NTIA Report 86-194

A Tutorial Review of Elements of Weak Signal Detection in Non-Gaussian EMI Environments

David Middleton
A.D. Spaulding

U.S. DEPARTMENT OF COMMERCE
Malcolm Baldrige, Secretary

Alfred C. Sikes, Assistant Secretary
for Communications and Information

May 1986

TABLE OF CONTENTS

TABLE OF CONTENTS (CONTINUED)

LIST OF FIGURES

LIST OF FIGURES (CONTINUED)

LIST OF FIGURES (CONTINUED)

LIST OF TABLES

A Tutorial Review of Elements of Weak Signal Detection in Non-Gaussian EMI Environments

David Middleton* and A. D. Spaulding**

New models of electromagnetic interference (EMI) have been developed by Middleton [1-11,48,49] over the last decade (1974-1983), which have provided canonical, analytically tractable, and experimentally well established quantitative descriptions of nearly all EMI environments. These models are (1) physically derived; (2) are canonical in the sense that they are invariant of the nature and waveform of the source and details of propagation, as far as their formal analytical structure is concerned; (3) are highly non-Gaussian; and (4) are analytically and computationally manageable. Their principal quantitative and most widely applied form is embodied in the first-order probability distributions of the (instantaneous) amplitude, and envelope, of the received waveform following the linear front-end stages of a typical receiver. Three basic EMI models are distinguished: Class A, B, and C, respectively involving sets of three, six and eight, physically derived parameters, which are measurable from observed EMI amplitude (or envelope) data. These three basic classes are defined in terms of receiver bandwidth vis-à-vis that of the EMI.

When receivers conventionally optimized for Gauss noise (i.e., matched-filter systems) are used in these highly non-Gaussian EMI environments, receiver performance can be greatly degraded [0(20-40 dB), typically], vis-à-vis that of receivers optimized to the actual EMI in force (e.g., Class A, B, or C noise) [2,13,14,21]. Specific examples of this behavior are provided. The physical bases and practical implications of the EMI models themselves and their impact on the reception process also are discussed.

The principal aim of this Report is to present a Tutorial Review of the main features of the work to date ($\leq$1985) on these models and their current and potential applications, particularly for weak-signal detection. Accordingly, this Report represents an updated and expanded version of an earlier tutorial review ([40], 1980). Various analytical details are reserved to an Appendix, and the full technical analysis and results are specifically cited in the extensive list of references, which themselves are briefly appraised from the viewpoint of the reader's further interest.

Key Words: Class A, B, C noise; electromagnetic interference environments (EMI); optimum and suboptimum detectors; optimum signal detection; performance comparison

---

*Contractor, Institute for Telecommunication Sciences, National Telecommunications and Information Administration, U. S. Department of Commerce, at 127 E. 91st St., New York, NY 10128.

**The author is with the Institute for Telecommunication Sciences, National Telecommunications and Information Administration, U. S. Department of Commerce, Boulder, CO 80303.

1. INTRODUCTION

In the last decade a variety of statistical-physical models of electromagnetic interference (EMI) have been developed [1-11,48,49], models that provide a canonical, analytically tractable, and experimentally well-established quantitative description of most EMI environments encountered in practice. Because of their impact both on measurement programs of real-world EMI situations and on the evaluation and prediction of receiver performance, it is appropriate at this stage to review the salient features of these models, with particular emphasis on their physical foundations and practical implications.

Accordingly, the present effort is an updated and expanded version of an earlier review [40]. It aims concisely to describe and explain the new EMI models, and their impact on receiver performance. This includes specifically the potentially significant improvements over conventional (matched-filter) techniques that are optimal for the usually postulated Gaussian noise environments. The present tutorial effort also includes suggestions for applications of these models and performance results, concepts, and methods, as well as important problems of implementation. In keeping with the tutorial character of this Report, it does not involve any new research efforts. Rather, it is intended to provide a useful, and moderately complete guide, at this stage, to the concepts, methods, results, and applications associated with these new EMI models, their experimental verification, and the performance of selected telecommunication receivers in such EMI environments. In these respects, we have borrowed freely from current technical reports and papers, emphasizing fundamental ideas and methods, as distinct from a detailed exposition of analytical procedures. The necessary mathematical apparatus, however, is fully described in the appropriate references and is partially summarized here in the Appendix .

Consequently, this report is organized in the following way: Part I - "Non-Gaussian EMI Models," consists of five sections, devoted respectively to the noise models, the measurement of model parameters, and a short review of the salient model features, their scope in application, etc., including the characterization of non-Gaussian EMI fields. Then, Part II-"Threshold Receiver Performance," contains five sections, concerned with optimum and suboptimum detection algorithms, performance, and the conditions for which the often large improvements in performance over the conventional matched-filter receivers may be expected. Simulation results for threshold detection in both Class A and Class B noise are presented, and the effects of spatial processing are included. Section 11 (of Part II) completes the principal body of the report with a short overview of the material described in the preceding sections. An extensive list of 73 pertinent references is included in Section 12.

PART I. NON-GAUSSIAN EMI MODELS

Here, in Part I, we shall consider the salient features of the recently developed EMI models referred to above, including the definition and measurement of their basic parameters, with empirical examples from various real-world interference environments.

2. GENERAL DEFINITIONS AND REMARKS

We distinguish three canonical EMI models, basically in terms of their temporal coherence structure vis-à-vis that of the receiver's response upon which they impact. Thus, we can classify this interference in the following three broad categories: A, B, and C (which is the sum of a Class A and Class B component). Specifically, Class A interference produces negligible transients in the typical receiver; i.e., is "coherent" as opposed to "impulsive," or "incoherent" interference (Class B), which is characterized by significant "transients" or "ringing" of the receiver (pre-detection/pre-processing) stages.

These effects may be more explicitly defined in terms of receiver (pre-detection/pre-processing) bandwidth (Δf_R) vis-à-vis the duration T_I of the typical interfering input waves. The necessary and sufficient condition for each class may be generally stated

Class A: $T_I \Delta f_R >> 1$: ignorable transients are produced in the (linear) RF/IF stages of the receiver; an essentially steady-state (possibly overlapping) set of signal waves is produced; (2.1)

Here Δf_N is the effective bandwidth of the incoming noise and Δf_R is the effective bandwidth of the (linear) RF/IF stages of the receiver.

Class B: $T_I \Delta f_R << 1$): essentially all transients are generated in the (linear) RF/IF stages of the receiver; i.e., overlapping "impulse" responses; (2.2)

Class C: $T_I \Delta f_R << 1$): an (additive) mixture of Class A and B is generated primarily "impulsive" if Class B dominates, etc. (2.3)

Thus, physically in Class A cases, (each) interfering signal is "on" long enough so that the initial and final transient buildup and decay are ignorable vis-à-vis the "on" period of the typical signal, while the reverse is the case for Class B.

The condition (2.1) significantly broadens the applicability of Class A models, heretofore, by removing the earlier condition $\Delta f_N \ll \Delta f_R$, as well as properly restricting Class B cases to those of "impulsive" noise transients generated by the receiver. (Thus the earlier Class B condition $\Delta f_R \ll \Delta f_N$ is necessary, but is not sufficient unless $\Delta f_N \doteq T_I^{-1}$ also.) The spectral relationship of the EMI interference and the front-end stages of the typical receiver, upon which the definition of the various interference classes is made, is shown in Figure 2.1.

Of course, strictly speaking, we must always have a "build-up" and transient decay period generated by the front-end stages of the receiver, when the incoming signal first appears, and next, terminates. For Class A interference these transient periods are negligible vis-à-vis the incoming emission's duration, so that typical Class A input signals are effectively undistorted by the receiver. On the other hand, for a Class B interference, the transient decays are dominant, in that the receiver rings for a period effectively longer than the input signal duration. For general waveforms entering the receiver, where $1 > T_I \Delta f_R$, the effect of the (front-end stages of the) receiver is noticeably to modify the original input waveforms. Thus, Class B (and Class C) "signals" are always transmitted with distortions, while Class A waveforms are passed essentially undistorted.

It is important to note that it is not necessary (although it is sufficient) that the bandwidth (Δf_N) of the Class A interference obey the previously stated condition: $\Delta f_N < \Delta f_R$. In fact, one can have $\Delta f_N > \Delta f_R$ for Class A disturbances, subject to (2.1) where now $T_I > \Delta f_N^{-1}$. Thus spectrally broad interference also can be Class A, as long as (2.1) is obeyed. An example of this is a coherent train of pulsed radar signals, where for each pulse duration, $\tau_0 < T_0$ (= pulse repetition rate (P.R.R.) $< T_I$, with $T_I \Delta f_R > 1$, for which, however, $\Delta f_R < 1/\tau_0 (\doteq \Delta f_N)$. On the other hand, an incoherent pulse train would be an example of Class B interference here, provided $(T_I = \tau_0) < T_R (\doteq \Delta f_R^{-1})$; i.e., each (incoherent) pulse in the train is sufficiently brief to appear "impulsive" to the receiver. In the former instance above, the transient effects in the receiver are ignorable and the typical interfering wave appears as a filtered pulse train, whereas in the latter case, the "transients" are now the interference.

A critical feature of these Class A and B (and C) models is that they are canonical; their analytic form remains invariant of the particular physical source mechanisms; such diverse mechanisms as fluorescent lights, power line signals, automobile ignition noise, atmospheric noise, ore-crushing machinery, etc., are

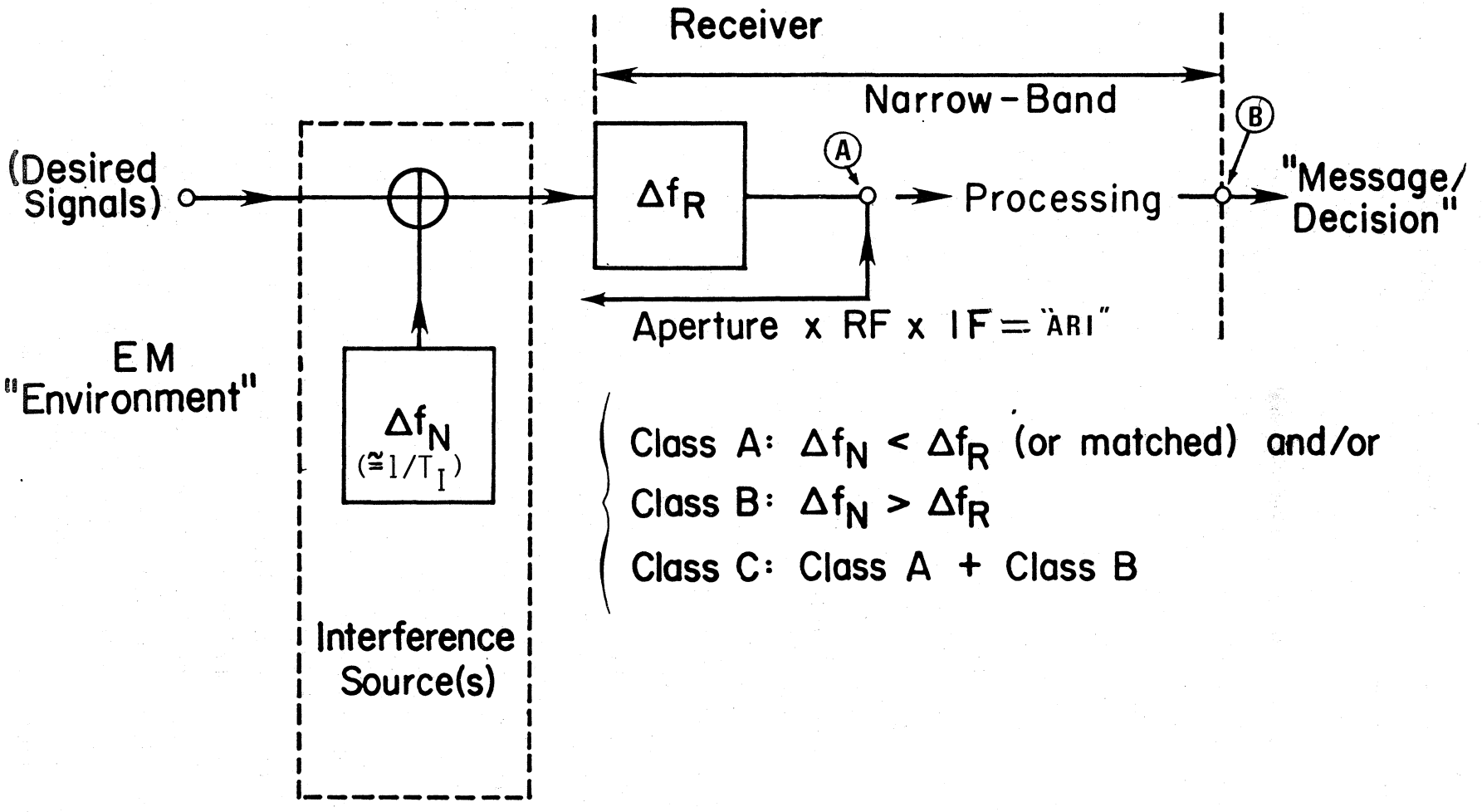

Figure 2.1. Schema of the EM interference and desired signal environment vis-à-vis a typical narrow-band receiver. The statistical properties of the EMI are obtained at (A). Performance of the particular receiver is assessed at (B).

readily accommodated without restriction (cf. Figures 3.1 to 3.9 below, in Section 3). In fact, the only limitations on the statistical-physical foundations of our models are that they

(1) represent independent (or independent sets of) radiation "events";

(2) that any number of sources can be emitting at any given instant; i.e., the available number of potential emitters is (mathematically) infinite;

and (3) that the output of the (linear) front-end stages of the receiver be narrow band (cf. Figure 2.1). (Extensions to the broadband (Class A noise) cases have recently been made [60, Sec. 7.4].)

The result is that the basic statistics are fundamentally Poissonian [1,6-11] (in particular, see Sec. 2 of [49]).

Most EM interference may be canonically represented by these models, invariant of waveform and the details of the propagation law of typical emitters, as far as formal analytical structure is concerned [1,2,7].

Of course, a particular interference field and communication system will have their specific numerical parameter values, which it is one task of a measurement program to obtain [6,12]. A second critical feature of these models is that they are analytically tractable, as well as computationally manageable. This is especially important when we go beyond the measurement program to apply the analysis to the prediction and evaluation of system performance, including optimum as well as suboptimum reception [14,17]. See Sections 7 to 10 following, and the Appendix.

Exceptions to the generality of our EMI models arise in two principal ways:

1. <u>For the class of situations where the interference is completely deterministic and known at the receiver</u>: These cases, of course, must be handled by the classical method of direct analysis and/or empirical study. However, in almost all "real-world" environments, the interference is at best only statistically related to the observer (receiver), at least for emission times, number of sources acting at any given instant, waveform structures, source locations, etc., so that a statistical treatment is necessary and inevitable.
2. <u>For the other class of situations, where condition (1) above does not hold</u>: This may occur when the total number of possible emitters is reasonably small (say, O(3,4) or less). Then, although the various emission times, and the actual number of sources active at any given instant, are random, the small maximum number of sources possible precludes Poissonian statistics, unless the emission times of each source are uniformly and, independently distributed (so that <u>each</u> source produces a Poisson distribution of emissions vis-à-vis our typical receiver), cf. Sec. 2 of [49].

Practically, it appears that the assumption that the number of possible (independent) emitters can be indefinitely large is sufficient to insure the desired basic Poisson statistics. This is well borne out by the ample empirical data obtained by various researchers [cf. Refs. 23-28, for example], of which Figures 3.1 to Figure 3.8 are typical. The final condition [(3) above], that the output of the linear front-end stages of the receiver be narrow-band (at Ⓐ, Figure 2.1), although not critical for the development of an analytically tractable theory, cf. Sec. 7.4--which is one of the major achievements of recent studies [1-10,47,49]--is nevertheless almost always satisfied in practice. By "narrow-band" is meant, as usual, that "envelope" and "phase" of the signal output (at point Ⓐ here) are slowly varying vis-à-vis the central or "carrier" frequency component(s) ($\cos \omega_0 t$, $\sin \omega_0 t$) of the signal. (For the broad-band cases, see Sec. 7.4 of I, [60].)

The above three categories (Classes A, B, and C) for interference, as the latter impacts on a typical (narrow-band) receiver, e.g., as (the linear, front-end of) that receiver responds to the EM environment, cf. Figure 2.1, provide a useful and meaningful way of distinguishing the different effects that these different categories have on reception. This categorization is important because receiver response is statistically different for each Class. As will be seen presently, these differences appear most generally and explicitly (as far as first-order statistics are concerned) in the experimentally derived (cf. Figure 3.1 to Figure 3.8), and theoretically determined exceedance probabilities (PD's). These are often called APD's (a posteriori probability distributions), such as $P_1(X > X_0)$, or $P_1(E > E_0)$. These are the respective probabilities that the instantaneous amplitude (X), or instantaneous envelope (E) observed at the receiver's IF output exceed some threshold X_0, or E_0, as these latter are allowed to assume values in the respective ranges $(-\infty,\infty)$, or $(0,\infty)$. The conditions "spectrally broader than," and "spectrally narrower than," cf. (2.1), (2.2), and Figure 2.1, are to be interpreted as "sufficiently broader or narrower," etc., where in any case, care is taken to refer to the definitions of Class A, B, etc., in terms of the residual transients vs. the "on"-time of the input emission that appears at the output of the IF stage of the receiver in question. [For a quantitative discussion, see Sec. 7, Ref. 7.]

It is instructive to extend the schmema of classification further, in order to distinguish between man-made and natural interference, and between "intelligent" and "nonintelligent" emissions. Accordingly, we define

(i) "Intelligent" noise* or interference as man-made and intended to convey a message or information of some sort;

whereas

(ii) "Nonintelligent" noise or interference may be attributable to natural phenomena; e.g., atmospheric noise or receiver noise, for example, or it may be man-made, but conveying no intended communication, such as automobile ignitions, or radiation from power lines, etc.

The importance of distinguishing man-made from natural noise or interference lies in the fact that the former is potentially controllable, sometimes to the point of elimination, whereas the latter cannot be eliminated at the source, and is usually not subject to control; one can seek only to investigate its effects on the communication process. Moreover, the distinction between "intelligent" and "nonintelligent" is always significant with regard to information transfer; the taxonomy of the former can have greatly different implications and consequences from that of the latter.

We can readily tabulate these different varieties of interference in a concise way, as suggested in Table 2.1. We have included a further refinement through the term "compatible." By definition, compatible interference here is one that is appropriately matched spectrally to the receiver band Δf_R, in the sense of being equivalent to Class A interference vis-à-vis the receiver and occupying a spectral region in Δf_R, and such as to produce ignorable transients in the ARI stages. "Incompatible" may mean that $\Delta f_N > \Delta f_R$ (Class A-C), or that only a portion of the incident emission is spectrally available to the receiver; Class A again, e.g., $1 \ll T_I \Delta f_R$, but now the interference is not wholly in the receiver band Δf_R. Class C in Table 2.1 reminds us that combinations of Class A and B noise can occur, as noted, cf. Figure 2.1.

However, before we go on to consider these new EMI models in a more quantitative fashion (Sec. 3 et seq.), it is appropriate to comment briefly on earlier attempt at EMI model-building. For the most part, earlier efforts at modeling man-made and natural interference (principally atmospheric noise) have produced a wide variety of analytical results, often with the virtue of mathematical simplicity, but severely limited in usefulness by lack of generality and physical insight, and

* We remark again [cf. Middleton, [15], Sec. 1.3.5] that by definition, "noise" or "interference" is any undesired "signal" at or in the receiver, regardless of origin.

Table 2.1. Interference Categories and Classes

TYPE	"INTELLIGENT"	CLASS	"NONINTELLIGENT"	CLASS
Man-made	1) Compatible	A	1) Automobile ignition	B
	2) Incompatible (Communication)	A,B,C	2) Other EM emissions: power lines, electric tools, etc.	A,B,C
	[3) Extra-terrestrial (Communication)	A,B,C]		
Natural			1) Atmospheric	B
			2) Extra-terrestrial solar, galactic, cosmic radiation, etc.	[A], B,C

a concomitant dependence on local, empirical data and circumstances, [12]. Somewhat less restricted, but still lacking detailed physical structure and limited to the Class B situation, are the quasi-empirical models of Hall [32].

Important exceptions to the above are the work of Furutsu and Ishida [29] on obtaining the APD's (and associated probability densities [pdf's]) of atmospheric noise under rather broad conditions, and the more recent studies of Giordano [30], and Giordano and Haber [31], similarly directed to atmospheric noise. These recent investigations, however, are (necessarily) constrained to Class B types of interference and generally do not attempt a canonical formulation, which is a key feature of the current efforts [1,4-11,49,50]. Recent work of Pevnitskii, Palozok et al. [42],[43], regarding man-made interference, and the new book of Remizov [66], concerning natural radio noise primarily, also are particularly to be noted.

Middleton's canonical formulation thus allows one to apply the new models formally by Class (A, B, etc.) to all types of (EM) interference (provided the conditions (2.1) hold), unrestricted in general structure by the particular physical mechanism involved. These latter mechanisms, of course, determine the generic properties of the model parameters. They must be specifically introduced into model building if the ad hoc and arbitrary empiricism of much of the earlier work is to be avoided. [For a more detailed review of earlier work vis-à-vis this newer approach, see Chapter 2 of Spaulding and Middleton [13,14]; and references therein; see [59], Sec. 3, also.]

3. BASIC MODEL PARAMETERS

The model statistics of principal interest and use are i) the various (first-order) moments, ii) the probability density functions (pdf's), and iii) the exceedance probabilities (or APD's) [1-11,49]. These quantities are defined respectively by the following relations:

i) first-order moments (of instantaneous amplitude, X, or envelope, E):

$$\langle X^m \rangle \equiv \int_{-\infty}^{\infty} X^m w_1(X|A,B, \text{ or } C)dX; \langle E^m \rangle \equiv \int_0^{\infty} E^m w_1(E|A,B, \text{ or } C)dE, \tag{3.1}$$

where X(=X(t)) and E(=E(t)), respectively, are the indicated instantaneous amplitude and envelope of the output of the front-end stages of the typical receiver, at (A), Figure 2.1. Here $w_1(\ |A,B, \text{ or } C)$ denotes the probability density function, or pdf, (of X or E) for Class A, B, or C interference. These (m^{th}) moments, $\langle X^m \rangle$, $\langle E^m \rangle$ are first-order, i.e., they are obtained from a first-order pdf, w_1, for any instant

(t). [For a discussion of first- and higher-order pdf's and the associated random processes, see Secs. 1.3, 1.4, Ref. 15.]

Physically, the lower degree moments (m=1,2) have their usual significances, $\langle X \rangle$ = mean values (=0), while $\langle E \rangle$ = mean value (>0) here. Similarly, we have $\langle X^2 \rangle$ (= $\langle E^2 \rangle /2 > 0$) represent the mean intensity of the interference, again as measured at (A), Figure 2.1.

ii) The probability density function (pdf's) of (X and E): these, as noted above, are $w_1(X|A,B,\text{ or } C)$, $w_1(E|A,B,\text{ or } C)$, for X's and E's at some time t. In more detail, we can write

$$w_1 = w_1(X,t|A,B,\text{ or } C),\ \text{etc.}, \tag{3.2}$$

where we include (t) explicitly, to indicate the dependence on time; different pdf's are often obtained for different times t. Thus, in practical applications it is important to note the time period in which data (X,E) are collected, to construct empirical pdf's (and APD's--(iii) below, and Sec. 4). This is because different EMI environments occur at different times of day (usually), and at different times of the week, etc., particularly in urban situations, for example, when a noticeable component of the EMI is automobile ignition noise [cf. Figure 3.6]. Similarly, atmospheric noise [cf. Figure 3.7] exhibits diurnal characteristics.

iii) The exceedance probabilities (or APD's): These are defined as the probabilities that (here X exceeds a level X_o, E exceeds E_o):

$$P_1(X \geq X_o) \equiv \int_{X_o}^{\infty} w_1(X,t|A,B,\text{ or } C)\, dX = 1 - D_1(X \leq X_o)\ , \tag{3.3a}$$

$$P_1(E \geq E_o) \quad \int_{E_o}^{\infty} w_1(E,t|A,B,\text{ or } C)\, dE = 1 - D_1(E \leq E_o)\ , \tag{3.3b}$$

where X_o,E_o are some threshold values of X, E, respectively, and D_1 is the familiar cumulative probability, or distribution (of X_o,E_o). [The P_1 also are often referred to in the literature as a posteriori probability distributions, or APD's.] Examples of experimental and theoretical APD's are shown in Figure 3.1 through Figure 3.9.

Finally, it is convenient to use normalized amplitudes (x or z) and envelopes ($\mathcal{E}$), in place of X,E. These normalized quantities are defined by

$$x \equiv \frac{X}{\sqrt{\langle X^2 \rangle}} = \frac{X}{(\Omega_2+\sigma_G^2)^{1/2}} \; ; \; \mathcal{E} \equiv \frac{E}{\langle E^2 \rangle^{1/2}} = \frac{E}{[2(\Omega_2+\sigma_G^2)]^{1/2}} \quad , \qquad (3.4)$$

where $\langle X^2 \rangle = \Omega_2+\sigma_G^2$, $\langle E^2 \rangle = 2(\Omega_2+\sigma_G^2)$ are expressed in terms of the respective mean intensities of the non-Gaussian and Gaussian components of the incoming noise, as seen at (A), Figure 2.1 above. (A more detailed definition of these and the other fundamental parameters of our interference models is presented below, in Section 3.1.)

With the above in mind, we can proceed to a more detailed description of the new EMI models.

3.1 The Basic Model Parameters of First Order Statistics

Class A interference is characterized (in the first-order approximations used) by three global parameters $\mathcal{P}_{3A} = \{A_A, \Gamma'_A, \Omega_{2A}\}$, and Class B by a six-fold set, $\mathcal{P}_{6B} = \{A_B, \Gamma'_B, \Omega_{2B}; \alpha, b_{1\alpha}, N_I\}$, similarly; [1,7,8]. For Class C interference there are eight global parameters, $\mathcal{P}_{8C} = \{A_A, A_B; \Gamma'_{AB}; \Omega_{2A}, \Omega_{2B} | \alpha, b_{1\alpha}, N_{IC}\}$. These parameters are briefly described below, in subsections A, B, and C. In any case, we emphasize that these parameters are not ad hoc, but are physically derived from the model, involving source distributions, radiation properties and geometries, and front-end receiver structure. As has been noted above, and in the discussion of Figure 3.1 through Figure 3.9 below, the analytical model is in excellent agreement with the empirical data, as well as being canonical, cf. Section 2 above.

Class A cases, however, range from the simplest forms, namely, the strictly canonical cases involving $\mathcal{P}_{3A}$ only, to the approximately canonical forms, which may involve more parameters, finally to the quasi-canonical models, which require at least one additional parameter. (The reasons for this stem from the nature of the source distributions, and are discussed in technical detail in Sections V and VII of [49], as well as in [48].)

Let us consider first the strictly and approximately canonical Class A models that require only a single approximating pdf.

A. Class A Parameters, $\mathcal{P}_{3A}$:

The Class A interference (in the first-order) is governed principally by three global parameters, $\mathcal{P}_{3A} \equiv (A_A, \Gamma'_A, \Omega_{2A})$. These are (cf. [1]):

A_A = the "overlap" or "unstructure" Index, which is defined as the average number of radiation "events" per second times the mean duration of a typical source emission (cf. [7], Part 2, Equations (2.16, 2.18), etc.). The smaller A_A, the more "structured" (in time) is the interference. Conversely, the larger A_A the more Gaussian and less structured is the noise. When $A_A \to \infty$, the noise is Gaussian. (3.5a)

$\Gamma'_A \equiv \sigma_G^2/\Omega_{2A}$ = the Gaussian factor = ratio of average intensity of the Gaussian component of the interference to that of the non-Gaussian component. (3.5b)

Ω_{2A} = the mean intensity of the non-Gaussian (or "impulsive")* noise component of the interference. (3.5c)

These parameters, $\mathcal{P}_{3A}$, are all measurable, either at the input to the receiver or at the output of the initial linear front-end stages, before nonlinear processing, c.f. Figure 2.1. Figure 3.1 through Figure 3.9 show typical Class A (and Class B) experimental data, along with the theoretical curves. (For a treatment of the approximately and quasi-canonical Class A cases, see [48], and Sections V and VII of [49].) We turn next to:

B. Class B Parameters, $\mathcal{P}_{6B}$:

Unlike Class A interference, we require for Class B noise, ultimately, a pair of approximating APD's, and pdf's, which are suitably joined at some appropriate threshold value $\mathcal{E}_B$ [10]. These approximations are $P_{1\text{-}I}$, $P_{1\text{-}II}$, joined at $\mathcal{E}_B$, cf. Equation 4.2.

In addition, we require now a basic global set of six parameters $\mathcal{P}_{6B} = \{A_B, \Gamma'_B, \Omega_{2B}; \alpha, b_{1\alpha}, N_I\}$, described below.

*The term "impulsive" for the noise is too restrictive; as already noted, these models are canonical in the waveform, which can be cw trains, structured pulses, etc., as well as "impulses" (which for the most part, are Class B, anyway).

The parameter subset, $\mathcal{P}_{3B} \equiv \{A_B, \Gamma'_B, \Omega_{2B}\}$, of $\mathcal{P}_{6B}$, is defined precisely as for the Class A cases, cf. (3.5). The additional parameters $\{\alpha, b_{1\alpha}, N_I\}$ required for first-order approximations, are:

$$\alpha = \frac{2 - \mu}{\gamma}\Bigg|_{\text{surface}}, \quad = \frac{3 - \mu}{\gamma}\Bigg|_{\text{volume}} \tag{3.6a}$$

$\equiv$ spatial density propagation parameter. Here μ, γ are, respectively, the power-law exponents associated with the range dependence of the spatial density distribution of the (possibly) emitting sources and their propagation law.

$$b_{1\alpha} = \frac{\Gamma(1 - \alpha/2)}{2^{\alpha/2}\,(1 + \alpha/2)} \left\langle \left(\frac{\hat{B}_{oB}}{\sqrt{2}} \right)^{\alpha} \right\rangle; \tag{3.6b}$$

($\hat{B}_{oB}$ = typical envelope after front-end stages of receiver, cf. Figure 2.1).

= a "structure" factor, which appears in the Index, $\hat{A}_\alpha$ (see Appendix A.2).

N_I = a scaling parameter on the normalized envelope $\mathcal{E}$, cf. (3.4), which is required to assist the joining process for the two approximations. (3.6c)

In effect, $\mathcal{P}_{3B} = \{A_B, \Gamma'_B, \Omega_{2B}\}$ are basically "structure" parameters, which govern the overall form of the APD and pdf, while the subset (3.6) represent essentially "scale" parameters, which primarily set the level and scale of the distribution (the Ω_{2B} is both a structure and scale parameter). Figure 3.3 through Figure 3.8 show typical experimental APD's and the analytic approximations $P_{1\text{-BI,II}}$, all exhibiting the characteristically excellent agreement between theory and experiment.

In place of the more complete Class B model involving six parameters, a useful approximation may be expressed in terms of three different global parameters $\hat{A}_\alpha$, α, and Ω. Here $\hat{A}_\alpha = f(\alpha, \langle \hat{B}_{oB}^{\alpha} \rangle, \Gamma'_B, A_B)$, while Ω is a suitable normalization factor. The specific pdf's and APD's here are summarized in Appendix A.5.

Finally, we mention the Class C cases.

C. Class C Parameter, $\mathcal{P}_{8C}$:

As noted elsewhere [10],[11], Class C interference can be represented approximately for first-order statistics, as a Class B form. In particular, just like the Class B cases, two approximating APD's (or pdf's) are again required in the general case. Specifically, [10],[11], in regard to the parameters, we now replace the Class B parameters by the set

$$\mathcal{P}_{8\text{-}C} = \{A_A, A_B; \Gamma'_{AB}; \Omega_{2A}; \Omega_{2B} | \alpha, b_{1\alpha}, N_{IC}\} \tag{3.7}$$

cf. $\mathcal{P}_{6B}$ above, where now $A_{AB} = A_A + A_B$; $\Gamma'_{AB} = \sigma^2_{GAB}/\Omega_{2AB}$, $\Omega_{2AB} = \Omega_{2A} + \Omega_{2B}$; $b_{1\alpha}$ = Eq. (3.5b), with $N_I \to N_{I\text{-}C}$, and $a_B^2 \to a_{AB}^2 = \{2\Omega_{AB}(1 + \Gamma'_{AB})\}^{-1}$. (When there is no Class B noise, $A_B \to 0$, $\sigma^2_{GB} \to 0$, $\Omega_{2B} \to 0$; with no Class A component, we have $\alpha_{AB} \to \alpha$, $A_A \to 0$, $\sigma_A^2 \to 0$, $\Omega_{2A} \to 0$.) The results above apply here, with the indicated substitutions, as do the various Class B procedures for parameter estimation, as discussed in Appendix A.3. (A more precise Class C, based on only four parameters, is developed in [11], cf. Eq. 2.20.)

3.2 EMI Scenarios

The various sets of statistical-physical parameters $\mathcal{P}_{3A}$, $\mathcal{P}_{6B}$ (or $\mathcal{P}_{3B}$), $\mathcal{P}_{8C}$, etc., which appear in the canonical noise models are all measurable, or inferable from direct measurement, as we shall note in Section 4, following. These sets of statistical parameters, and their component elements, also are the elements of what we have called the EMI scenario, which, conversely, allows us to calculate a priori these measurable parameters, in many instances. Thus, the EMI scenario embodies all the relevant knowledge regarding how a typical interfering source radiates and where it is located. Also, it provides an explicit structure for the resulting, typical waveform as seen following the (linear) front-end stages of the receiver.

The (first-order) EMI scenario is specifically defined by:

(i) the propagation law ($\lambda^{-\gamma}$); cf. (3.6a)

(ii) the distribution law of sources $\sigma_s(\lambda,\phi)$ in the source domain; e.g., σ_s is $\lambda^{-\mu} w_1(\phi)$, cf. (3.6a);

(iii) the statistics of the waveform parameters (a = fading scale; ε = epoch; beam-patterns; envelope, $\hat{B}_0$; etc.);

(iv) the average emission characteristics of the sources, as embodied in the overlap indices, A_A, A_B;

(v) the level of the Gaussian component; and

(vi) the pertinent statistics of any other emission parameters.

For example, $\Omega_{2A,2B}$, cf. (3.5c), is given by $\Omega_2 \equiv A\langle \hat{B}_o^2 \rangle/2$. Thus, given the typical envelope structure, we have

$$\hat{B}_o = aG_o(\phi,t)/\lambda^{\gamma} , \tag{3.8}$$

where

$$G_o(\phi,t) = |\mathcal{A}_{RT}(\phi)|\, b\, u_o(t,\underline{\theta}') \tag{3.9}$$

embodies the transmit-receiving beam patterns, $\mathcal{A}_{RT}$, u_o = normalized basic interference waveform in the linear receiver output (before "processing") and b = appropriate dimensional parameter. We can determine Ω_2, based on $\sigma_s(\lambda,\phi)$, etc. For details of scenario construction, see, for example, Sections 3.1, 3.2 of [59], and Section V, B, pp 90-93, of [49].

3.3 Comparisons with Experiment

In this subsection we include a variety of comparisons of our new theoretical models with experiment, for both Class A and Class B interference (Figure 3.1 through Figure 3.9). (For analytical details, see Appendix A.1,2, and [1,2].) Four significant features are at once evident:

(1) The agreement between theory and experiment is excellent; i.e., the approximating forms are effective, analytical relations for predicting the desired first-order statistics.

(2) The canonical nature of our models is demonstrated: the form of the results [here APD's: $P_1(\mathcal{E} > \mathcal{E}_o)$] is invariant of the specific source mechanism, whether ignition noise, atmospherics, fluorescent light, etc., man-made or natural, within the distinct Class A or B types.

(3) Class A and Class B interference are observably and quantitatively different noise types (vis-à-vis the narrow-band receiver used).

(4) The governing, physically structured parameters of these PD's and pdf's, which are likewise also canonical, can be obtained from approximate experimental data (usually expressed as an APD). (The procedure is discussed in Section 4 below.)

The importance of the canonical character of these models cannot be overstressed: with such models we avoid the vary limited and nonpredictive quality of all ad hoc models, whose structure must be verified and whose parameters provide little or no physical insight into the underlying process itself. Second, because these models are derived from physical principles [1,4,49], their parameters are

physically defined, are consequently canonical, and are quantifiable in specific instances from empirical data. Their structure, however, is independent of any particular measurement.

Figures 3.1 and 3.2 show APD's, e.g., $P_1(\mathcal{E} > \mathcal{E}_0)_A$ vs. the normalized envelope threshold $\mathcal{E}_0$, for Class A interference, respectively, from ore-crushing machinery in a mine (data from Adams, Bensema, and Kanda [23]), and from a powerline (from E. C. Bolton [25]). Observe the characteristic very steep rise following the Rayleigh region (constant slope), followed in turn by the expected bending over of the APD for the rarer "events" in each case. [Similar examples of Class A interference, but from man-made intelligent sources, also have been observed (e.g., Figure 3.9).]

Figure 3.3 through Figure 3.5 show APD's of Class B interference, respectively, for (i), primarily urban automotive ignition noise (Spaulding and Espeland, [28]); (ii) atmospheric noise (Espeland and Spaulding [26]); (iii), fluorescent lights, in a mine shope office (Adams et al. [23]). Observe the more gradual departure from the straight-line Rayleigh region, and the continuing rise, with constantly increasing slope in the figures (which is equivalent to $\eta \to 0$ for $\exp(-a^2\mathcal{E}_0^\eta)$, as $\mathcal{E}_0 \to \infty$). In these particular examples, the inevitable "bend-over" points, $\mathcal{E}_B$, lie outside the range of data taken, e.g., for $P_{1\text{-}B} < 10^{-6}$, so that we are able to obtain all the global parameters, except for A_B, cf. [10]. This is not the case, however, for the Class B examples of Figure 3.6 through Figure 3.8,* e.g., respectively for (i) ignition noise from vehicles moving on a freeway (Shepherd [27]); (ii) atmospheric

*Note that $\Gamma_B' \equiv \sigma_B^2/\Omega_{2B}$, where σ_G^2 is the independent Gaussian component, which is different from the <u>total</u> Gauss component $\Delta\sigma_G^2 = \sigma_G^2 + b_{2\alpha}A_B$. Thus, in Figure 3.6 and Figure 3.8 we must calculate Ω_{2B} from the data curve and then obtain σ_G^2 from Γ_B'. On the other hand, for Figure 3.7 Ω_{2B} occurs at 0 dB, by normalization. Since $P_1 = 0.36$ determines the total Gauss component ($\Delta\sigma_G^2$ for Class B, σ_G^2 for Class A noise), from the data of Figure 3.7 we get ($\Delta\sigma_G^2 \doteq -17$ dB ($= 2 \cdot 10^{-2}$) and $\therefore \sigma_G^2 = \Gamma_B'\Omega_{2B} = 10 \log_{10}(8 \cdot 10^{-3}) \doteq -21$ dB, which gives in turn $b_{2\alpha}A_B \doteq 0.012$ (in units of Ω_{2B}).

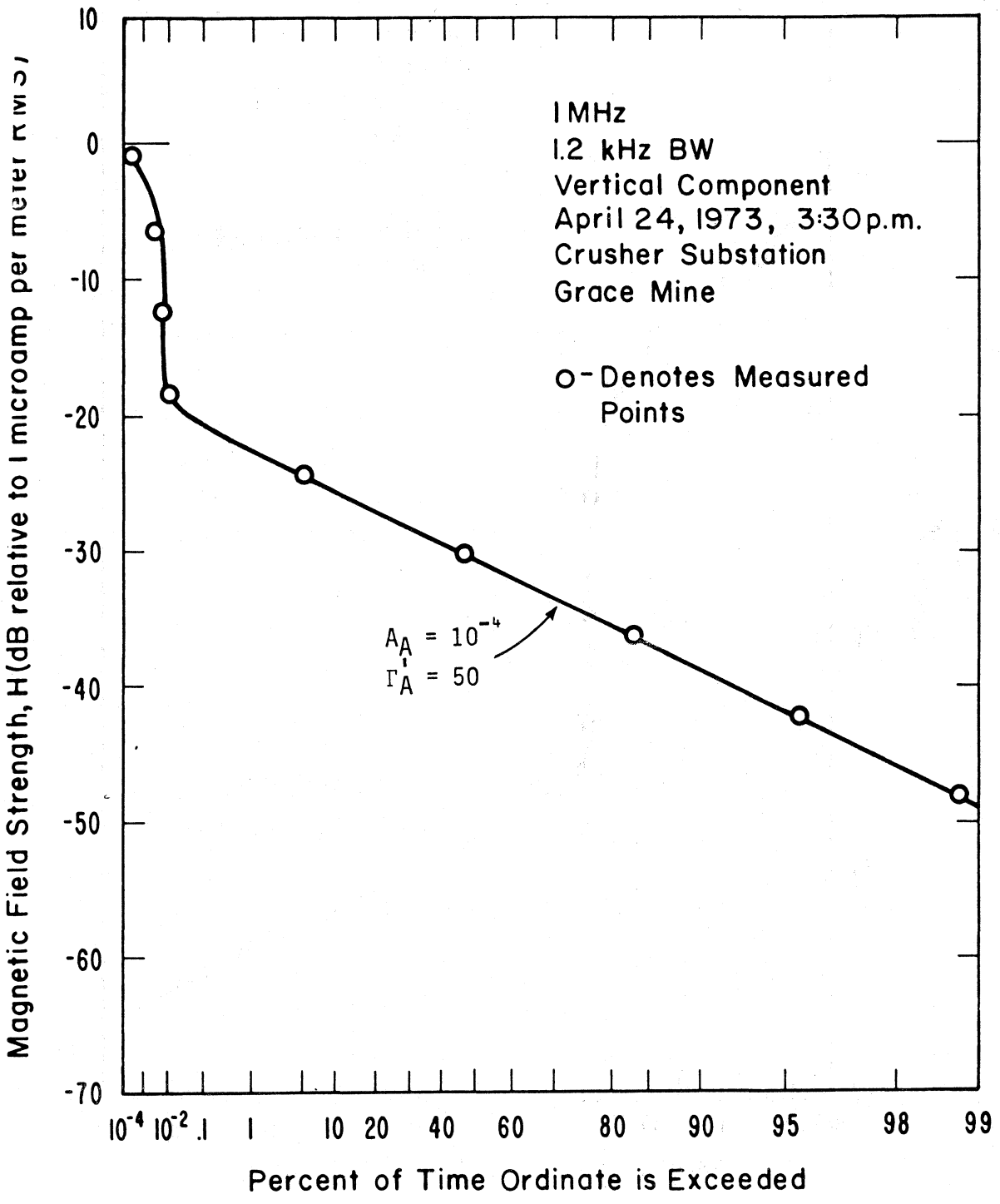

Figure 3.1. Comparison of measured envelope distribution, $P_1(\mathcal{E}>\mathcal{E}_0)_A$, with Class A model. Interference from ore-crushing machinery [Data from Adams et al, Ref. 23].

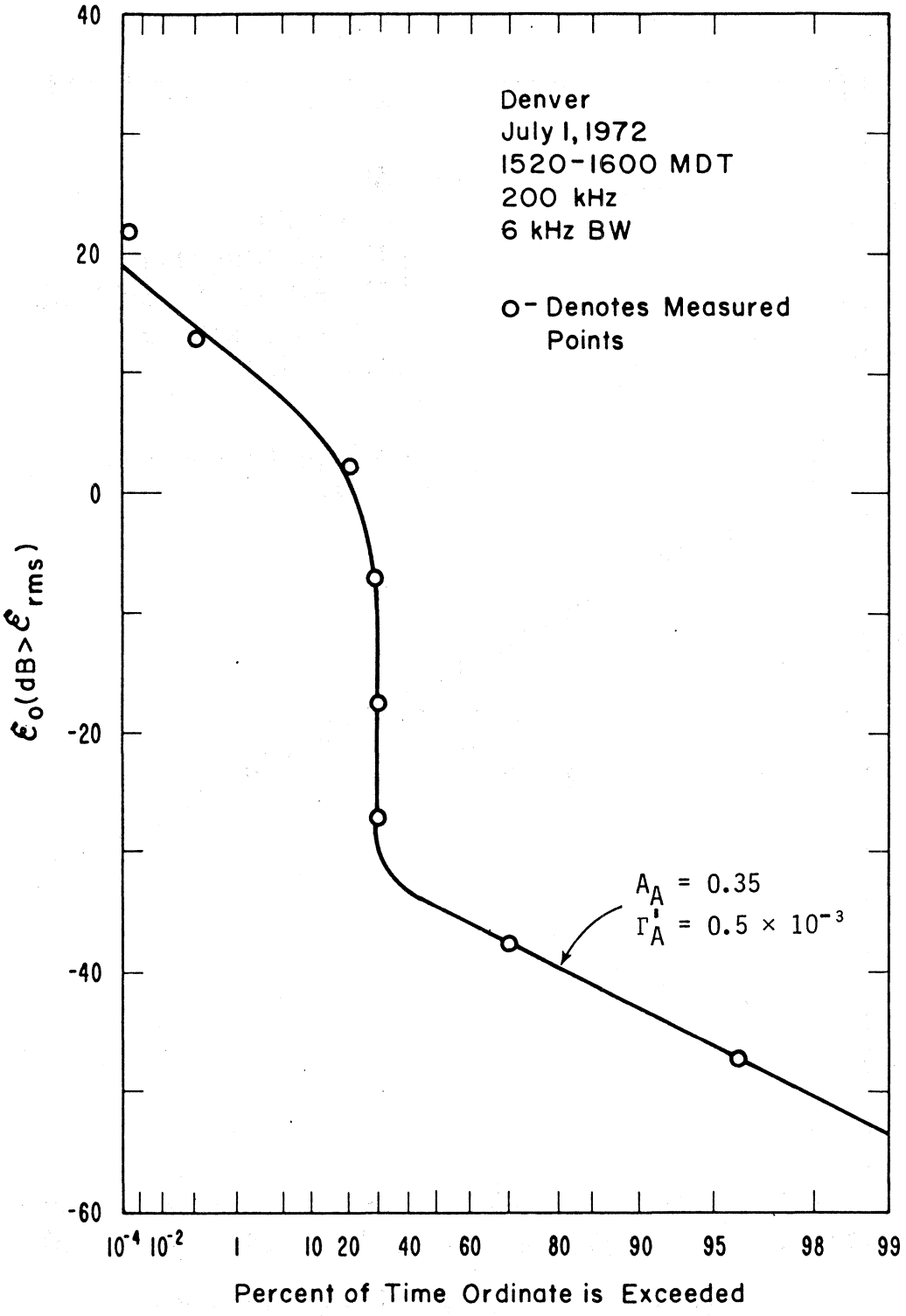

Figure 3.2. Comparison of measured envelope distribution, $P_1(\mathcal{E}>\mathcal{E}_o)_A$, with Class A model. Interference (probably) from nearby powerline, produced by some kind of equipment fed by the line [Data from Bolton, Ref. 25].

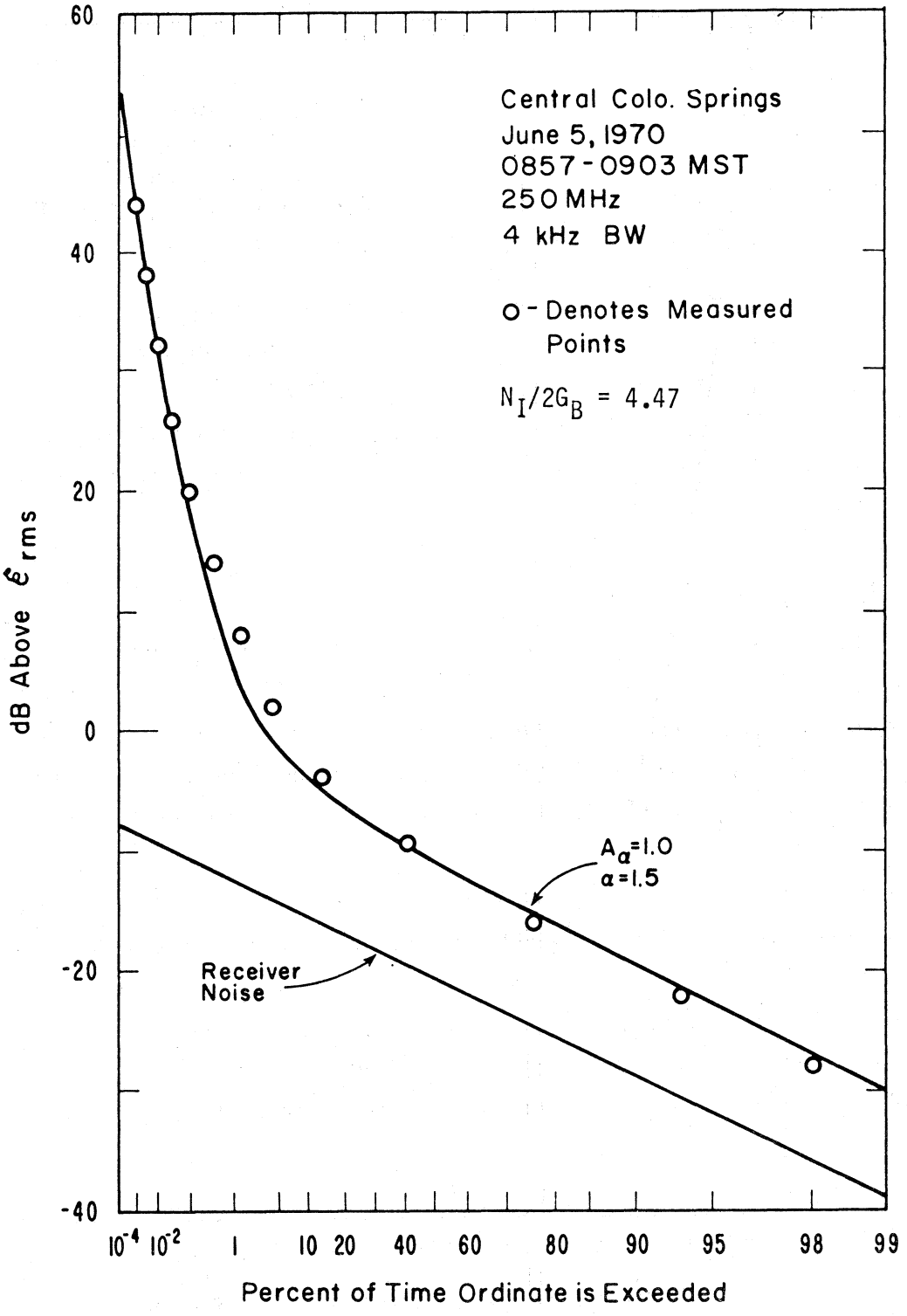

Figure 3.3. Comparison of measured envelope distribution, $P_1(\mathcal{E}>\mathcal{E}_o)_B$, of man-made interference (primarily automotive ignition noise) with Class B model. [Data from Spaulding and Espeland Ref. 28.]

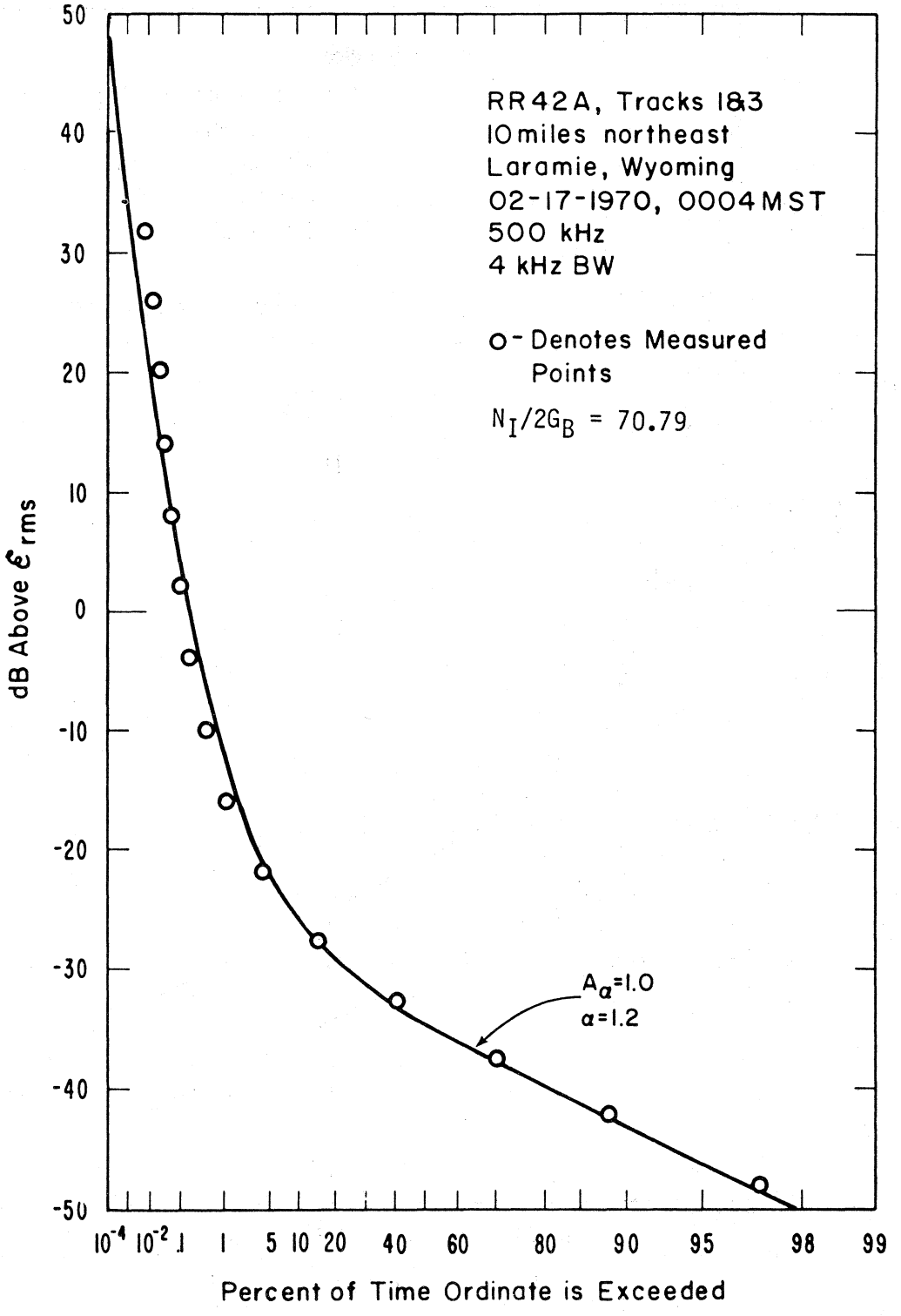

Figure 3.4. Comparison of measured envelope distribution, $P_1(\mathscr{E}>\mathscr{E}_0)_B$, of atmospheric noise with Class B model. [Data from Espeland and Spaulding, Ref. 26.]

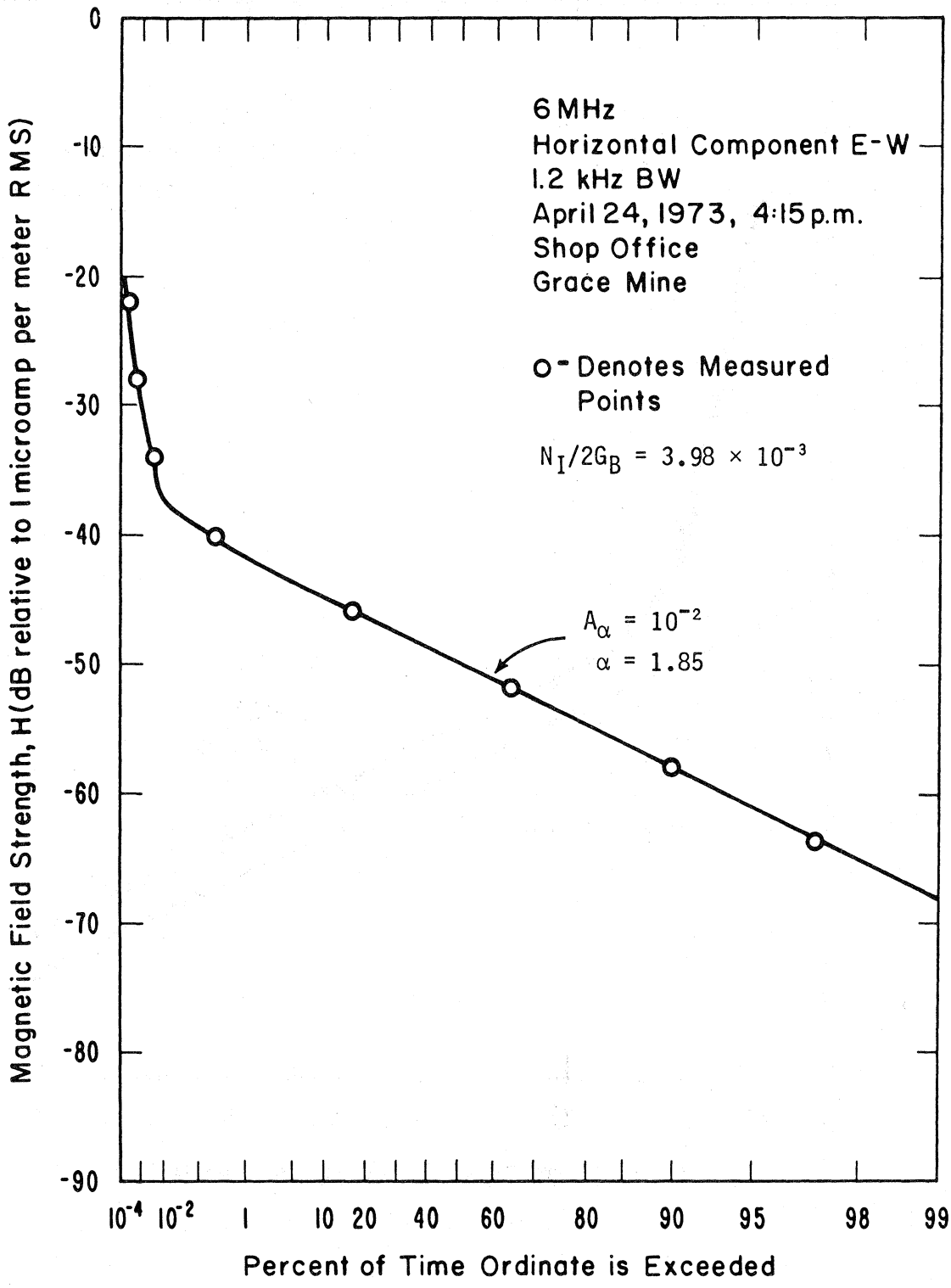

Figure 3.5. Comparison of measured envelope distribution, $P_1(\mathscr{E}>\mathscr{E}_0)_B$, of man-made interference (fluorescent lights in mine shop office) with Class B model. [Data from Adams et al., Ref. 23.]

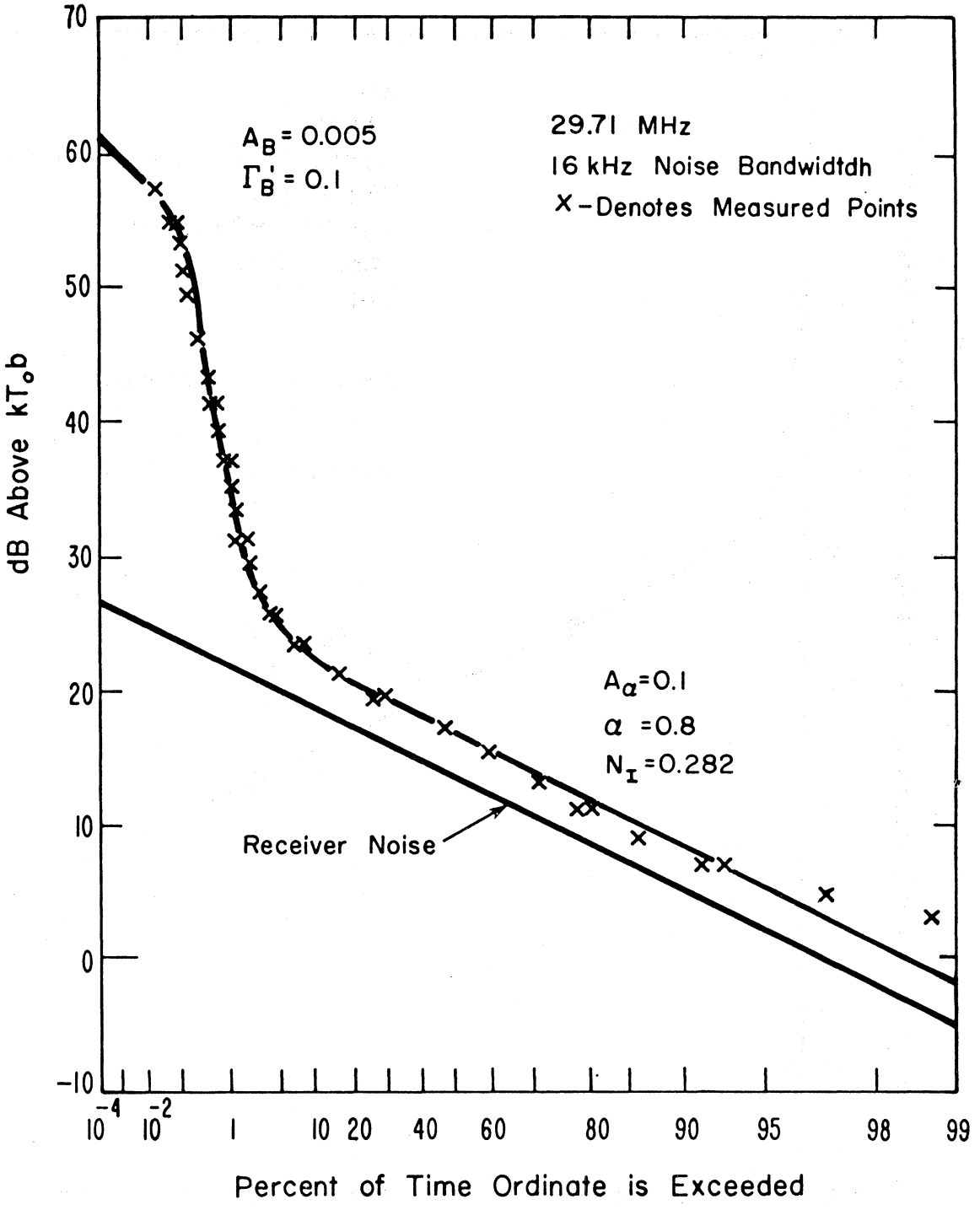

Figure 3.6. Comparison of measured envelope distribution, $P_1(\mathcal{E}>\mathcal{E}_0)_B$, of automotive ignition noise from moving traffic with full Class B model. [Data from Shepherd, Ref. 27, Fig. 14.]

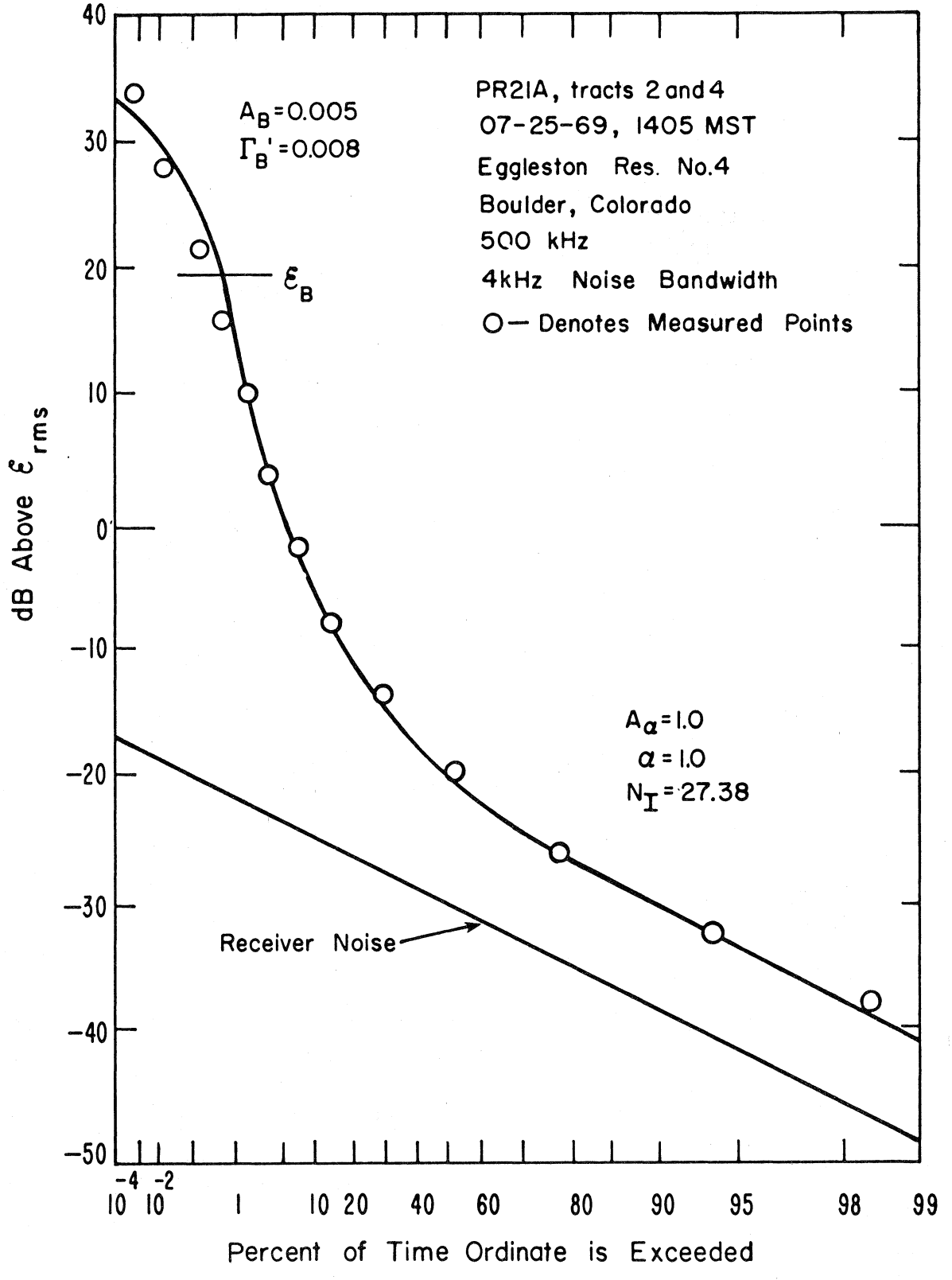

Figure 3.7. Comparison of measured envelope distribution, $P_1(\mathcal{E}>\mathcal{E}_0)_B$, of atmospheric noise with full Class B model. [Data from Espeland and Spaulding, Ref. 26. p. 42.]

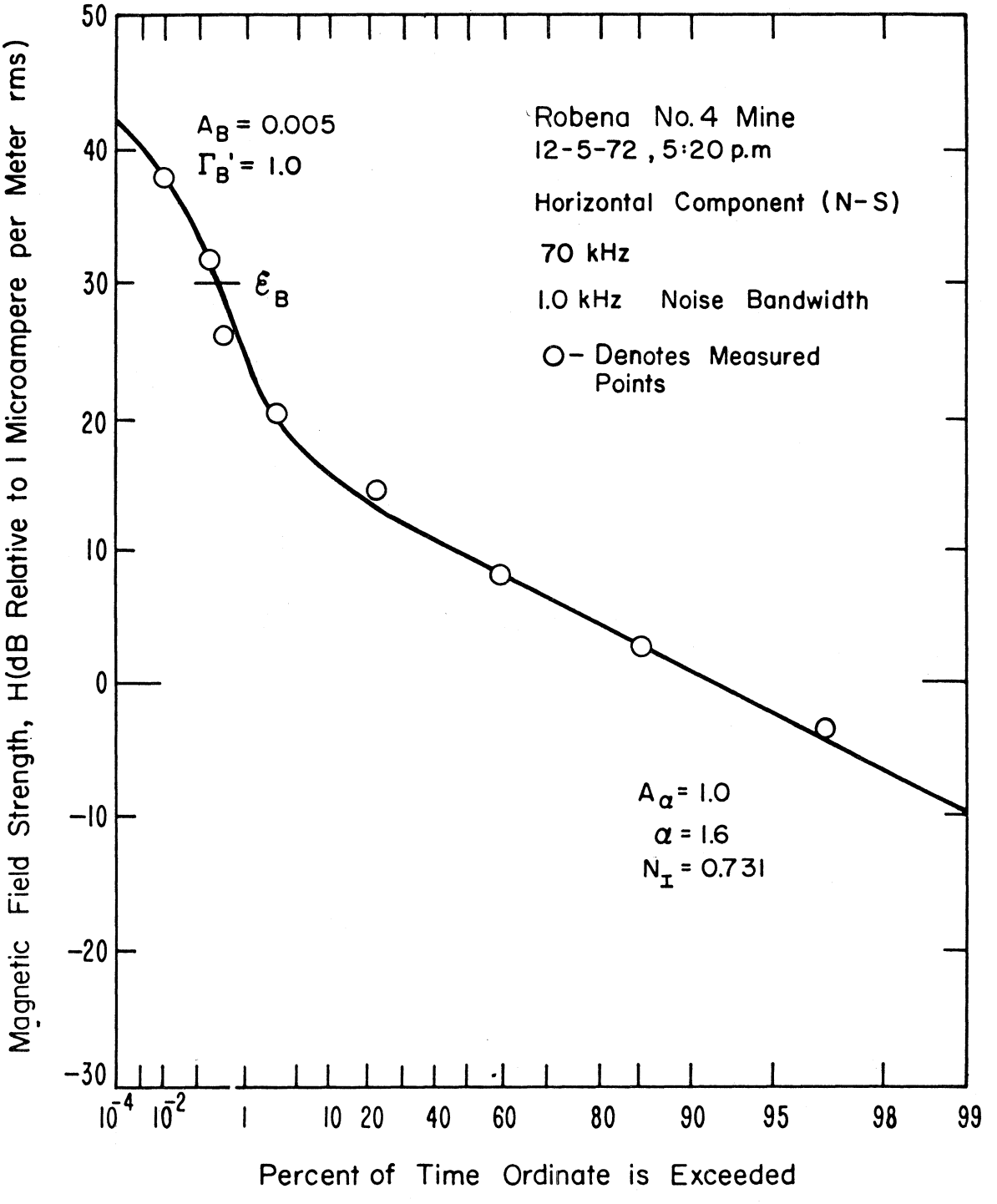

Figure 3.8. Comparison of measured envelope distribution, $P_1(\mathcal{E}>\mathcal{E}_0)_B$, of man-made interference (mining machinery noise) with the full Class B model. [Data from Bensema et al., Ref. 24, Fig. 67, p. 115.]

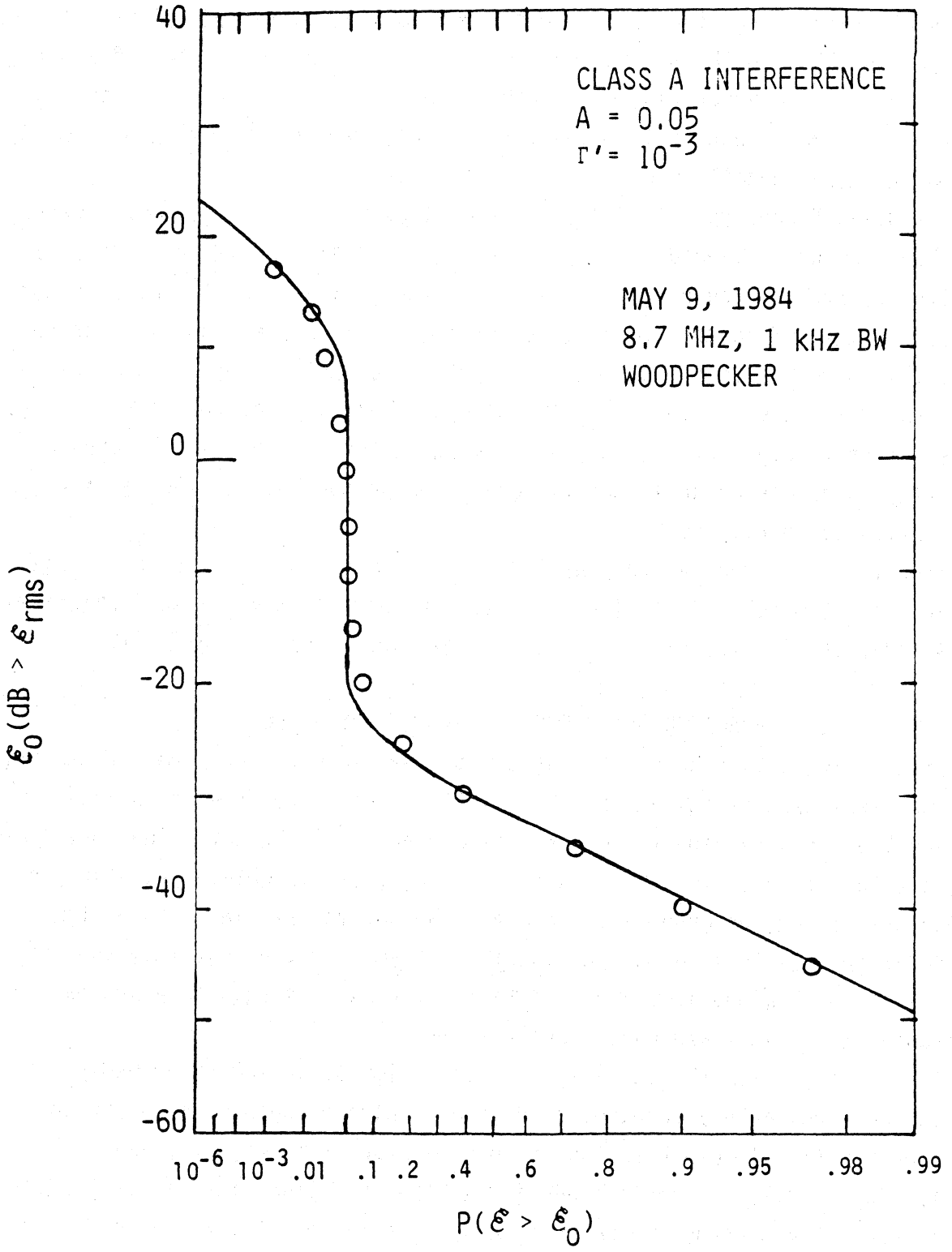

Figure 3.9. Comparison of measured envelope distribution with the Class A model. Interference is Soviet high power over-the-horizon radar (coherent pulses).

noise (Espeland and Spaulding [26]); and (iii) machinery noise in a coal mine (Bensema et al. [24]). Here the bend-over of the APD's is exhibited, along with the inflexion points, $\mathcal{E}_B$. In these cases we can obtain numerical estimates of all the six global parameters characteristic of each example of interference (see footnote on page 17), man-made or natural, by the methods briefly cited below in Section 4, and in more technical detail in [2,10].

Figures 3.1-3.9 are typical of Class A and Class B interference, man-made and natural. They are not intended to be exhaustive. Extensive additional APD data (mostly Class B) are available. [We have not included Class C APD data, although these appear in the references, because we limit our analysis and comparisons here to essentially "pure" Class A and Class B interference environment, some (analytical) conditions for which are examined in [7]. Also, the analysis of the Class C cases is not yet entirely complete.] Again, a striking feature of the present approach is its ability to handle an unlimited variety of noise sources, as long as the dominating Class is identified.

Finally, it is instructive to consolidate and compare some of the principal features of our EMI models. A concise comparison of some of the salient properties of Class A and Class B interference is accordingly presented in Table 3.1.

4. PARAMETER MEASUREMENTS FOR THE EMI MODELS

We present here only a summary treatment of the important problems of measuring the defining parameters of the various EMI models. There are three principal problems involved in obtaining the desired parameters: (1) to determine what Class the noise data corresponds to, viz. Class A, B, or C; (2) to obtain analytic procedures for specifying, or otherwise deducing, the parameters, in terms of the acquired data; and (3) to account, in actual practice, for the fact that the desired parameters must be obtained from finite data samples, and as such they are estimates, which are both statistical and consequently inexact.

For the first problem (1), empirical construction of an APD is probably the quickest and most reliable procedure for distinguishing between Class A and the other Classes; if the APD exhibits the sharp rise characteristic of Class A EMI inputs, cf. Figures 3.1, 3.2 above, then it is Class A. Otherwise, it is a Class B or Class C type. One procedure here is to assume it to be Class B, and estimate the parameters ($\mathcal{O}_{6B}$) according to the methods outlined below. If the resulting analytical APD is a "good-fit" (in the sense of (4.5) below), then we accept that our empirical data belong to a Class B ensemble; if not, then Class C is the governing model.

Table 3.1. Class A vs. Class B Interference

CLASS A	CLASS B
1. New models and results	"Classical" (30 yrs. old), but new approach; new results
2. 3 global parameters: "strictly canonical" model $\mathcal{P}_{3A} = \{A_A, \Gamma'_A, \Omega_{2A}\}$ [3 or more parameters: approx. canonical model] 4 global parameters: (:quasi-canonical") model; [49]	6 global parameters: $\mathcal{P}_{6B} = \{A_B, \Gamma'_B, \Omega_{2B}; \alpha, b_{1\alpha}, N_I\}$ $\mathcal{E}_B$: empirical parameter of approximation
3. All moments $\langle \mathcal{E}^\beta \rangle$, $0 \leq \beta$ exist	All moments $\langle \mathcal{E}^\beta \rangle$, $0 \leq \beta$ exist (3 parameters in practical approximation Section A.5.) (No moments exist.)
4. Insensitive to source distribution in space and propagation law for strictly canonical model; progressively sensitive, as one approaches quasi-canonical cases	Sensitive to source distribution and propagation law (α); quasi-canonical forms
5. Waveform in IF output: "gaps" in time [$P_1(\mathcal{E} = 0) > 0$]	Waveform in IF output: no "gaps" in time [$P_1(\mathcal{E} = 0) = 0$]
6. No gaps in time if Gaussian background $\left\{\begin{matrix}X \text{ Gauss P.D.} \\ \mathcal{E} \text{ Rayleigh P.D.}\end{matrix}\right\}$ as $A_A \to \infty$ and/or $\sigma^2 \to \infty$	No gaps in time ($\sigma_G^2 \geq 0$) $\left\{\begin{matrix}X \text{ Gauss P.D.} \\ \mathcal{E} \text{ Rayleigh P.D.}\end{matrix}\right\}$ as $A_\alpha, A_\beta) \to \infty$ and/or $\bar{\sigma}_G^2 \to \infty$
7. No Hall models exist [7,32].	Hall models for special values of α [7].

Having thus determined that the data belong to the appropriate Class, we then proceed to a detailed evaluation, along the lines outlined below.

4.1 A Summary of Procedures for Parameter Evaluation

As we have just noted above, once the Class of interference has been established, a key problem in the practical application of these general interference models is the determination of the basic parameter sets, $\mathcal{P}_{3A}$, $\mathcal{P}_{6B}$, etc. (and $\mathcal{P}_{8C}$). Here, we must distinguish between the infinite (or ideal) ensemble of data and the finite, limited-sample data sets available to us in practice.

First let us postulate the idealized condition of the infinite ensemble population. [In Section 4.3 we shall comment briefly on the effects of finite data ensembles.] We summarize here a number of procedures for evaluating the parameters of the models, from the data ensemble:

A. Procedures for Obtaining $\mathcal{P}_{3A}$:

The simplest, and often surprisingly accurate [O(10 percent, or less error)] procedure in the Class A cases is to use the following empirical observations derived from the APD and based on both computation and experiment. These are

$$A_A \doteq P_1 (= 10^{-b}), \text{ at the point where the sharp rise in } \mathcal{E}_0 \text{ versus } P_1 \text{ occurs (cf. Figure 4.1) for } A_A = O(0.5 \text{ or less}); \tag{4.1a}$$

and for the Gauss factor Γ'_A:

$$\Gamma'_A \doteq \text{the abscissa } (\mathcal{E}_0) \text{ value, at the point where } P_1 \text{ departs from its straight line (i.e., Rayleigh) behavior; for } \Gamma'_A \leq O(1/2). \tag{4.1b}$$

This result, coupled with $\langle E^2 \rangle_{xpt} \doteq 2\Omega_{2A}(1 + \Gamma'_A)$, where $\langle E^2 \rangle_{xpt}$ is obtained directly from the experimental data set {E}, then gives us directly

$$\Omega_{2A} \doteq \langle E^2 \rangle_{xpt}/2(1 + \Gamma'_A) > 0; \quad \Gamma'_A \leq O(1/2) \tag{4.1c}$$

for the estimated intensity of the non-Gaussian component. For example, for the Class A noise of Figure 4.1, we find that using the above procedure yields

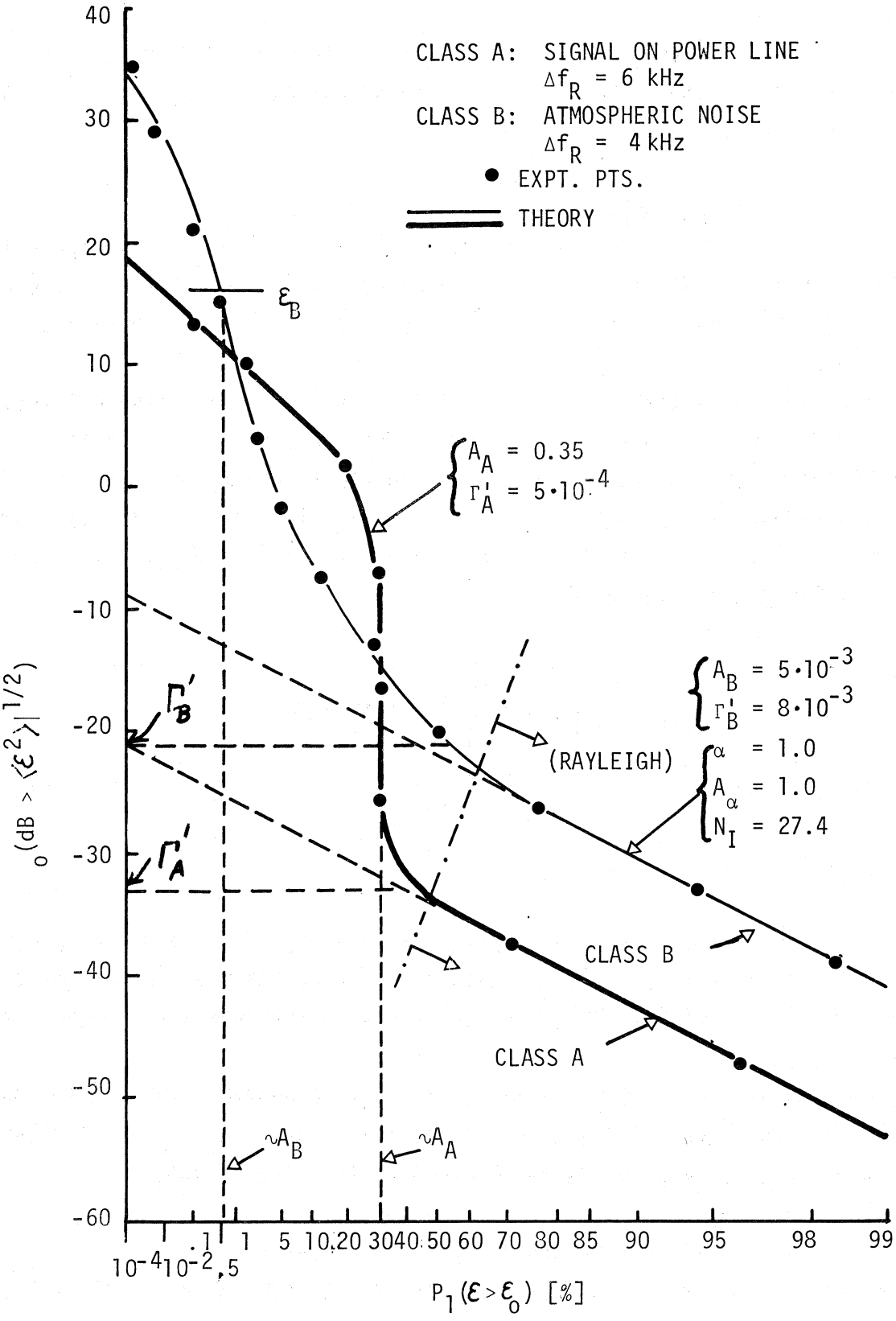

Figure 4.1. Measured and theoretical envelope probability distributions (APD's), $P_1(\mathcal{E}>\mathcal{E}_0)$, for Class A and B interference. Data from Figs. 3.2, 3.7. Class A here is a narrow-band signal on a power line; Class B is atmospheric noise.

$A_A \doteq 0.31$, $\Gamma'_A = -32.7$ (dB), versus $A_A = 0.35$, $\Gamma'_A = 5 \cdot 10^{-4} = -33.0$ (dB), of the original, more-refined parameter search determined by computer [1,7] (see also the discussion in [10], Section 3.1).

B. Procedures for Obtaining $\mathscr{P}_{6B}$

Similar approaches (except for explicit analytic forms like those of Appendix A) are available for Class B interference, but, of course, the procedures are necessarily more elaborate, since six basic global parameters, $\mathscr{P}_{6B}$, cf. Section 3.1-B, are now involved.

An empirical procedure like (4.1) above is also available for Class B noise, but is more elaborate and somewhat less accurate than for the Class A cases. A detailed discussion of the empirical procedure is given in the Appendix and [8,10].

A more exact procedure, using the empirical one for initiating the domain of a computer search, employs the following set of six relations for $\mathscr{P}_{6B}$, relating analytical and (ideal) experimental APD's:

$$P_{1\text{-}I} = P_{1\text{-}II} = (P_1)_{i\text{-}xpt}; \quad \frac{dP_{1\text{-}I}}{d\mathscr{E}_B} = \frac{dP_{1\text{-}II}}{d\mathscr{E}_B} \; ; \; @ \; \mathscr{E}_o = \mathscr{E}_B$$

$$\lim \mathscr{E}_o \to 0: \quad P_{1\text{-}I} - P_{1\text{-}II} = (P_1)_{i\text{-}xpt} \tag{4.2}$$

$$\left\langle E_B^2 \right\rangle = 2\Omega_{2B}(1 + \Gamma'_B) = \left\langle E_B^2 \right\rangle_{i\text{-}xpt} \; .$$

The $P_{1\text{-}I}, P_{1\text{-}II}$ are respectively the two approximating forms of the APD, P_1, needed adequately to describe the true P_1 of Appendix A-2. Here, the "bend-over" point $\mathscr{E}_B$, cf. Figure 4.1 plays a critical role. Other related procedures along these lines also are available [9,10].

For the more usual and practical 3-parameter Class B models described in the Appendix (A-5), one uses the procedures given in [10] to get α and A_α; Ω is determined from the measured energy in the noise process, as noted in A-5.

4.2 Parameter Evaluation via the EMI Scenario

When the elements of the EMI scenario are known (cf. Section 3.2), it is then possible to calculate a priori, as opposed to inferring from measurement, the model (global) parameters. Usually, in practice, we employ a combination of empirical and analytical methods, i.e., measurement and EMI scenario.

4.3 Some Practical Observations on Parameter Estimation in Finite Data Samples

In the analysis reviewed above, we have assumed (for the most part) that we have been dealing with idealized, infinite data populations so that the analytic and empirical statistics (moments, APD's, etc.) are equal (probability 1). The consequence of this is that the various parameter estimates are precise (probability 1).

Practically, however, we are always limited to the empirical situation of finite data samples. This limitation, in turn, ensures that the estimates are never precise. In fact, they are themselves random variables, with their various statistics. Thus, we may employ the sample moments

$$\left\langle E^{2k} \right\rangle_e = \frac{1}{n} \sum_{j=1}^{n} E_j^{2k} \qquad (k \geq 1) \tag{4.3}$$

for the empirical estimates of the moments $\left\langle E^{2k} \right\rangle$. Similarly, although the APD's and pdf's of the Appendix are analytic forms, it is always their experimental values, and parameters with which we deal, and which are consequently approximate, and random (over the ensemble).

Because of the finite sample sizes ($n < \infty$), and their basic statistical background, we must first establish the independence and homogeneity of the data samples [18], the former in order to apply the usual and convenient statistical methods of analyzing the data [19,20], and the latter, to ensure (in some reasonable, statistical fashion) that the data are generated by a common statistical mechanism; i.e., belong to the same parent population. This process we call <u>validation of the data</u> [18], which consists essentially of the following procedures in sequence.

(i) Test the sample data (E_n) for statistical independence [18]; e.g, of the E_j vis-à-vis the $E_k (j \neq k)$, $[j,k \in n]$.

(ii) Test the sample data for homogeneity; i.e., whether or not the $\{E_n\}$ belong to the same statistical population.

One such test for (i) is the "runs test" [18] and for (ii), nonparametric tests, like the Kolmogoroff-Smirnov [18], are particularly useful because of their small-sample, as well as large-sample capabilities.

Having validated the data as a first step in estimating the accuracy of the model parameter estimates, we next apply a combination of classical theory of sample statistics and "goodness-of-fit" tests [18-20] to the various scale and structure parameters, including the various moments and distributions of the sample moments (4.3), as well. In principle, this approach includes interval estimates, optimum estimators, etc., and associated average-risk measures [15].

There are, however, two major technical difficulties in attempting a direct application of standard sampling and risk theory. These are: (i) the nonindependent character of the direct (envelope) data ($\underline{E}_n$), which are the most convenient in practice, and (ii), the analytic complexity of the estimators themselves, which are for the most part highly implicit functions of the sample data (cf. Appendix A-4). Accordingly, an indirect approach is required [10].

"Goodness-of-Fit" Approach: Since we know the (approximate) analytic form of the APD's, $P_{1-A,B}$, we use a "goodness-of-fit" procedure, whereby we test how closely these analytic APD's fit the experimental APD data, when the experimental parameter estimates are used in the analytic forms [18].

This approach is appropriately natural here, for the aforementioned reasons. Again, Kolmogoroff-Smirnov tests [18], are particularly useful, especially for the small-sample conditions attending the data acquired at small probabilities; i.e., the "rare-events," when P_1 is $O(10^{-4}$ or less), typically, cf. Figure 4.1

Finally, we remark that the models are robust. Small changes in parameter values produce correspondingly small changes in the basic APD (or pdf). Robustness (or its lack) is a measure of parameter inaccuracies and their effects on the statistics. This feature is most easily studied computationally, by varying the parameter values. Various examples of this are shown in [7,8].

In addition to the question of robustness of the model is that of model stability. Does the underlying probabilistic mechanism remain invariant during the data-acquisition period (and during any period for which we may wish to employ the model)? This is a particularly pertinent question when long data acquisition periods are required, as they are often, for example, to obtain sufficient data to establish the "tails" or "rare-event" probability portions of the APD (and pdf). The "stability" problem is essentially the same problem of validating the data and involves appropriate tests of homogeneity.

At this point we emphasize that the data are basically (stationary) ensemble data, and as such apply at any instant. They also are independent of the time duration of the observation period, as long as the underlying statistical mechanism itself is stable. This means, also, that these models, with their associated parameters, are entirely appropriate for short, as well as long, observation times, as long as stability applies for the interval in question.

5. NON-GAUSSIAN EMI FIELDS

In many cases the physical size of a typical receiver's aperture (antenna) is only a small fraction of a wavelength, so that the received field is essentially uniform over the aperture. Beam-forming is, of course, still possible, and is often used to achieve directionality, when needed. However, there also are situations where the receiving aperture is large compared to the wavelength, and then, in addition to directionality, it is also possible to obtain additional gain in reception by taking advantage of the nonuniformity of the interference field, when the field of the desired signal is comparatively uniform over the receiving array. This advantage is accomplished by placing the array sensor elements in the noise field so that interelement correlations are small (or, ideally, zero).

One way to do this is to employ "sparse sampling"; i.e., placing the array elements sufficiently far apart compared to the correlation distance of the noise field. In many cases this may be uneconomical, because of the large arrays required, particularly when the wavelength is large, so that one is forced to examine the noise field in more detail, i.e., establish (at least its spatial correlation function and then separate sensor elements by distances equal to that producing the (first) zeros of the correlation function.

In order to accomplish the above, then we need to (i) construct a representation of the noise field; (ii) obtain its covariance, at least, and examine it for "zeros." This analysis has been carried out in [60]. For example, the covariance of these (Poisson) interference fields is shown to be

$$K_I(\underline{\Delta R},\tau) = A_{(A \text{ or } B)} \frac{C^2}{2} \left\langle R_o^{-2\gamma} \right\rangle \mathrm{Re}\left\{ M_a(\underline{\Delta R},\tau) D_1(\omega_o \tau) \left\langle e^{ik_o \underline{\Delta R}\cdot \hat{\underline{i}}_o} \right\rangle_{\hat{\underline{i}}_o} \hat{K}_o(\tau)_{in} \right\}, \quad (5.1)$$

where

$$\underline{\Delta R} = \underline{R}_2 - \underline{R}_1 \; ; \; \tau = t_2 - t_1 \quad ; \quad k_o = \omega_o / c_o = \lambda_o^{-1} \; ; \quad (5.2a)$$

$\hat{\underline{i}}_o$ = random unit vector, normal to wavefront of a typical incoming noise source ,

with C^2 = scaling constant; R_o = distance of typical source to receiver; $\hat{K}_{o\text{-}in}$ = narrow-band covariance of a typical source emission. Here $\underline{R}_1, \underline{R}_2$ are two (spatial) points in the noise field. The quantity M_a is a fading covariance, viz.:

$$M_a(\underline{\Delta R},\tau) = A_a(\underline{\Delta R},\tau)\, e^{-i\Phi_a(\underline{\Delta R},\tau)} \quad , \tag{5.2b}$$

while $D_1(\omega_o\tau)$ incorporates the effects of doppler spread, for each of the interfering signals, and is given by

$$D_1(\omega_o\tau) = e^{i\omega_o\tau} F_1(i\tau)_{\omega_d} \quad ; \quad F_1(i\tau)_{\omega_d} \equiv \left\langle e^{i\omega_o\tau} \right\rangle_{\omega_d} \quad . \tag{5.2c}$$

The quantity principally governing the random spatial character of the noise field is given by the directional spread factor

$$\left\langle e^{ik_o\underline{\Delta R}\cdot\hat{\underline{i}}_o} \right\rangle_{\hat{\underline{i}}_o} \equiv E_1(k_o\underline{\Delta R}|) \quad , \tag{5.2d}$$

which takes into account the random wavefront orientation of individual noise sources, as seen at $\underline{R}_1,\underline{R}_2$. Since

$$\hat{\underline{i}}_o = \hat{\underline{i}}_x \cos\phi_o \cos\theta_o + \hat{\underline{i}}_y \sin\phi_o \cos\theta_o + \hat{\underline{i}}_z \sin\theta_o \quad , \tag{5.3}$$

(θ_o,ϕ_o) here are random angles. For example, in some situations θ_o and ϕ_o may be uniformly distributed, e.g.,

$$w_1(\theta_o,\phi_o) = \frac{1}{\pi} \cdot \frac{1}{\pi} \quad ; \quad -\pi/2 \leq \theta_o \leq \pi/2 \quad ; \quad o \leq \phi_o \leq \pi \quad , \tag{5.4}$$

so that then, in the vertical direction,

$$E_1\big|_{vert} = J_o(k_o\Delta R) \quad ; \quad \Delta R = |\underline{\Delta R}| \quad , \tag{5.5a}$$

while in the horizontal direction,

$$E_1\big|_{hor} = J_o^2(k_o\Delta R/2) \quad . \tag{5.5b}$$

(The simplicity, or complexity, of E, will naturally depend on wavefront (angle) distribution and how the points $(\underline{R}_1,\underline{R}_2)$ of observation are chosen.)

Continuing our example, clearly, now, if the conditions leading to (5.5a,b) hold, we see that to obtain more reasonable spatial independence of the noise field samples (i.e., field sampled at indistinct spatial points), we should select, for a vertical array in the field,

$$k_o \Delta R = Z_1 [= \text{1st zero of } J_o = 2.4048],$$

or (5.6a)

$$\left.\frac{2\pi\Delta\ell_1}{\lambda_o}\right|_{vert} = Z_1 \; ; \; \therefore \; \left.\Delta\ell_1\right|_{vert} = \frac{Z_1\lambda_o}{2\pi} = 0.383\lambda_o \quad ,$$

while for a horizontal array, cf. (5.5b),

$$\left.\Delta\ell_1\right|_{hor} = \frac{Z_1\lambda_o}{\pi} = 2\left.\Delta\ell_1\right|_{vert} = 0.765\lambda_o \tag{5.6b}$$

here. Of course, spacings between nonadjacent pairs of sensors will not be uncorrelated, but they will be comparatively weakly correlated.

Finally, we remark again that, in a general way, the increased processing gains achievable by spatial sampling depends on the extent of the (spatial) nonuniformity of the noise field vis-à-vis that of the desired signal field. For a concise account of spatial sampling and its effect on weak-signal detection of desired signals in EMI environments, see [62].

6. SUMMARY REMARKS ON THE EMI MODELS: PROPERTIES AND APPLICATIONS

Let us now briefly comments on A, the principal properties of these new EMI models; and B, on the areas of major application. Remembering the basic definitions of Class A, B, and C noise, we begin with

A. The principal key properties: These are

(1) The Class A, B (and C) models are in a general way canonical, varying from "strictly canonical" to "quasi-canonical." They have analytic forms independent of the particular noise mechanisms involved (Section 3).

(2) The model parameters are similarly canonical. They are not ad hoc, but are physically constructed and derived.

(3) These models are analytically tractable and their parameters are (at least) indirectly determinable.

(4) The models are robust.

(5) The models also are typically in excellent accord with experiment, whatever the source, cf. Figures 3.1-3.9.

(6) These models apply to nearly all types of interference, provided only that the individual sources radiate independently, that the number of potentially emitting sources be large, and that the received interference following the (linear) front-end stages of the receiver is narrow-band (this condition can be removed [60]). Statistically, such models are compound Poisson processes.

(7) The (first-order) model statistics are canonical in the emitted waveforms: "impulsive" or "spikey" waveforms, long cw train, other, structured waveforms--all are handled similarly. (The term "impulsive interference" [13,14], accordingly, should not be limited to very-short-duration waveforms, but should include all types of emissions, subject only to the broad conditions above.)

It is also important in many applications to distinguish between "intelligent" and "nonintelligent" interference, as well as that of man-made and natural noise or interference [cf. Table 2.1]. Such distinctions often enable us to identify, eliminate, and/or reduce unwanted noise sources. At the least, one very important aim of any evaluation of the EMI environment is to identify its specific and general quantitative character. This brings us to a brief taxonomy of practical applications of these EMI models. We list

A. Evaluation of EMI Environments [12]:

(i) Spectrum occupancy;

(ii) Interference characteristics of urban and other environments (APD's, other lst-order statistics).

B. Spectrum Management [33-38]:

(i) Land-mobile telecommunications;

(ii) Electromagnetic compatibility evaluations (civilian and military);

(iii) Other telecommunication services [12].

C. Performance Measures in EMI Environments [7,13,14]:

(i) Detection - optimum and suboptimum [cf. Part II below];

(ii) Extraction - optimum and suboptimum estimation of desired signal parameters [72].

To all of the above these "canonical" EMI models appear essential for realistic quantitative treatment of the above classes of problems, which are particularly important, since the "real world" is a world primarily characterized by non-Gaussian interference and emissions.

PART II: THRESHOLD RECEIVER PERFORMANCE

With the establishment of effective analytic, canonical models of essentially the main classes of interference, which are in turn independent of the particular physical mechanisms generating the noise, we can proceed next to evaluate typical reception situations.

Thus, signal detection, as is well-known, is a form of test of statistical hypotheses, where the desired signal (and noise) is designated the alternative hypothesis (H_1), and the state "noise alone" is termed the null hypothesis (H_0). For optimal processing and performance, we use, of course, the well known standard techniques of Statistical Communication Theory (SCT, [15,16]). These designate the (generalized) likelihood ratio $\Lambda_n(\underline{X}|S)$ as the optimum processor in detection, and whose pdf's under the null (H_0) and alternative (H_1) hypotheses yield the associated error probabilities, or equivalently, the detection and false alarm probabilities as the application may require.

However, these error probabilities are particularly difficult to acquire explicitly, particularly for non-Gaussian noise, like the canonical Class A, B (and C) interference currently described here, and previously [1-11]. Accordingly, a variety of ingenious analytical and numerical procedures must be employed, in order to evaluate receiver performance and to make needed comparisons between optimum and suboptimum processors. This has been done in [13,14,21], mainly for Class A interference situations, but including, more recently, some Class B noise examples [21,59]. Some typical detection examples are discussed below and are illustrated in Figures 8.1-8.4. For details, see especially [14,59].

We consider first the usual EMI cases where the received noise field (cf. Section 5) is uniform over the receiving aperture, so that only temporal processing is in effect.

7. THRESHOLD DETECTION ALGORITHMS: RECEIVER STRUCTURE

In the critical limiting cases of threshold reception [16,17,59], ($S \to 0$, $n(= N) \to \infty$), it is possible to obtain canonical expressions for optimum detector processing, independent of the particular noise statistics and type of decision.

We shall confine our analytical illustrations here to the basic "on-off" detection situation for the most part, referring the reader to [14] (and Figure 8.1) for other telecommunications applications. Some typical algorithms (e.g., "structures"),

are given below in terms of a test statistic $g(x)$, or $g(x)^*$, respectively, for suboptimum and threshold optimum detection. These test statistics, g, g*, embody the functional, i.e., data processing structure of the receivers in question. We consider first, for independent noise data sampling:

7.1 "On-Off" Coherent Threshold Detection

Coherent reception means that the signal epoch is known at the receiver [cf., [15], Section 19.4.3]. Thus, we have

(1) LOBD: (= "locally optimum Bayes detector," cf. [17])

$$g(\underline{x})^* = \hat{B}(N, \langle s^2 \rangle)^*_{coh} + \sum_j^N g(x_j)^* \tag{7.1a}$$

$$\doteq \hat{B}(N, \langle s^2 \rangle)^*_{coh} - \sum_j^N \langle s_j \rangle \frac{d}{dx_j} \log w_1(x_j|H_o) ,$$

$$= \hat{B}^*_{coh} - \sum_j^N \langle s_j \rangle \ell(x_j) . \tag{7.1b}$$

where

$$\ell(x_j) \equiv \frac{d}{dx_j} \log w_1(x_j|H_o) , \tag{7.1c}$$

is usually a highly nonlinear operation on the $\{x_j\}$.

(2) Correlation Detection

$$g(\underline{x}) = \hat{B}(N, \langle s^2 \rangle)^*_{coh} + \sum_j^N g(x_j) = \hat{B}(N, \langle s^2 \rangle)^*_{coh} + \sum_j^N \langle s_j \rangle x_j . \tag{7.2}$$

The decision rule, e.g., reception process, is

$$g(x)^*, g(x) \begin{cases} < \log K: & \text{decide } H_o\text{: "no signal"} \\ \geq \log K: & \text{decide } H_1\text{: "signal present"} \end{cases} \tag{7.3}$$

The quantity $\hat{B}^*_{N\text{-coh}}$ is a "bias," which depends on sample size (N) and on the input signal-to-noise ratio, $\langle s^2 \rangle$. These biases are required to insure strong consistency as $N \to \infty$, $\langle s^2 \rangle \to 0$, i.e., the proper vanishing of the error probabilities for indefinitely large statistical samples. More important, these biases are needed to insure that the algorithm remains (threshold) optimum for the very large samples ($N >> 1$) required in weak-signal detection, i.e., retain their asymptotically optimum (AO) character, as $N \to \infty$ (see the remarks in Section 7.3 ff.) The threshold is K ($= \kappa/\mu = \kappa q/p$), where κ is a cost ratio, $p + q = 1$, $0 \leq p, q \leq 1$; (p,q) are a priori probabilities of the $H_{0,1}$ states, in the usual way.

Here we have postulated the simplest case of independent sampling, with $\underline{x} = \{x_j\}$ the (normalized) sampled data set on the observation interval $(0,T)$. Thus, N is equivalent to the conventional time-bandwidth product, or "processing gain" for the case of Gaussian noise backgrounds. The normalization of the data and desired signal is with respect to the total mean noise intensity $(\Omega_2 + \sigma_G^2)$; e.g.,

$\underline{x} = \underline{X}/(\Omega_2 + \sigma_G^2)^{1/2}$, $\underline{s} = \underline{S}/(\Omega_2 + \sigma_G^2)^{1/2}$, where $\underline{x}$ is the instantaneous amplitude data (3.4).

Figure 7.1 shows the structure of the optimum and suboptimum receivers (7.1), (7.2). We note, incidentally, that the (cross) correlation detector, g(x), (7.2), is, of course, optimum in Gaussian noise, and as we observe in Figures 8.1-8.3 (see also Section 9 ff.) can be very suboptimum (vis-à-vis g*) in non-Gaussian interference.

Similarly, for incoherent reception, where now signal epoch is unknown, we have:

7.2 "On-Off" Incoherent Threshold Detection

1. LOBD

$$g(x)^* = \hat{B}^*(N, \langle s^2 \rangle)_{inc} \cdot + \sum_{ij}^{N} [\ell(x_i)\ell(x_j) + \ell_i' \delta_{ij}] \langle s_i s_j \rangle \quad , \qquad (7.4a)$$

$$\text{with } \ell_i' = \frac{d}{dx_i} \ell(x_i) \ ,$$

2. Correlation Detection:

$$g(x) = \hat{B}(N, \langle s^2 \rangle)_{inc} + \sum_{ij}^{N} \langle x_i x_j \rangle s_i s_j \quad , \qquad (7.4b)$$

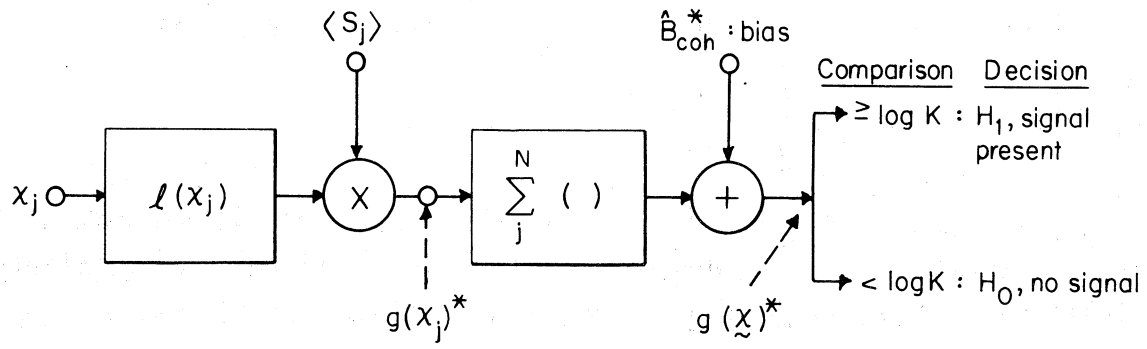

Figure 7.1a. LOBD locally optimum threshold receiver, Eq. (7.1), for "on-off" coherent signal detection in a general EMI environment.

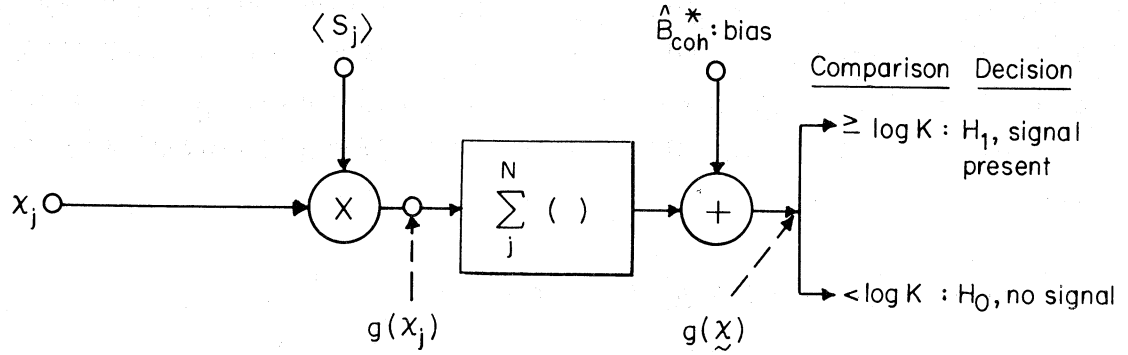

Figure 7.1b. (Cross-) correlation detectors, Eq. (7.2), for "on-off" coherent signal reception in a general EMI environment.

again where $\hat{B}^*$, $\hat{B}$ are "biases," which depend on sample size (N) and the input signal-to-noise ratio, $\langle s^2 \rangle$. Once more the decision rule is given by (7.3). In addition, it can be shown that a proper choice of bias for (7.4b) is

$$\hat{B}(N, \langle s^2 \rangle)_{inc} = \hat{B}^*_{inc} - \sum_j^N \langle s_j^2 \rangle , \tag{7.5}$$

where $\hat{B}^*_{(coh,inc)}$ is determined by the methods of [17,Section V], and more generally, as noted in Section 7.3. The auto-correlation detector, (7.4b), can similarly be very suboptimum O(30 dB, or more) vis-à-vis $g(x)^*$, (7.4a), as Figures 8.1 and 8.2 indicate, even though this correlation detector is optimum in Gaussian noise.

The structures of the above incoherent receivers, (7.4a,b), respectively, for optimum (threshold) and suboptimum detection, are considerably more complex than those for coherent reception, as can be seen from Figure 7.2.

7.3 Role of the Bias

In Sections 7.1 and 7.2 we have noted the presence of an appropriate bias term, $\hat{B}^*$, in both the coherent and incoherent threshold algorithms. This bias term is critical to effective threshold receiver performance, both to retain optimality as sample size N becomes very large (asymptotic optimality) and to maintain the LOB character of the algorithm under these circumstances.

The proper bias, $\hat{B}^*$, is found, technically, by taking the average over the $\{x_j\}$ with respect to the null hypothesis (H_o:noise alone), of the next order non-vanishing term in the expansions of the likelihood ratio, $\Lambda_N(\underline{x}|\theta)$, about $\theta = 0$. (Here $\theta \equiv$ input signal-to-noise ratio.) Thus, for threshold optimal algorithms, g^*, we have

$$\log \Lambda_N \doteq g(\underline{x})^* = \theta f_1(\underline{x}) + \frac{\theta^2}{2} f_a(\underline{x}) + O(\theta^3, \theta^4) , \tag{7.6}$$

and

$$g^*_{coh} = \theta f_1(\underline{x}) + \frac{\theta^2}{2} \langle f_2(\underline{x}) \rangle_{H_o} \; ; \cdots \hat{B}^*_{coh} = \frac{\theta^2}{2} \langle f_2(\underline{x}) \rangle_{H_o} , \tag{7.7}$$

in the coherent cases. For incoherent reception, we get

$$g^*_{inc} = \frac{\theta^2}{2} f_2(\underline{x}) + \langle O(\theta^4, \underline{x}) \rangle_{H_o} \; ; \; \hat{B}^*_{inc} = \langle O(\theta^4, \underline{x}) \rangle_{H_o} \tag{7.8}$$

(this last for suitably symmetric distributions). For independent noise samples (which can usually be achieved by sampling at suitable (time) intervals) f_1, f_2 are

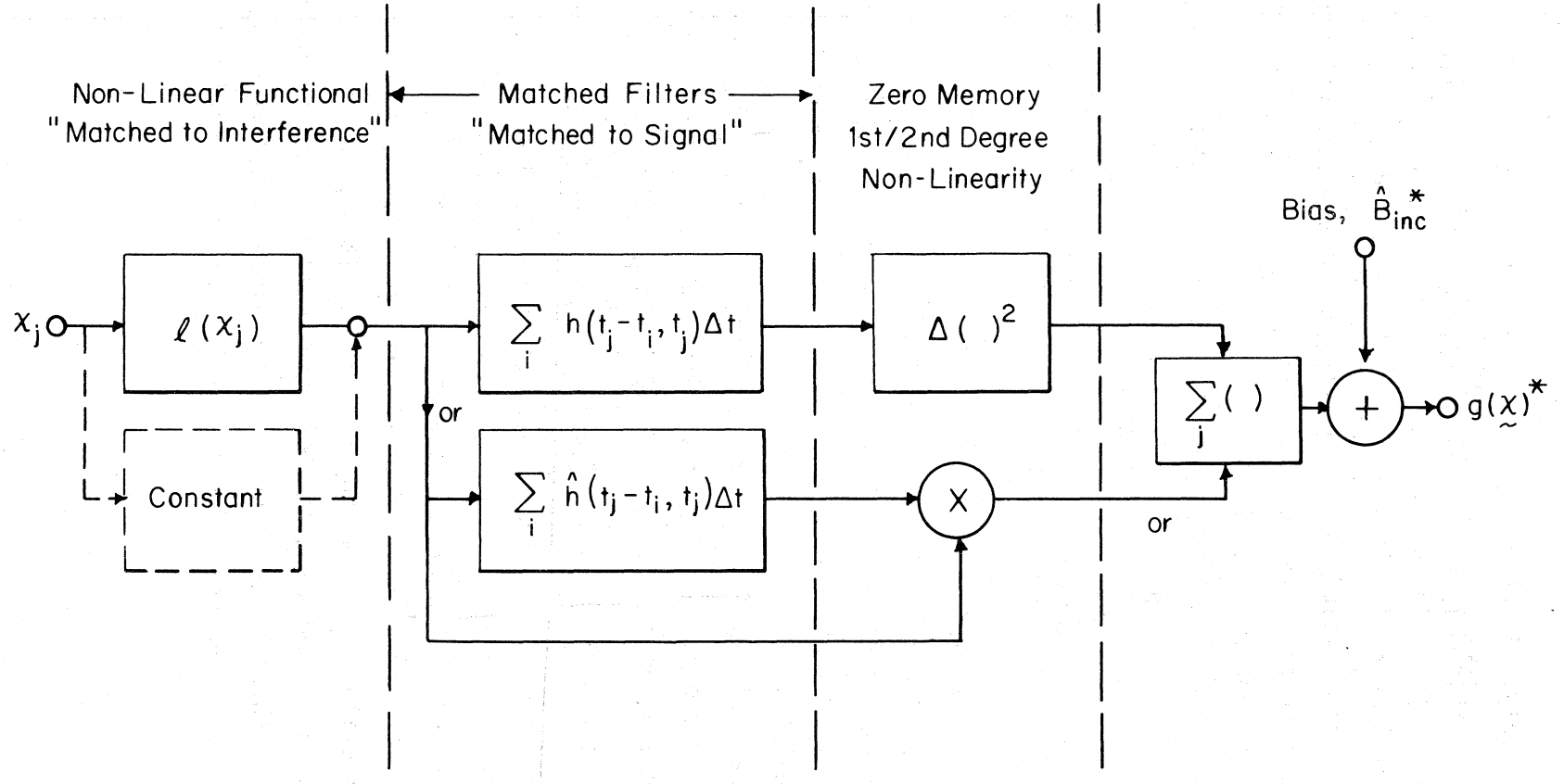

Figure 7.2. LOBD for optimum, "on-off" incoherent signal detection in a general EMI environment, Eq. (7.4a). (The dotted portion, ----, applies for the usually suboptimum auto-correlation detector, Eq. (6.4b). The matched filters here, h, $\hat{h}$, are functionals of the signal auto-correlation function $\langle s_i s_j \rangle$; (see pp. 84-87 of [16] for the explicit relations between h, $\hat{h}$ and $\langle s_i s_j \rangle$).)

functions of $w_1(x_j|H_o)$ only. In any case, given Λ_N (and $\therefore$ log Λ_N) one can accordingly determine the appropriate bias, by the procedures indicated above. In other words, with the proper bias, our algorithm, g*, retains its optimum structure and performance as the data sample ($N \to \infty$) becomes indefinitely large. The corollary of this is that g* has only a fixed number of terms here, whereas, without the correct bias, more and more terms in the expansion (7.6) would be needed to give the same performance, as N becomes larger.

It can further be shown [59,61] that the bias in these optimum threshold cases is equivalent to

$$\hat{B}^* = -\frac{1}{2}\,\mathrm{var}_{H_o}\, g_N^* = \frac{1}{2}\left[\left\langle g_N^{*2}\right\rangle_{H_o} - \left\langle g_N^*\right\rangle_{H_o}^2\right] \doteq -\frac{1}{2}\,\sigma_{ON}^{*\,2}\,, \qquad (7.9)$$

A sufficient condition for asymptotic optimality (AO) of g_N^* (or $N \to \infty$) is that g_N^* itself be asymptotically Gaussian, with means $\mp\,\sigma_{ON}^{*2}/2$ (respectively under H_o and H_1), and with variance σ_{ON}^{*2}, cf. Appendix 3,[59]. This means, here, that the error probabilities determined from the operations of the algorithm g_N^*, <u>vanish</u> for nonzero (but small) input signals, as $N \to \infty$.

This, in turn, leads to a definition of "smallness" of the (normalized) input signal (power), $\langle\theta^2\rangle$, where still $\langle\theta^2\rangle > 0$. Thus, the associated <u>threshold signal condition</u> is established by requiring that if σ_{IN}^{*2} ($\equiv \mathrm{var}_{H_1} g_N^*$) $= \sigma_{ON}^{*\,2} + F_N^*(\theta)$ is such that $\sigma_{IN}^{*\,2} \doteq \sigma_{ON}^{*\,2}$, or $|F_N^*| \ll \sigma_{ON}^{*\,2}$, then $|F_N^*(\theta)| \ll \sigma_{ON}^{*2}$ sets an <u>upper</u> limit on the small values θ can have, providing a least upper bound on the "weak" input signals for which (7.9) is effectively valid. We shall see practical examples of this in Section 9 following, in our discussion of robustness of the threshold detection algorithms. The point is, practically, that if the input signal is too large, the "threshold" optimum algorithm g_N^* is no longer optimum. It may, in fact, be quite suboptimum and exhibit rather pathological behavior, unless suitable modification of the algorithm is made at these larger signals. An example of highly suboptimum performance when the bias is incorrect (or omitted) is noted in Section IV of [61].

7.4 Adaptive and Matched Filtering

In Figure 7.3 we give a general schematic of optimum coherent or incoherent threshold detection in a changing, generally non-Gaussian EMI environment, in particular, to show where the "adaptive" portions of the reception process appear. For the threshold signals specifically considered here, the optimum detector is the appropriate LOBD, of which examples are given explicitly in Sections 7.1 and 7.2. [For general input signal levels, the optimum nonlinear processor analogous to the $\ell(x_i)$, $\ell'(x_i)$ combinations above (cf. Figure 7.1) is, of course, the generalized likelihood ratio $\Lambda(\underline{X}|S)$ noted above, (at the beginning of Part II), which, however, is not usually a simple matter to diagram or implement in practice.]

The central feature to observe here from equations (7.1) and (7.4), and in Figure 7.3, and generally, is that the LOBD g*, including the process of parameter estimation, is a nonlinear adaptive filter. [This is true even in Gauss interference, where g* reduces to $g \to g_{opt}$ in Gauss, and where the parameter to be estimated is $P_{1G} = \sigma_G^2$, the mean intensity of the noise.] The processor g* is adaptive because it must determine $w_1(x_1|H_0)$, and various functionals of w_1. For Class A and B noise this means specifically estimating the parameter sets $\mathcal{P}_{3A}$, $\mathcal{P}_{3B}$, or $\mathcal{P}_{6B}$. [Note again that since Class A,B noise essentially describe (almost) all real-world interference, and detection is always a fundamental reception process, this situation emphasizes, again, the role and importance of these canonical interference models.]

Operations more complex than (7.1,7.4) are required for more complex observation conditions, but the essential task for the processor remains to estimate the appropriate parameter set from the received data. In addition, since these interference models are robust (cf. Section 4 above), we may expect the processing algorithms (7.1,7.4) likewise to be robust: (numerical) changes in parameter estimates yield comparable changes in the various probabilities of decision.

First, the adaptive portion of the receiver (cf. Figure 7.3) identifies the noise class and then carries out the calculation of the needed parameter (estimates) for the particular interference class in which reception is taking place. These parameters are accordingly supplied to the detection processor (or algorithm), which operates as follows. We see from Figures 7.1 or 7.3 that, for coherent reception (cf. Section 7.1) the optimum (threshold) detector processor, or LOBD, in non-Gaussian interference performs two successive operations:

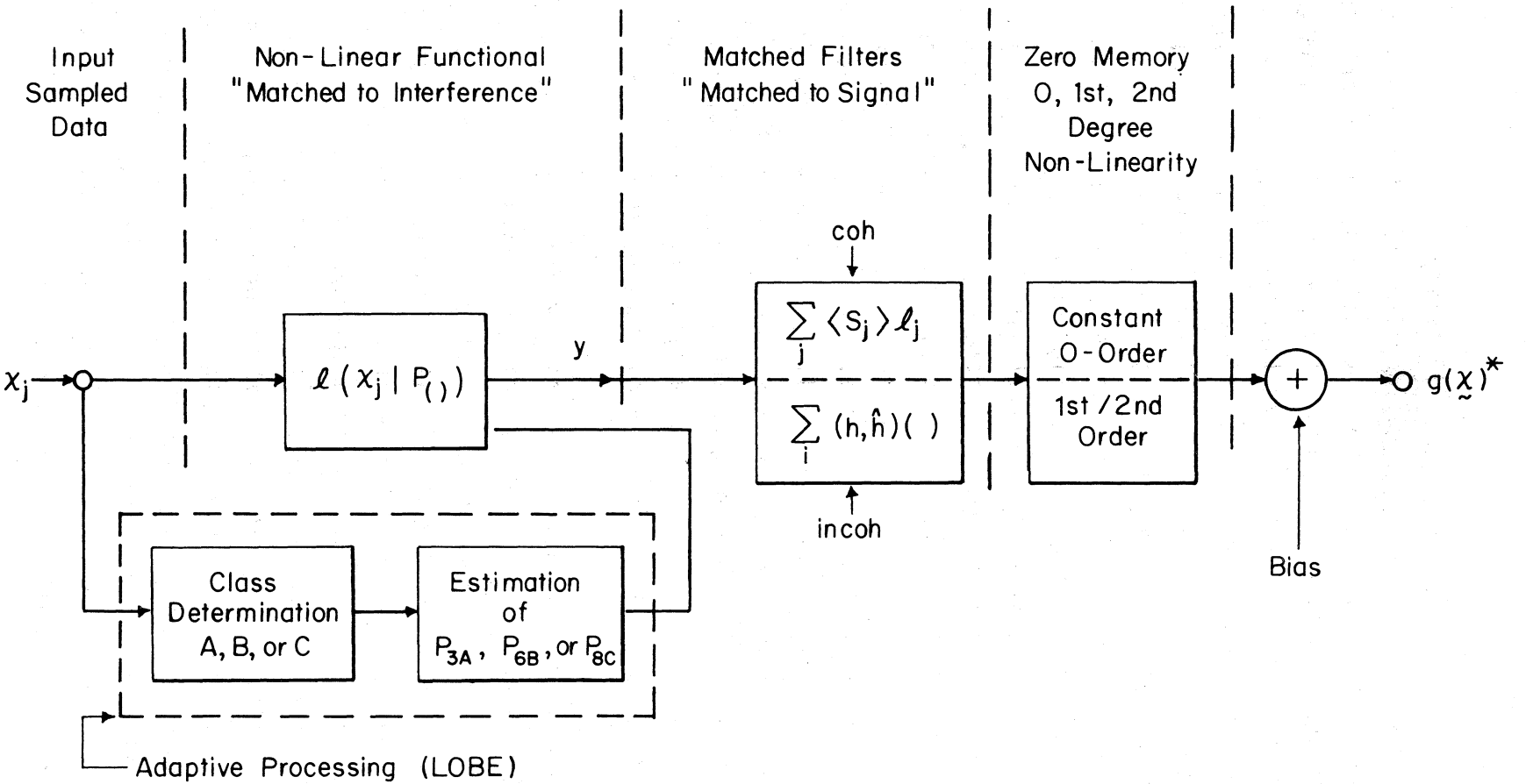

Figure 7.3. The full LOBD for optimum ("on-off") threshold detection of signals in a general EMI environment, for coherent/incoherent reception, and showing the adaptive portion of the optimum receiver [cf. Figs. 7.1a,b, 7.2].

1. It first "matches" the receiver to the noise, in that it adapts [i.e., determines the class of interference and then estimates the noise parameters ($\mathscr{P}_{3A}$, $\mathscr{P}_{3B}$, $\mathscr{P}_{6B}$, etc.)] to generate a non-Gaussian functional ($\ell(x_i)$, etc.) of the input data.

2. Next, the optimum processor then "matches" the signal to this new input $\ell(x_i)$, etc., to form an appropriate correlation detector for the non-Gaussian functional $\ell(x_i)$. These matched filters are always linear, and realizable (i.e., causal), cf. Figures 7.1 - 7.3.

For incoherent detection, there is an additional, third operation, which follows the "matching" process (Figure 7.2). This is usually a non-linear operation plus summation, where the nonlinearity may be a memoryless quadratic process, or a multiplication (e.g., a second-order, or finite-order, zero-memory nonlinearity). More complicated nonlinearities can arise in the cases of partially coherent reception, etc. [14,59].

It is essential to observe that Step 1, above, is not an attempt to "Gaussianize" the noise background. Rather, it is the key step by which the entire (here first-order) pdf of the real-world noise as it comes, is acknowledged, and employed, in the detection processing. Step 2 then incorporates the a priori signal characterstics, known at the receiver, in the classical "matching" sense [22], but now with respect to the nonlinearly processed data $\ell(x_i)$, etc.

If the interference is Gaussian, the first operation 1) is simply linear in the data (7.2,7.4) and we are left with the appropriate conventional matched filter [22,59,61], which is basically a second-moment processor, since (zero-mean) Gauss noise is completely specified by its correlation function. It is the strong non-Gaussian "tails" of the pdf and APD (Figures 3.1-3.9) that are critical in degrading receiver performance vis-à-vis that in Gauss noise, and that the nonlinear adaptive processor of Step 1 above takes into account optimally (for threshold signals).

7.5 Extensions: Composite and Binary Detection

The composite detector algorithm is formed from the usual threshold expansion of the likelihood ratio by including both the coherent terms $O(\theta)$ and the incoherent terms $O(\theta^2)$, again with suitable bias. Thus (cf. Section 6.5 of [59]), we have for the LOBD here, specifically,

$$g^*_{N\text{-comp}} = g^*_{N\text{-coh}} + g^*_{N\text{-inc}} - \log \mu \ , \tag{7.10a}$$

or, explicitly,

$$g^*_{N\text{-comp}} = \log \mu + \hat{B}^*_{N\text{-comp}} + \frac{1}{2} \sum_{ij}^{N} [-2\ell_i \langle \theta_i \rangle \ \delta_{ij} + (\ell_i \ell_j + \ell'_i \delta_{ij}) \langle \theta_i \theta_j \rangle] \ , \tag{7.10b}$$

where the composite bias is

$$\hat{B}_{N\text{-comp}} = \hat{B}_{N\text{-coh}} + \hat{B}^*_{N\text{-inc}} \ . \tag{7.10c}$$

The variance of $g^*_{N\text{-comp}}$ (under H_o) is similarly found to be

$$\sigma^{*2}_{ON\text{-comp}} = \sigma^{*2}_{ON\text{-comp}} + \sigma^{*2}_{ON\text{-inc}} \ . \tag{7.11}$$

It is $\sigma^{*2}_{ON\text{-comp}}$ that is now used to obtain performance measures, e.g., error probabilities, etc., in the usual way.

This composite LOBD (7.10a,b), also is an asymptotically optimum (threshold) algorithm, as required of its individual LOBD components. The practical importance of the composite detector is that it allows us to treat those (coherent) cases where $\bar{\theta} > o$, and include additional relevant information, contained in the "incoherent" term ($O(\theta^2)$). Thus, improvement in performance over the purely coherent cases is possible, and can sometimes be sizeable O(3-6 dB). The same is true for suboptimum composite detectors, constructed analogously to (7.10a,b). Again, in each case, the role of the proper bias is critical.

So far, we have considered only "on-off" detection situations. In many telecommunication applications "binary" signals are used, so that the receiver's decision problem is specified by

$$\begin{aligned} H_1 &: S_1 + N : \quad \text{decide } S_1 \text{ in noise, if } \log \Lambda^{(12)} < \log K_{12} \\ H_2 &: S_2 + N : \quad \text{decide } S_2 \text{ in noise, if } \log \Lambda^{(12)} \geq \log K_{12} \end{aligned} \tag{7.12}$$

Here, optimum threshold algorithms are formed, as before, now from the expansion of

$$\log \Lambda_N^{(12)} = \log \Lambda_N^{(2)} - \log \Lambda_N^{(1)} \tag{7.13}$$

where $\Lambda_N^{(1)} = \Lambda_N^{(1)}(\underline{x}|S_1)$, etc. Thus, we have

$$g_N^{(21)*} = g_N^{(2)*} - g_N^{(1)*} \text{ , etc.,} \tag{7.14}$$

and $g_N^{(21)*} = \text{var}_{H_o} g_N^{(21)*}$, etc., with analogous expression for suboptimum detectors. The use of binary signals allows us to achieve "symmetric" channel operation, usually, which simplifies the problem of the proper bias; e.g., $\hat{B}^*_{N-(12)} = 0$, usually, and increases the useful signal energy transmitted, with a consequent improvement in performance, as well as potentionally increasing the information rate for the same bandwidth.

8. OPTIMUM AND SUBOPTIMUM PERFORMANCE

Applying the general approaches of [14,17], we can obtain upper (i.e., conservative) bounds on detector performance for all signal levels, but this procedure must ultimately be done numerically.

In the limiting threshold situations, however, direct analytic approximations are possible, since the test statistic g, and (LOBD) g*, are asymptotically normally distributed [17] (by the Central Limit Theorem). Moreover, with the proper bias [cf., Section 7.3], g* remains asymptotically optimum (AO) as $N \to \infty$, as required for very small input signals. For these cases we accordingly find, for the "on-off" types of signal reception, where false alarm probabilities ($P_F = \alpha_o q$) are preset, that the probability of correct signal detection is (when $\hat{\sigma}_o \doteq \hat{\sigma}_1$) (8.2),

$$P_D = pp_D = p(1 - \beta)$$

$$\simeq \frac{p}{2}\left\{1 + \theta\left[-\theta^{-1}(1 - 2\alpha_o) + \frac{\langle h\rangle_1 - \langle h\rangle_o}{\hat{\sigma}_o\sqrt{2}}\right]\right\} \text{ ;} \tag{8.1a}$$

$$\alpha_o \simeq \frac{1}{2}\left\{1 - \theta\left[\frac{\log K - \langle h\rangle_o}{\hat{\sigma}_o\sqrt{2}}\right]\right\} \text{ ,} \tag{8.1b}$$

where h = g, or g* (7.1,7.4), for example. In particular, we have

$$\langle h^k \rangle_{0,1} \equiv \int_{-\infty}^{\infty} h(\underline{x})^k w_N(\underline{x}\, H_{0,1}) \underline{dx} \quad (k \geq 1)$$

$$\hat{\sigma}^2_{01} \equiv \langle h^2 \rangle_{0,1} - \langle h \rangle^2_{0,1} \quad , \quad (h = g, g^*) \; , \tag{8.2a}$$

and here, for the assumed independent sampling,

$$w_N(\underline{x}\,|H_{0,1}) = \prod_{j=1}^{N} w_1(x_j|H_{0,1}) \; . \tag{8.2b}$$

In addition, since signal and noise are postulated to be additive, in the above, we have $w_1(x_j|H_1) = w_1(x_j - s_j|H_0)$. The quantity θ is the familiar error function:

$$\theta(x) = \frac{2}{\sqrt{\pi}} \int_0^x \exp(-t^2)dt \; . \tag{8.3}$$

On the other hand, for many common communication applications, where the channel weightings are usually equal, e.g., $\kappa = 1$, $\mu = p/q = 1$, e.g., $K = 1$, so that we have the Ideal Observer situation in which α_0 and β are jointly adjusted, we find that the probability of error, P_e, is in these threshold cases,

$$P_e \cong \frac{1}{2} \left\{ 1 - \theta \left[\frac{\langle h \rangle_1 - \langle h \rangle_0}{2\hat{\sigma}_0 \sqrt{2}} \right] \right\} . \tag{8.4}$$

In particular, it can be shown [59] that

$$\langle h \rangle_1 - \langle h \rangle_0 = \sigma_0^{(*)2} = \mathrm{var}_{H_0}\, g^{(*)} = \mathrm{var}_{H_0}\, h \quad , \tag{8.5}$$

so that, in more familiar form we have for (8.1) and (8.4)

$$P_D^{(*)} \cong \frac{p}{2} \{ 1 + \theta [\frac{\sigma_0^*}{\sqrt{2}} - \theta^{-1} (1 - 2\alpha_0)] \} \tag{8.6a}$$

$$P_e^{(*)} = 1/2 \left\{ 1 - \theta \left[\frac{\sigma_o^{(*)}}{2\sqrt{2}} \right] \right\} \tag{8.6b}$$

Various canonical performance curves for $P_D^{(*)}$ and $P_e^{(*)}$ are given in Figures 1 and 2 of [61] and in Section 7 of [59].

8.1 Performance Examples and Comparisons

We shall confine our explicit examples here to coherent cases, both optimum and suboptimum. (Various examples of the performance of incoherent detectors are discussed and evaluated in [13,16,59,61].) There is no loss in qualitative generality in so doing, since the relative differences between the optimum and suboptimum receivers remain essentially invariant of whether reception is coherent or incoherent, for most cases (cf. Figure 8.1).

Accordingly, for the "on-off" coherent cases (7.1,7.2), we obtain explicitly

Optimum Detection:

$$(\langle g^* \rangle_1 - \langle g^* \rangle_o)/\hat{\sigma}_o^* \sqrt{2} \doteq \sqrt{\langle s^2 \rangle NL^{(2)}/2} \equiv \sqrt{\phi^*/2} \quad , \tag{8.7a}$$

$$(\langle g \rangle_1 - \langle g \rangle_o)/\hat{\sigma}_o \sqrt{2} \doteq \sqrt{\langle s^2 \rangle NL^{(2)}/2} \cdot \sqrt{\langle -x\ell(x) \rangle / L^{(2)}} \tag{8.7b}$$

$$\equiv (\sqrt{\phi^*/2})(\sqrt{\phi_{c|o}}) \quad ,$$

which defines $\phi^* \equiv \langle s^2 \rangle NL^{(2)}$ and $\phi_{c|o} \equiv \langle -x\ell(x) \rangle / L^{(2)} = 1/L^{(2)}$, respectively, where,

$$\langle x\ell(x) \rangle \equiv \int_{-\infty}^{\infty} x \frac{d}{dx} \log w_1(x|H_o)dx = -1$$

$$L^{(2)} \equiv \int_{-\infty}^{\infty} \ell(x)^2 w_1(x|H_o)dx \quad : \quad (S^2 L^{(2)} << 1, \quad N >> 1) \; . \tag{8.8}$$

The quantity ϕ^* is defined as the average output signal-to-noise ratio, or $(S/N)_{in}^2$ times the equivalent time-bandwidth product (or threshold processing gain) for the optimum detector (7.1), and the particular noise statistics involved. An extension

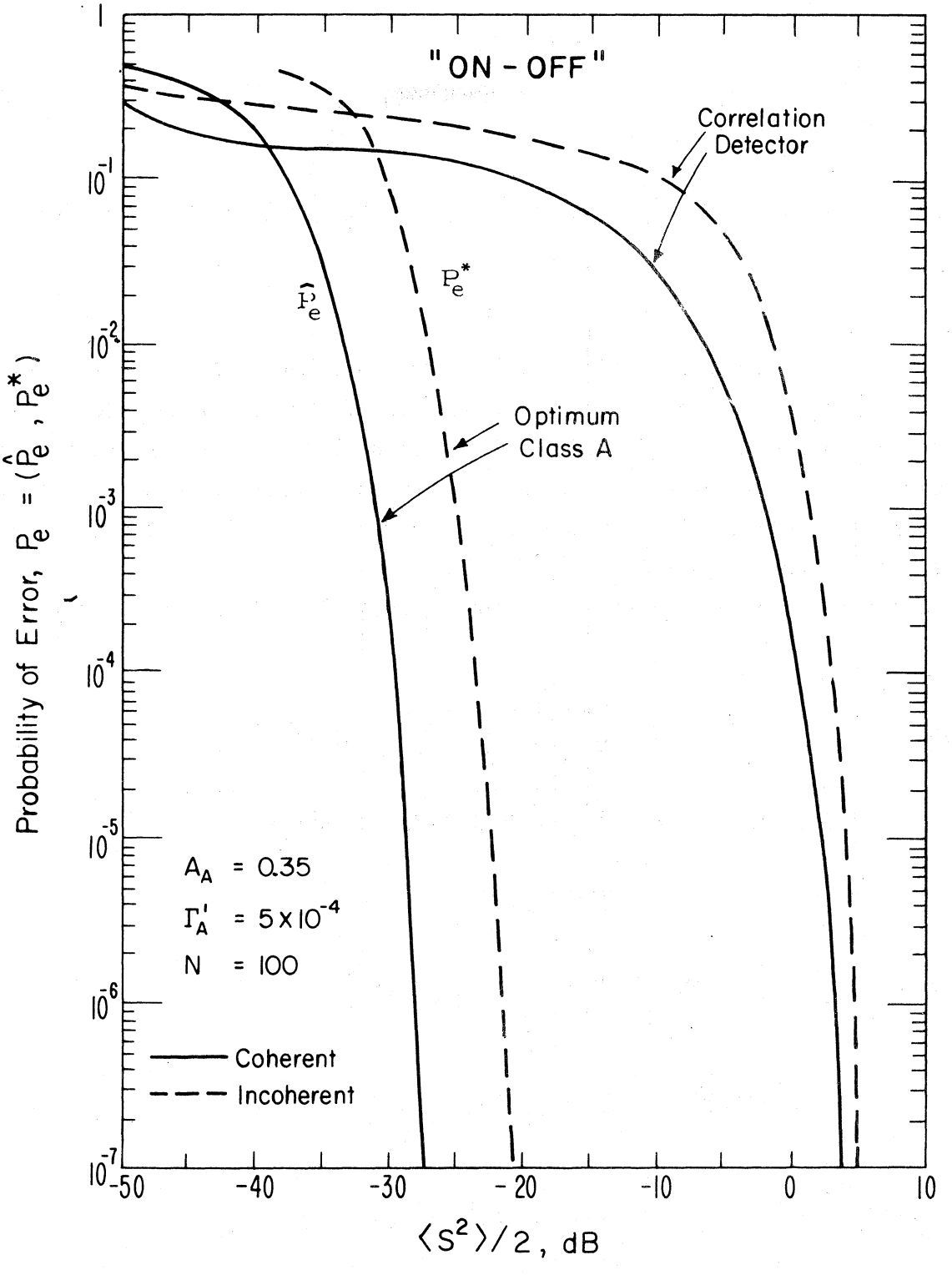

Fig. 8.1. Performance of optimum "on-off" detectors for coherent and incoherent (CW) signal reception (K=1) in Class A noise ($A_A = 0.35$, $\Gamma_A' = 5 \cdot 10^{-4}$), compared with corresponding (cross) correlation and (auto-) correlation detectors (optimum in gauss noise). (P_e, $\hat{P}_e$, P_e^* = probability of error, upper bound on probability of error, estimate of probability error; from Ref. 14, Part II, Figures 5 and 8).

of this concept to include specific minimum detectable signals and processing gains, on a systematic basis, for both optimum and suboptimum threshold detectors is given in [59,61,67].

The functional $\phi_{c|o}$ is the degradation measure of the suboptimum (other than in Gauss) cross-correlation detector (7.2). (For the particular parameters of Figures 8.1 and 8.2, we find that $\phi_{c|o} \tilde{=}$ -30 dB, as can be seen from these figures.) In general, $0 \leq \phi_{c|o} \leq 1$, and $\phi_{c|o}$ is unity only when the interference reduces to Gaussian noise.

Figure 8.1 is based on [14], while Figure 8.2 is calculated from (7.1a), and Figure 8.3 is taken from Spaulding [21]; Figures 8.1 and 8.2 are for (both strictly and quasi-canonical) Class A noise, whereas Figure 8.3 represents detection in Class B interference. In all instances, we observe the very considerable degradation, O(30 dB), of the conventional correlation detector vis-à-vis the corresponding optimum processor. Furthermore, as the interference becomes more non-Gaussian (i.e., smaller A, Γ'), we may expect even larger degradation of conventional processing, and consequently increased gains using the required optimum algorithms.

8.2 Practical Conditions for Significant Improvement Over Conventional Receivers

To appreciate fully why such optimum (threshold) detection algorithms as g*, (7.1), (7.4), etc. are so effective (cf. Figures 8.1-8.3) vis-à-vis the conventional optimum processors, e.g., "matched filters" or correlation detectors, of the earlier, more classical treatments (and most current engineering practice!), we must note the following.

In order for there to be significant improvement in the LOBD detection performance over conventional matched filter (or correlator) systems, which are optimal in Gauss noise, i.e., to justify the computational complexities of the former, adaptive nonlinear receivers, the following four conditions must be fulfilled.

The interference must be moderately to strongly non-Gaussian; e.g.,

1. $A_{(A,B)} <$ O(1,2 or less): i.e., a small overlap index, for "structured" noise:
2. $\Gamma'_{(A,B)} <$ O(1/2 or less): small Gaussian factor;
3. $\Omega_{2A,B} > \langle s^2 \rangle$: there must be a detection (or reception) problem, e.g., the desired signal is "weak" vis-à-vis the noise, at the receiver input;

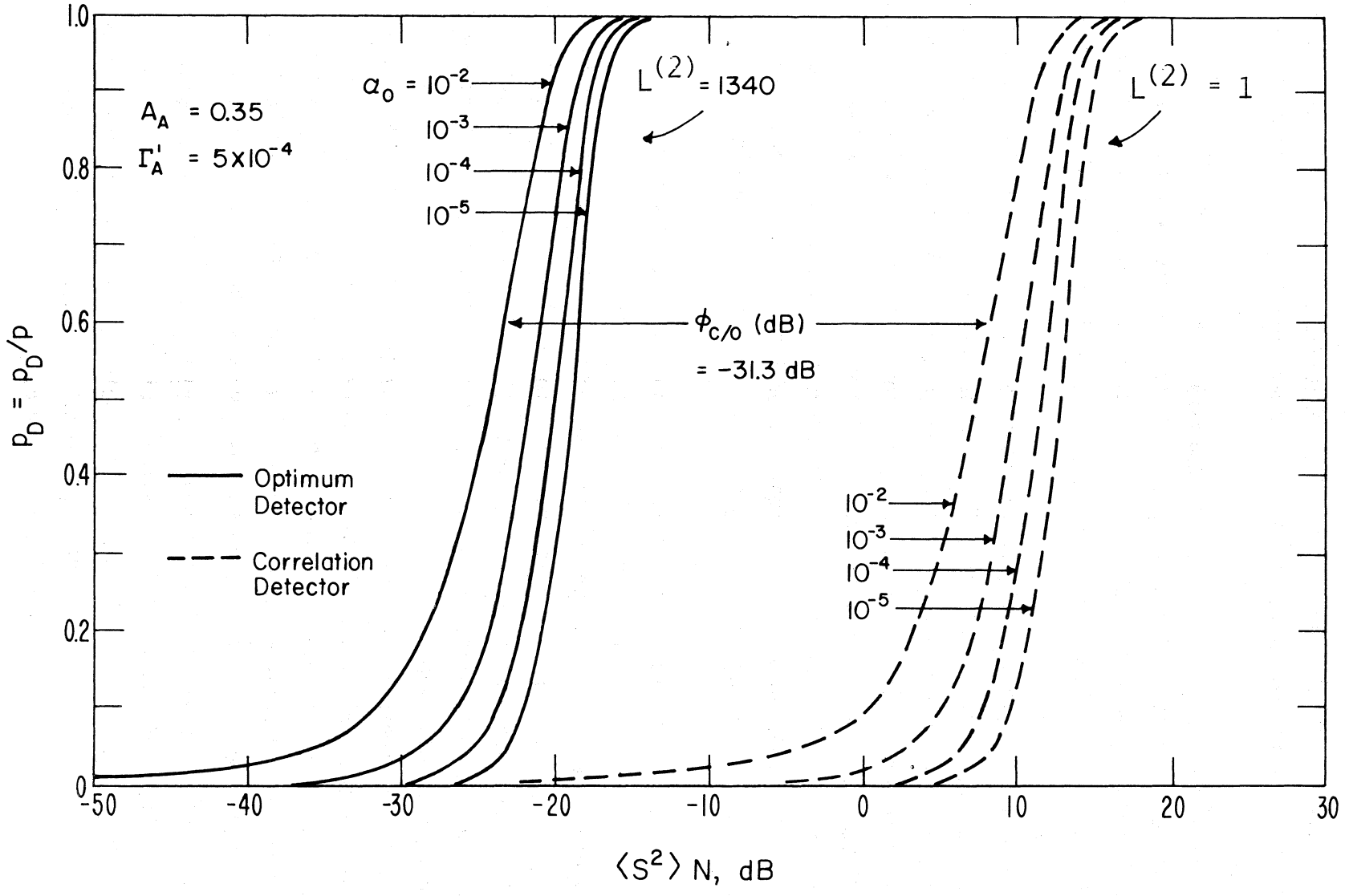

Figure 8.2. (Conditional) probability of signal detection p_D (=p_D/p), (8.1), (8.7), (8.8), for coherent threshold detection with fixed false alarm probability α_o (=p_F), for optimum and cross correlation receivers in Class A noise (A_A = 0.35, Γ'_A = $5 \cdot 10^{-4}$).

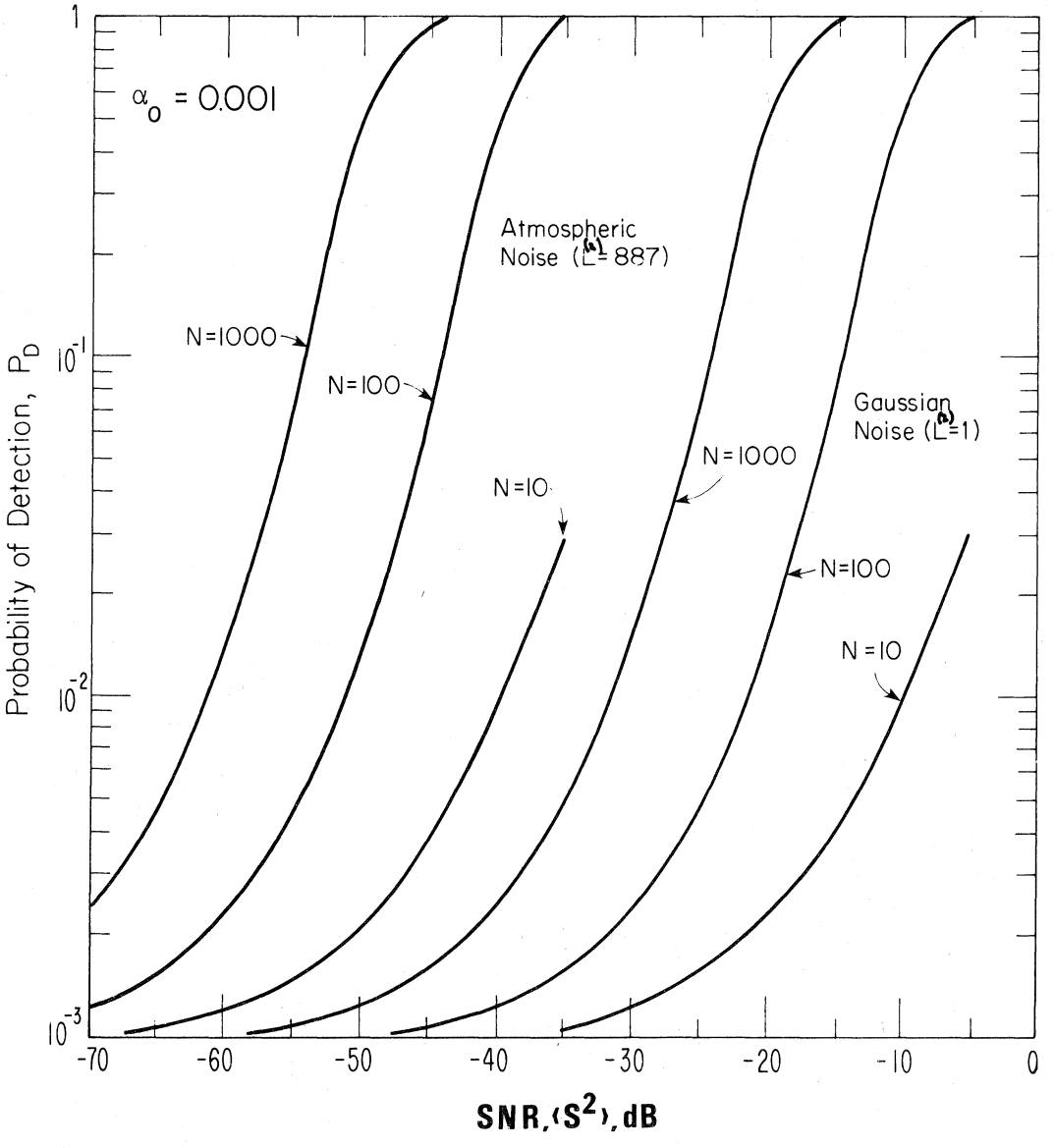

Figure 8.3. (Conditional) probability of detection versus input SNR for a probability of false alarm α_o = 0.001. Coherent "on-off" detection, Class B noise (A_α = 1.0, α = 1.2, Ω = $7.94 \cdot 10^{-4}$) ($\mathcal{E}_o^2 = \mathcal{E}_o^2/\Omega$).

and

4. $N >> 1$: the time-bandwidth product (e.g., number of independent noise data samples) should be reasonably large, e.g., O(20,30 or more). Thus, equivalently, the longer the observation time (under stable conditions), the smaller the input signal that can be detected.

It is generally found that the conditions 1-4 are obeyed for real-world interference processes so that the large predicted performance gains vis-à-vis conventional processing may be expected.

The large improvements over conventional detectors, optimized against Gauss noise, show how seriously "mismatched" such detectors can be in the highly non-Gaussian EMI environments in which we customarily operate. However, simple suboptimum detectors, such as those employing limiters, can offer considerable improvement against this non-Gaussian noise and can be "close" to the optimum detector. Thus, the optimum detector characteristic may be well approximated (in performance) by comparatively simple nonlinearities, which are then the economical ones to use. An extended treatment of suboptimum vs. optimum detectors is given in [59]; see also Section 9 ff.

9. ROBUSTNESS AND SIMULATION RESULTS FOR CLASS A AND CLASS B NOISE

The performance results above are the results expected for the desired signal level sufficiently small (but >0) and for N, the number of independent samples $\to\infty$. ("Sufficiently small" is precisely defined in Middleton and Spaulding [59].) In actual cases, the LOBD derived detectors will probably be used in situations where the signal level is larger than "sufficiently small" and/or N is not particularly large. In this section, then, we present performance results of actual LOBD detectors (simulated) to display their actual performance, in order to compare with the theoretical limiting performance.

In order to construct an LOBD, we need to determine the appropriate model parameters (Class A or B), and we also need to know to what degree of accuracy we need to do this estimation. That is, the robustness of a given detector is required knowledge. Here, we will also demonstrate that the LOBD can be quite robust.

9.1 Robustness

Consider binary CPSK. Our problem is to decide optimally between the two hypotheses:

$$H_1 : X(t) = S_1(t) + Z(t) \qquad 0 \leq t < T$$

$$H_2 : X(t) = S_2(t) + Z(t) \qquad 0 \leq t < T \,. \tag{9.1}$$

In (9.1), $X(t)$ is our received waveform in detection time T and this waveform contains either the completely known signal $S_1(t)$ plus the noise $Z(t)$ or the completely known, equi-probable, signal $S_2(t)$ plus $Z(t)$. The LOBD receiver for this case (9.1) is shown in Figure 9.1, where S_{1i} and S_{2i} are samples of the signals $S_1(t)$ and $S_2(t)$, and $\ell(X_i)$ is the standard LOBD nonlinearity, i.e.,

$$\ell(x_i) = - \frac{d}{dX_i} \ell n \; w_1(x_i|H_1) \tag{9.2}$$

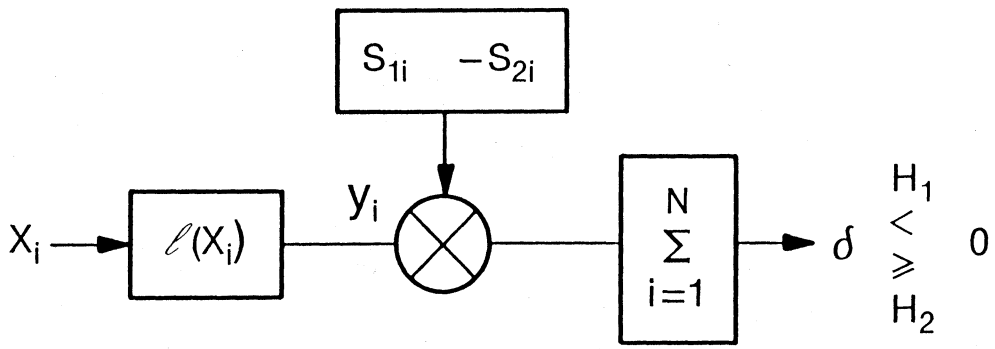

Figure 9.1. LOBD for binary symmetric purely coherent signals.

For binary symmetric signals,

$$S_1(t) = \sqrt{2S}\cos(\omega_o t) \qquad 0 \leq t < T$$

and

$$S_2(t) = -\sqrt{2S}\cos(\omega_o t) \qquad 0 \leq t < T \quad , \tag{9.3}$$

the standard LOBD analysis gives the performance (probability of error, P_e) estimate as

$$P_e \overset{\sim}{=} 1/2 \; \text{erfc} \; (\sqrt{SNL^{(2)}/2}) \; , \tag{9.4}$$

where S is the signal power (9.2) and $L^{(2)}$ is the "performance improvement factor" (improvement over the linear receiver) given, as before, by

$$L^{(2)} = \int_{-\infty}^{\infty} \frac{[w_1'(z)]^2}{w_1(z)}\, dz \ . \tag{9.5}$$

In order for (9.4) to be valid, we must have $SL^{(2)} << 1$. [Note that if the noise process has been normalized so that the noise power = 1, then S is also the **signal-to-noise ratio.**] Also note that (9.4) is the result (now precise) that is obtained for the linear receiver in Gaussian noise ($L^{(2)} = 1$). This is the consequence of using the Central Limit Theorem argument in the LOBD analysis, which requires S to be "small" and N large.

Suppose now that we have a LOBD detector based on the assumption that our interference is $\hat{w}_1(z)$, and the actual interference is $w_1(z)$. We can carry out the LOBD analysis using $\hat{w}_1$ where appropriate to determine the effects of "mismatching" the interference, or we can use this to determine the sensitivity of the LOBD performance to changing interference (robustness). This approach also gives results that can be easily used to evaluate the small signal performance of any ad hoc nonlinearity. The result is that $L^{(2)}$ is replaced by a parameter L_{eff}, for "L effective," where, $L_{eff} = L_1^2/L_2$,

$$L_1 = \int_{-\infty}^{\infty} \left[\frac{\hat{w}_Z'(z)}{\hat{w}_Z(z)}\right] w_1'(z)\, dz \ , \qquad \text{and} \tag{9.6}$$

$$L_2 = \int_{-\infty}^{\infty} \left[\frac{\hat{w}_1'(z)}{\hat{w}_1(z)}\right]^2 w_1(z)\, dz \ . \tag{9.7}$$

If $\hat{w}_1(z) = w_1(z)$, then $L_1 = L_2 = L^{(2)} = L_{eff}$.

We can quickly compute the performance of any arbitrary nonlinearity, $\ell(x)$, used in the detector of Figure 9.1. For example, for the hard-limiter, $\ell(x) = 1$, if $x \geq 0$ and $\ell(x) = -1$, if $x < 0$. We can solve the resulting expression

$$\ell(x) = -\frac{d}{dx} \ell n\, \hat{w}_1(x) \ , \tag{9.8}$$

to obtain the corresponding $\hat{w}_1(z)$, to compute L_{eff} via (9.6) and (9.7) above. For the hard-limiter case, we obtain

$$L_{eff} = 4\, w_1^2(0) \tag{9.9}$$

where w_1 is the actual interference pdf. (For a different, and much more involved derivation of this result, see [68], section 4.2.) Performance is given by (9.4), so that the degradation caused by using the hard-limiter is simply the difference between $L^{(2)}$ for our actual interference (LOBD performance factor) and L_{eff} for the hard-limiter (or similarly, for any other nonlinearity).

Figures 9.2 and 9.3 give results for the hard-limiter performance compared to the LOBD performance. The degradation obtained by using a hard limiter in place of the LOBD nonlinearity is, as noted above, given by the difference between L_{eff} (9.9) and $L^{(2)}$ (9.5). The hard-limiter is the simplest nonparametric detector and, as Figure 9.2 shows, is very robust in Class B noise and also gives performance that is "close" to that obtained by the LOBD. Figure 9.4 shows robustness results for the Class A LOBD, where the "actual interference" is given by $A = 1.0$ and $\Gamma' = 10^{-4}$, and the LOBD nonlinearity used is given by various $\hat{A}$ and $\hat{\Gamma}'$. On Figure 9.4, degradation is given by $L^{(2)}$ (in dB) - L_{eff} (in dB), using (9.6) and (9.7). Note that, for this example at least, the Class A LOBD is quite robust, and we do not need to estimate the parameter values closely in order to obtain near optimum results.

All these above results are limiting results (S "small" and $N \to \infty$), and next we will investigate, via computer simulation, the "truth" of these results when the detectors are used in actual possible operational situations.

9.2 Simulation Results

The receiver of Figure 9.1 for the signal given by (9.3) has been implemented on a large scale computer. Monte Carlo simulation results for the linear receiver, the bandpass limiter receiver, and the LOBD (bandpass) receiver are given in this section. By "bandpass" we mean that the nonlinearity acts on the received complex (magnitude and phase) sample of the received waveform. For example, the bandpass limiter nonlinearity is $X_i/|X_i|$, where X_i is the complex waveform sample (Figure 9.1).

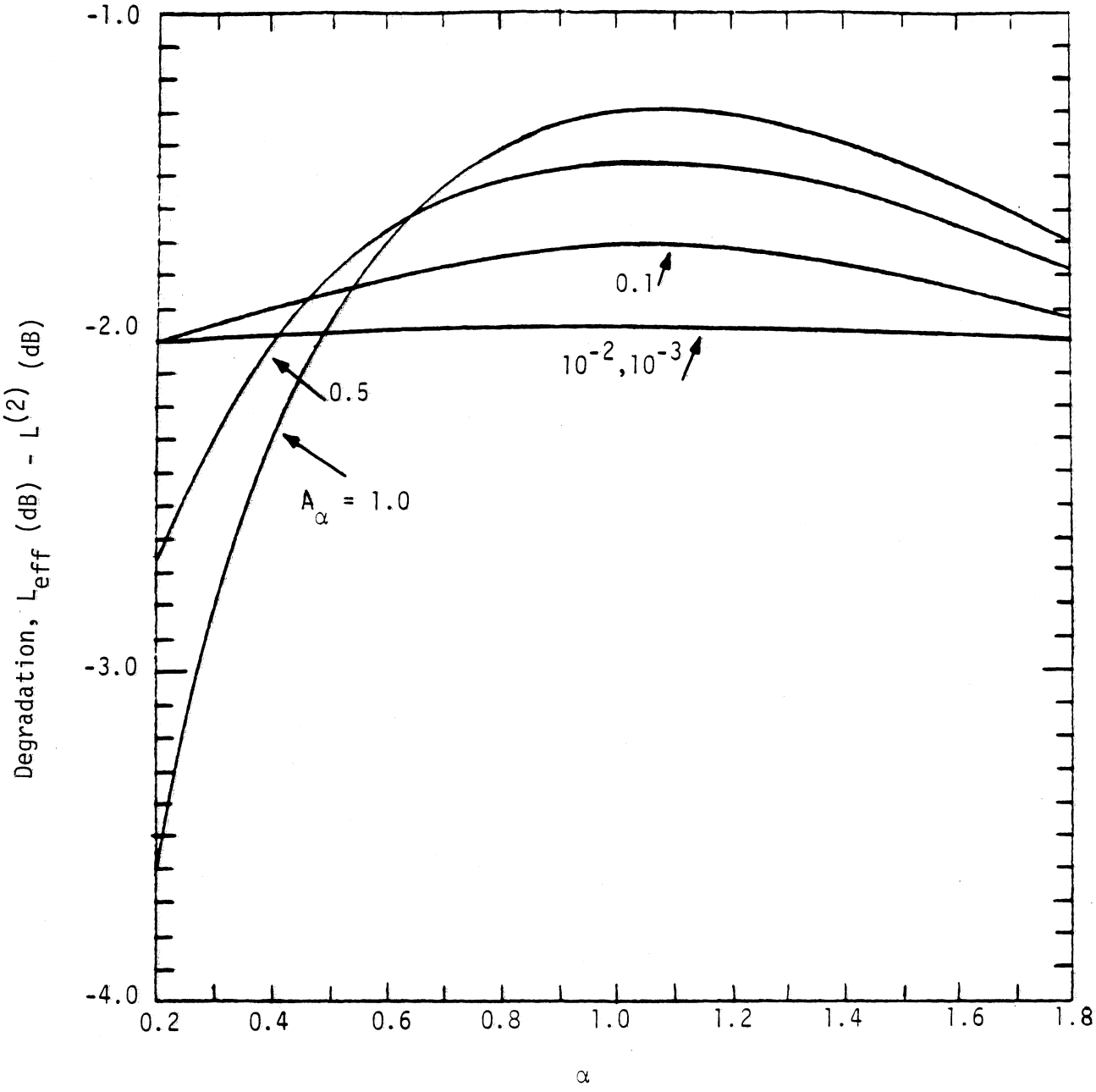

Figure 9.2. Comparison of the optimum nonlinearity for Class B noise with the hard-limiter.

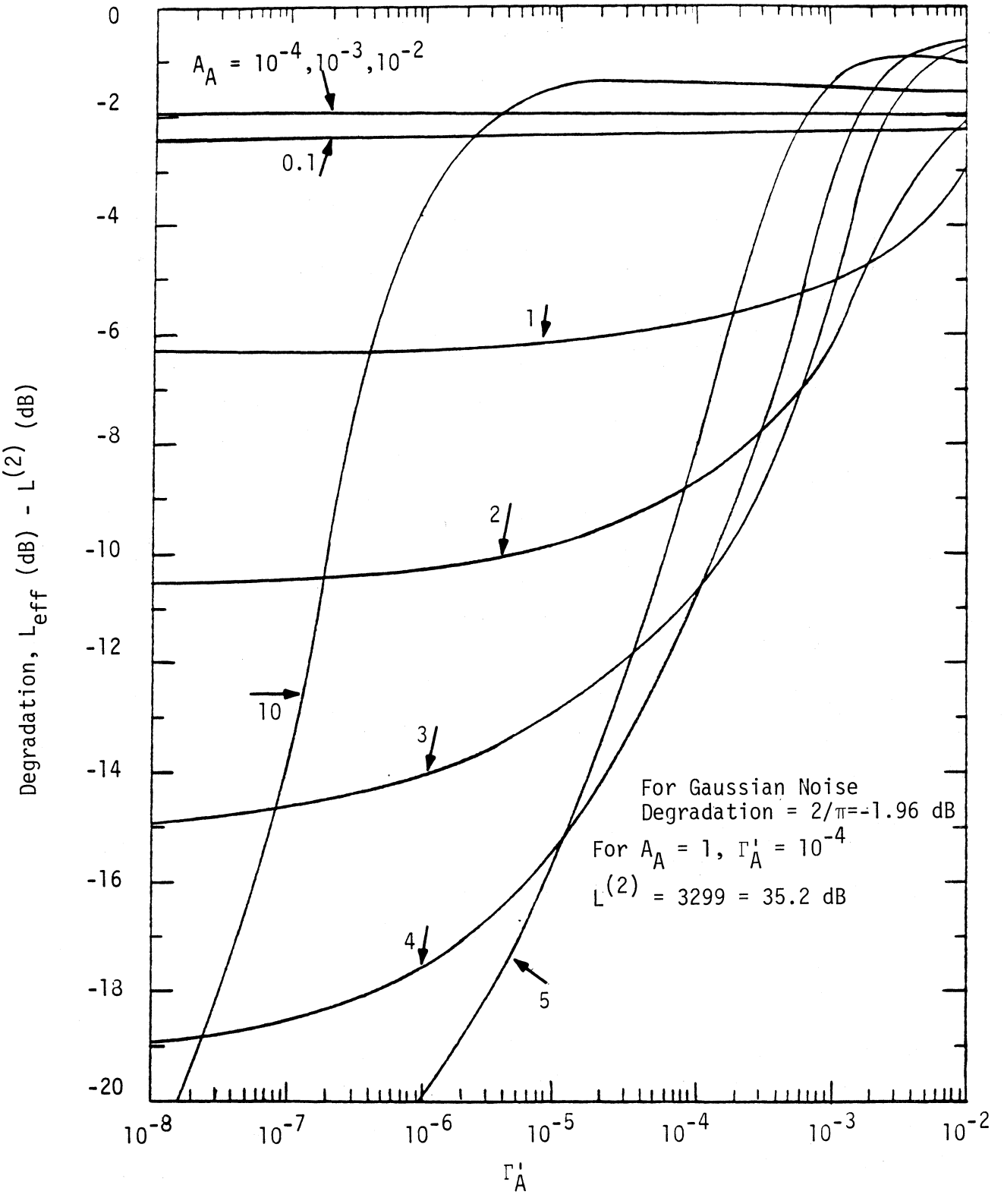

Figure 9.3. Comparison of the optimum nonlinearity for Class A noise with the hard limiter.

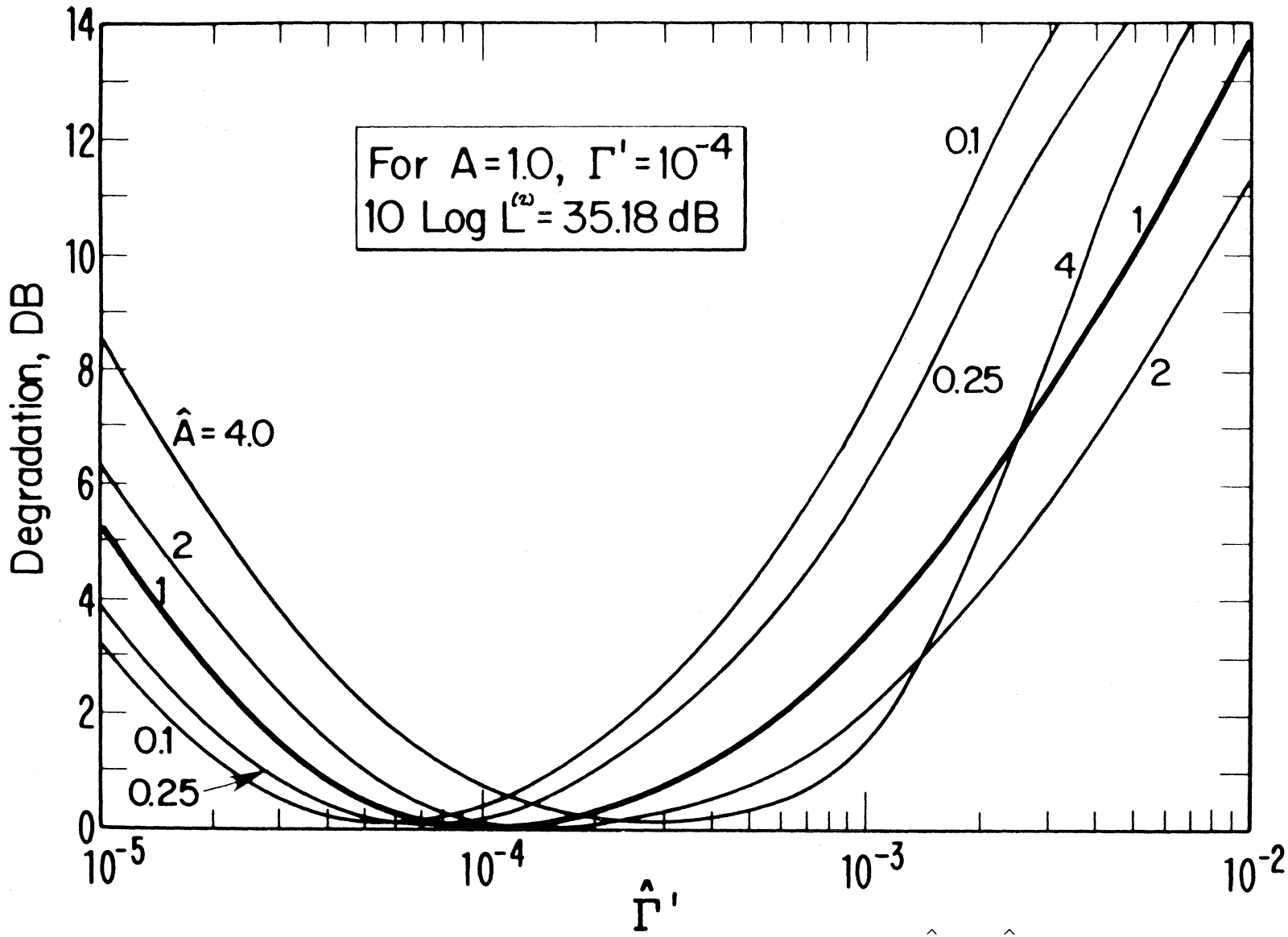

Figure 9.4. Comparison of Class A nonlinearity for various estimates $\hat{A}$ and $\hat{\Gamma}'$ with the nonlinearity for the particular case $A = 1$, $\Gamma' = 10^{-4}$.

The Class B model is given by

$$w_1(z) = \frac{e^{-z^2/\Omega}}{\sqrt{\Omega}} \sum_{m=0}^{\infty} \frac{(-1)^m}{m!} \hat{A}^m \Gamma\left(\frac{m\alpha + 1}{2}\right) {}_1F_1\left(-\frac{m\alpha}{2}; \frac{1}{2}; \frac{z^2}{\Omega}\right), \quad -\infty < z < \infty, \tag{9.10}$$

and

$$P_1[\mathcal{E} > \mathcal{E}_0] = e^{-\mathcal{E}_0^2/\Omega}\left[1 - \frac{\mathcal{E}_0^2}{\Omega} \sum_{n=1}^{\infty} \frac{(-1)^n}{n!} \hat{A}_\alpha \times \Gamma\left(1 + \frac{n\alpha}{2}\right) {}_1F_1\left(1 - \frac{n\alpha}{2}; 2; \frac{\mathcal{E}_0^2}{\Omega}\right)\right], \tag{9.11}$$

$$0 \leq \mathcal{E} < \infty.$$

For actual implementation of the required nonlinearity $\ell(x)$ (9.2), or for generation of random samples from the interference process, the models (9.10) and (9.11) are much too complex, and much simpler, approximate models must be used. Some time ago Hall [32] developed an ad-hoc mathematically simple model for atmospheric noise (Class B), and Middleton [1] has shown that his Class B model reduces, approximately, for special parameter values, to expressions of the Hall type. The Hall model has two parameters, θ and γ, and is given by

$$w_1(z) = \frac{\Gamma\left(\frac{\theta}{2}\right)\gamma^{\theta-1}}{\Gamma\left(\frac{\theta-1}{2}\right)\sqrt{\pi}\left[z^2 + \gamma^2\right]^{\theta/2}} \tag{9.12}$$

and

$$P[\mathcal{E} > \mathcal{E}_0] = \frac{\gamma^{\theta-1}}{\left(\mathcal{E}_0^2 + \gamma^2\right)^{(\theta-1)/2}} . \tag{9.13}$$

The closest match between the Middleton model (9.10) and the Hall model (9.12) are for the Middleton parameters $\alpha = 1$, $\hat{A}_\alpha = 1$, and $\Omega = 4 \times 10^{-4}$, with the corresponding Hall parameters $\theta = 2$ and $\gamma = \sqrt{2} \times 10^{-2}$. For both the Middleton model ($\alpha = 1$) and the Hall model ($\theta = 2$), the second moment does not exist, so the normalizing parameters Ω and γ are set to match measured data. For $\theta = 4$, however, the first three moments exist. For the Hall model, the required nonlinearity, $\ell(x)$, is simply given by (Figure 9.1),

$$y_i = \frac{\theta x_i}{x_i^2 + \gamma^2} \cdot \tag{9.14}$$

In actual systems, the various nonlinearities operate on the magnitude of the complex received waveform sample; that is, the phasor sum of the signal vector and the noise vector. For the noise (Hall), random samples from the envelope pdf are efficiently obtained from

$$E = \gamma \left(U^{\frac{-2}{\theta-1}} - 1 \right)^{1/2} \tag{9.15}$$

where U is uniformly distributed on [0,1]; and the noise phase angle is uniformly distributed on $[0,2\pi]$. Figure 9.5 shows the two examples of Class B noise (Hall) for which we will present simulation results. The case $\theta = 2$ results can be compared against the theoretical results for the Middleton model, $\alpha = 1$ and $\hat{A}_\alpha = 1$. The first simulation results are given in Figure 9.6 for the Hall model ($\theta = 2$) normalized to represent Middleton's model. First note the interesting results for the linear receiver. Identical results were obtained for N = 1, 10, and 100. This is, of course, not physically meaningful and is the result of using a model for which the moments do not exist. This "infinite power" problem does not exist whenever a nonlinearity is employed, as with the other results of Figure 9.6. For a linear receiver, for N = 10, say, detection is based on a "noise sample" that is the sum of the ten noise samples from the basic underlying distribution.

Except for Gaussian noise, the distribution of the "sum sample" is different from the distribution of each individual sample, and approaches Gauss via the Central Limit Theorem. This makes it difficult to analytically determine the performance of linear systems in non-Gaussian noise for time bandwidth products other than 1. On Figure 9.6, the performance of a linear receiver for N = 100 is estimated. This is based on the parameter $L^{(2)}$ (37 dB) and the simulation results for N = 100 for the LOBD receiver. The linear receiver simulation results for N = 1 match the analytical results (which for N = 1 are shown by the dashed curve). The next point to note is that for N = 1, the same results are obtained for the various nonlinearities as for the linear receiver demonstrating the known result that nonlinearities give improvement only for "large" N (37 dB, here for N = 100). The results for Hall, $\theta = 4$ (Figure 9.7) also show this. For N = 10 (Figure 9.6) note

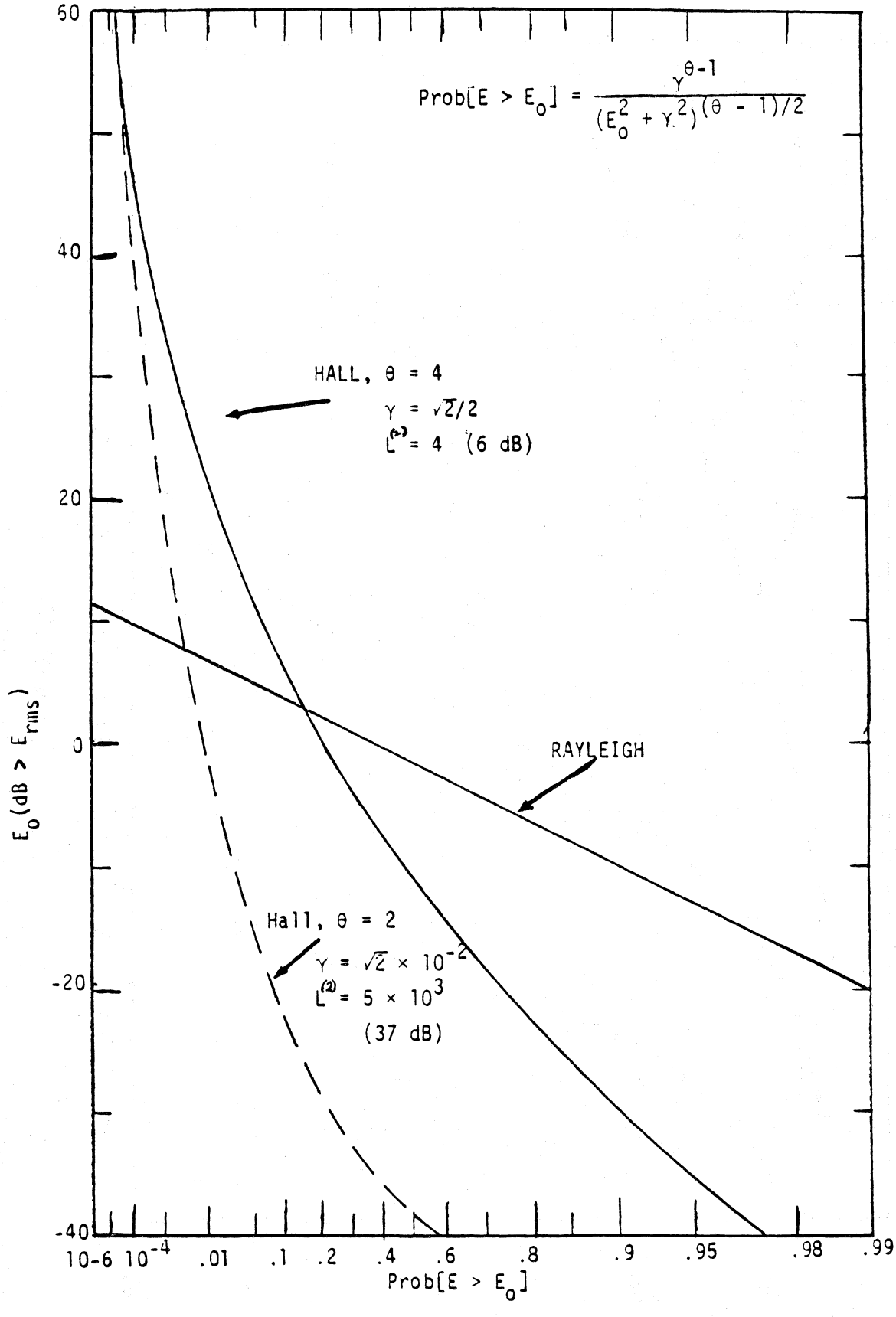

Figure 9.5. The Hall Class B noise model for θ = 2 and θ = 4. The APD is normalized to the rms envelope level (θ = 4) and to the rms of measured data (θ = 2).

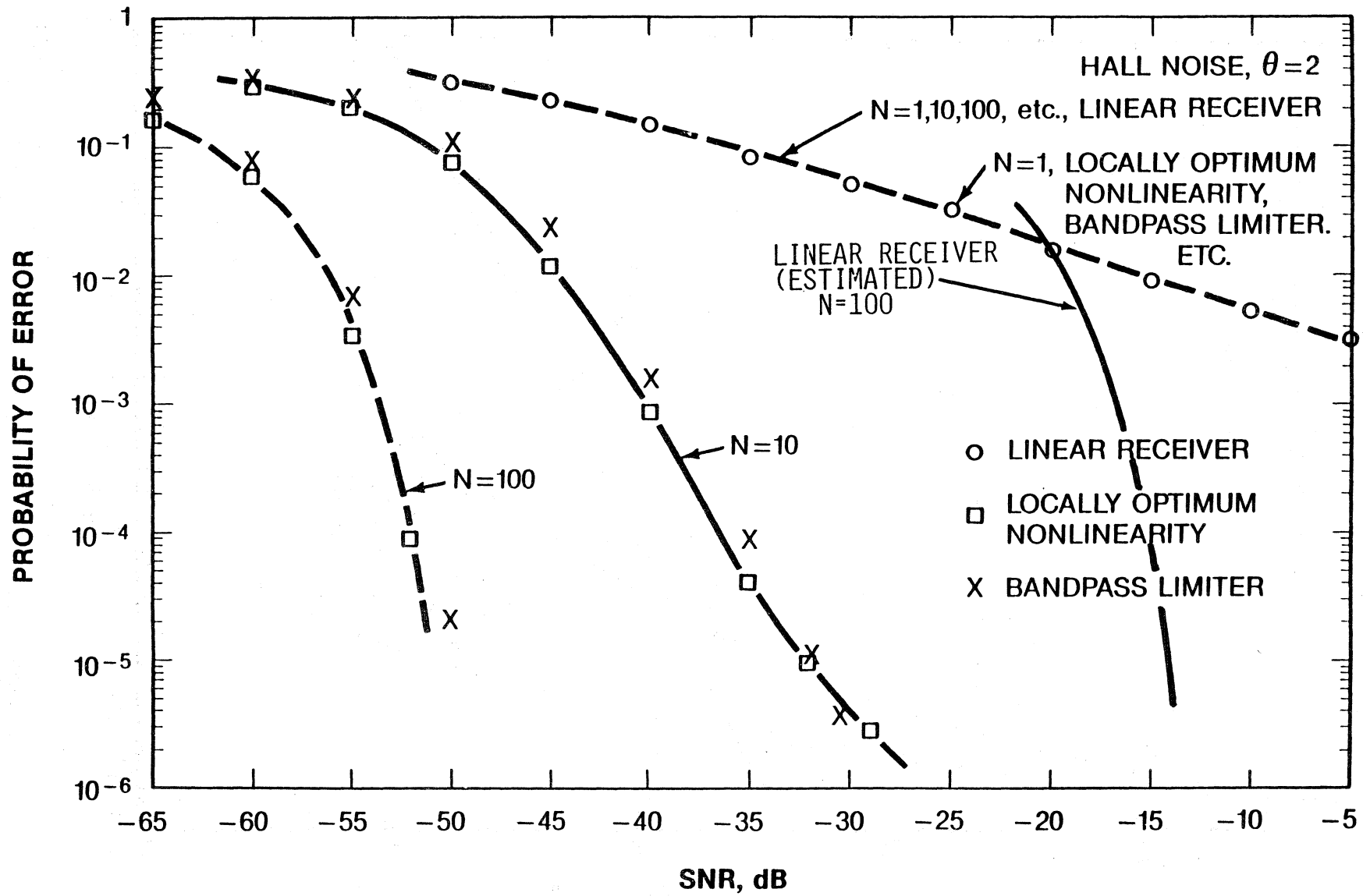

Figure 9.6. Simulation results with Hall noise, θ = 2, CPSK and constant signal.

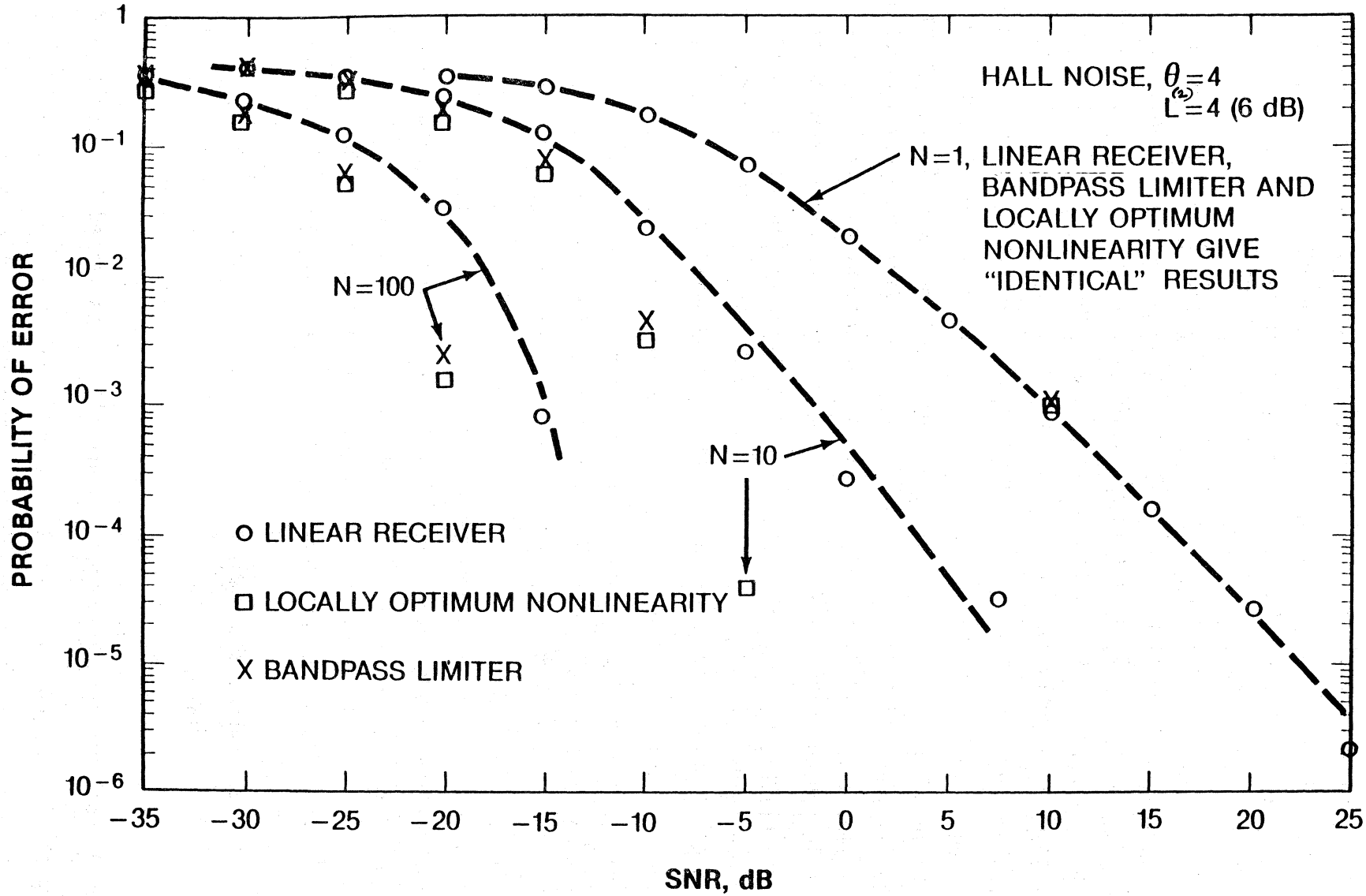

Figure 9.7. Simulation results with Hall noise, θ = 4, CPSK and constant signal.

the important result that the bandpass limiter outperforms the "optimum" LOBD detector for large enough signal level. This also has been indicated analytically [63]. For N = 100, the simulation results match the analytical results (9.4) and (9.9). Note the limiting result that the bandpass limiter is only approximately 1.5 dB inferior to the LOBD nonlinearity.

Figure 9.7 shows simulation results for the Hall model, $\theta = 4$. First note that as before, use of nonlinearities for N = 1 gives no improvement over the linear receiver, but, of course, does give improvement for N = 10 and 100. For N = 100, the improvement is only 6 dB as predicted by $L^{(2)}$. Note that the LOBD nonlinearity here also is only slightly superior to the bandpass limiter. For $\theta = 4$, the moments (first three) exist (i.e., finite energy) and we obtain "normal" results for the linear receiver for N = 1, 10, 100. On Figure 9.7, a SNR of approximately -20 dB is required for P_e of 10^{-3} (N = 100), whereas from Figure 9.6, a SNR of approximately -53 dB is required for P_e of 10^{-3}. This difference was indicated by the two $L^{(2)}$ values. Figure 9.5 shows that both distributions ($\theta = 2$ and $\theta = 4$) "look" highly non-Gaussian. This shows that we cannot arbitrarily say, by inspection, that a noise process that is "tremendously" non-Gaussian can result in "tremendous" improvement over the corresponding Gaussian or linear receiver situation.

The Middleton model for Class A narrowband "impulsive" noise is,

$$w_1(z) = e^{-A_A} \sum_{m=0}^{\infty} \frac{A_A^m}{m!\sqrt{2\pi\sigma_m^2}} e^{-z^2/2\sigma_m^2} , \tag{9.16}$$

where

$$\sigma_m^2 = \frac{m/A_A + \Gamma'_A}{1 + \Gamma'_A} , \tag{9.17}$$

and, for the envelope,

$$P(\mathcal{E}>\mathcal{E}_o) = e^{-A_A} \sum_{m=0}^{\infty} \frac{A_A^m}{m!} e^{-\mathcal{E}_o^2/\sigma_m^2} . \tag{9.18}$$

The Class A model has two parameters: A_A and Γ'. A_A is termed the overlap index, and as A_A becomes large ($\sim$10), the noise approaches Gaussian (still narrowband)

and Γ' is the ratio of the energy in the Gaussian portion of the noise to the energy in the non-Gaussian component. This model also is too complex mathematically for implementation of the nonlinearity $\ell(x)$ or for generating random samples for computer simulation. The following approximation, based on the characteristic function for the Class A model, however, can be used. Without going into detail, it turns out that the Class A APD can be closely approximated by

$$P[\mathcal{E}>\mathcal{E}_0] = \frac{1}{1+\hat{A}} \left\{ e^{-\mathcal{E}_0^2/\sigma_0^2} + \hat{A}\, e^{-\mathcal{E}_0^2/\sigma_1^2} \right\} \tag{9.19}$$

where $\sigma_0^2 = \Gamma'/(1+\Gamma')$,

and

$$\sigma_1^2 = \frac{1+\hat{A}-\sigma_0^2}{\hat{A}} \ .$$

Extensive use has been made of the particular Middleton Class A example, $\Gamma_A' = 0.5 \times 10^{-3}$, $A_A = 0.35$. To match this with (9.19), the appropriate parameters are $\Gamma_A' = 0.5 \times 10^{-3}$ and $\hat{A} = 0.40$. Using (9.19), we obtain random samples for the pdf of the Class A envelope from:

$$\mathcal{E} = \left(-\sigma_0^2 \ln \left[(1+\hat{A})(1-U) - \hat{A}\, e^{-E_B^2/\sigma_1^2} \right] \right)^{1/2} , \quad 0 \le U \le U_1 \ , \tag{9.20}$$

and

$$\mathcal{E} = \left(-\sigma_0^2 \ln \left[\frac{1+\hat{A}}{\hat{A}} (1-U) \right] \right)^{1/2} , \quad U_1 < U \le 1 \ ,$$

where,

$$U_1 = 1 - \frac{1}{1+\hat{A}} \left\{ e^{-E_B^2/\sigma_0^2} + \hat{A}\, e^{-E_B^2/\sigma_1^2} \right\} \ .$$

The parameter E_B must be determined "experimentally." For our Class A case above ($\Gamma'_A = 0.5 \times 10^{-3}$, $A_A = 0.35$) ($\hat{A} = 0.4$), $E_B = 0.1$. Figure 9.8 shows the APD for our Middleton Class A example and the corresponding APD (9.19) along with points generated via 10,000 random samples using (9.20).

The above gives the Class A approximation for the envelope. We also need the corresponding result for the pdf of the instantaneous amplitude in order to implement the LOBD nonlinearity, $\ell(x)$. Since the phase angle is uniformly distributed, this pdf can be obtained from

$$w_1(x) = \int_x^\infty \frac{1}{\pi\sqrt{\mathcal{E}^2 - x^2}}\, p(\mathcal{E})d\mathcal{E} \quad , \tag{9.21}$$

where $p(\mathcal{E})$ is the pdf of the (normalized) envelope $\mathcal{E}$. The result is

$$w_1(x) = \frac{1}{1+\hat{A}}\left\{\frac{1}{\sqrt{\pi\sigma_0^2}}\, e^{-x^2/\sigma_0^2} + \frac{\hat{A}}{\sqrt{\pi\sigma_1^2}}\, e^{-x^2/\sigma_1^2}\right\} . \tag{9.22}$$

The result (9.22) now is used to implement the LOBD nonlinearity. Figure 9.9 shows the LOBD nonlinearities for the two Hall model (Class B) cases and also for the Class B example, both the approximation (9.22) and the Middleton model (9.18). Also, numerical integration, using (9.5) gives $L^{(2)} = 34$ dB for both the Middleton model (9.16) and the approximation (9.22). Note that the Class A nonlinearity looks much like a hole puncher with the "punching" level fixed at about - 24 dB (i.e., for this "hole puncher," $y_i = 0$ for $|x_i| > -24$ dB).

Figure 9.10 gives Class A simulation results. First, for the linear receiver, we obtain "normal" results for N = 1, 10, 100, with the N = 1 results matching analytical results (indicated by the solid curve). Next, consider the N = 10 results for the LOBD and bandpass limiter nonlinearities. Figure 9.3 indicates that in the limit the limiter should be 3 dB inferior to the LOBD and on Figure 9.10, N = 10, things start out this way, but the limiter becomes much more inferior as SNR increases. Also, the N = 10 results are approximately 34 dB better than the linear receiver results as predicted by $L^{(2)}$, but as the SNR increases past approximately -27 dB, the LOBD performance degrades very rapidly and becomes inferior to even the linear receiver.

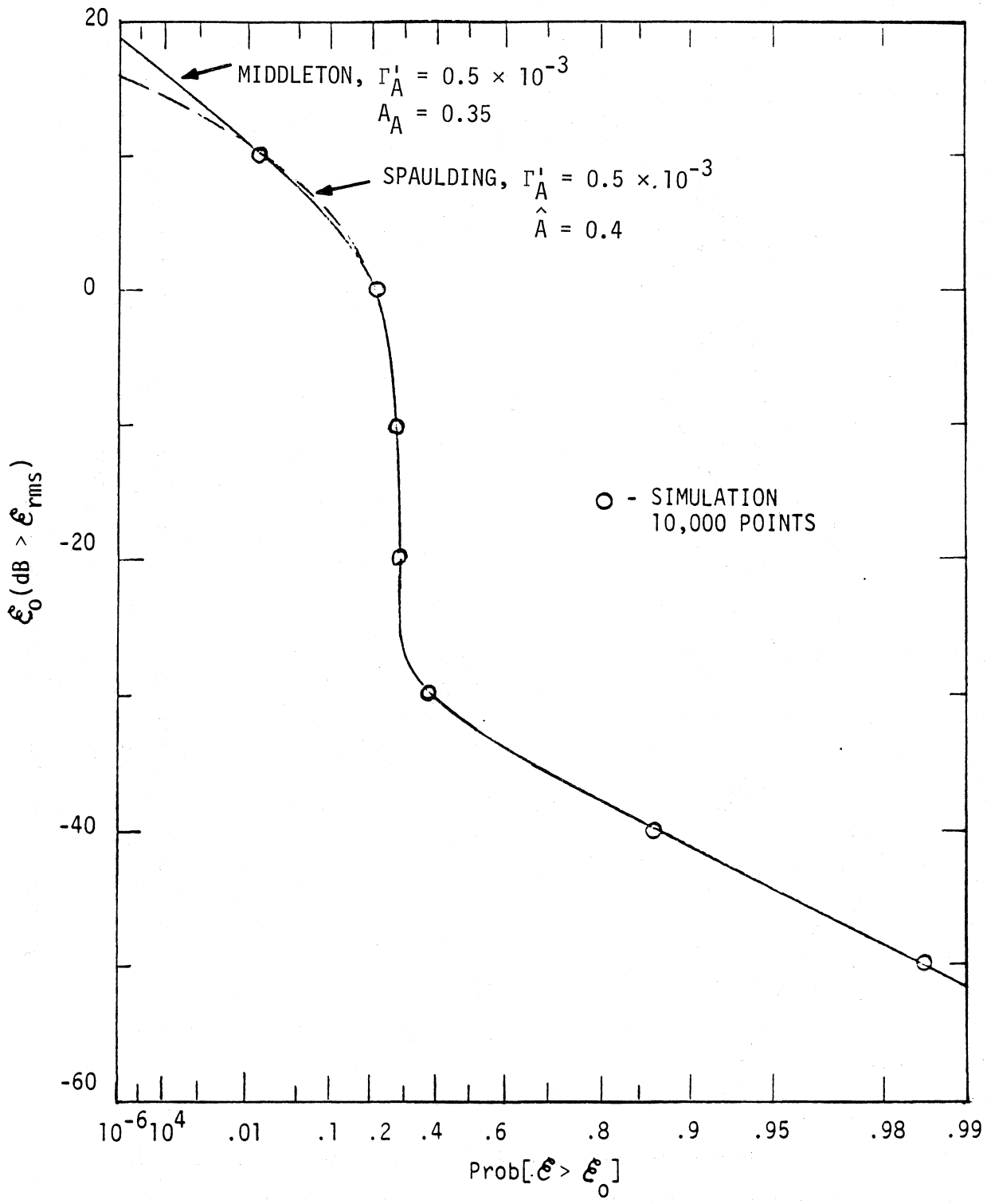

Figure 9.8. An example of Middleton's Class A distribution and corresponding simple approximation along with values obtained via computer simulation using the simple approximation.

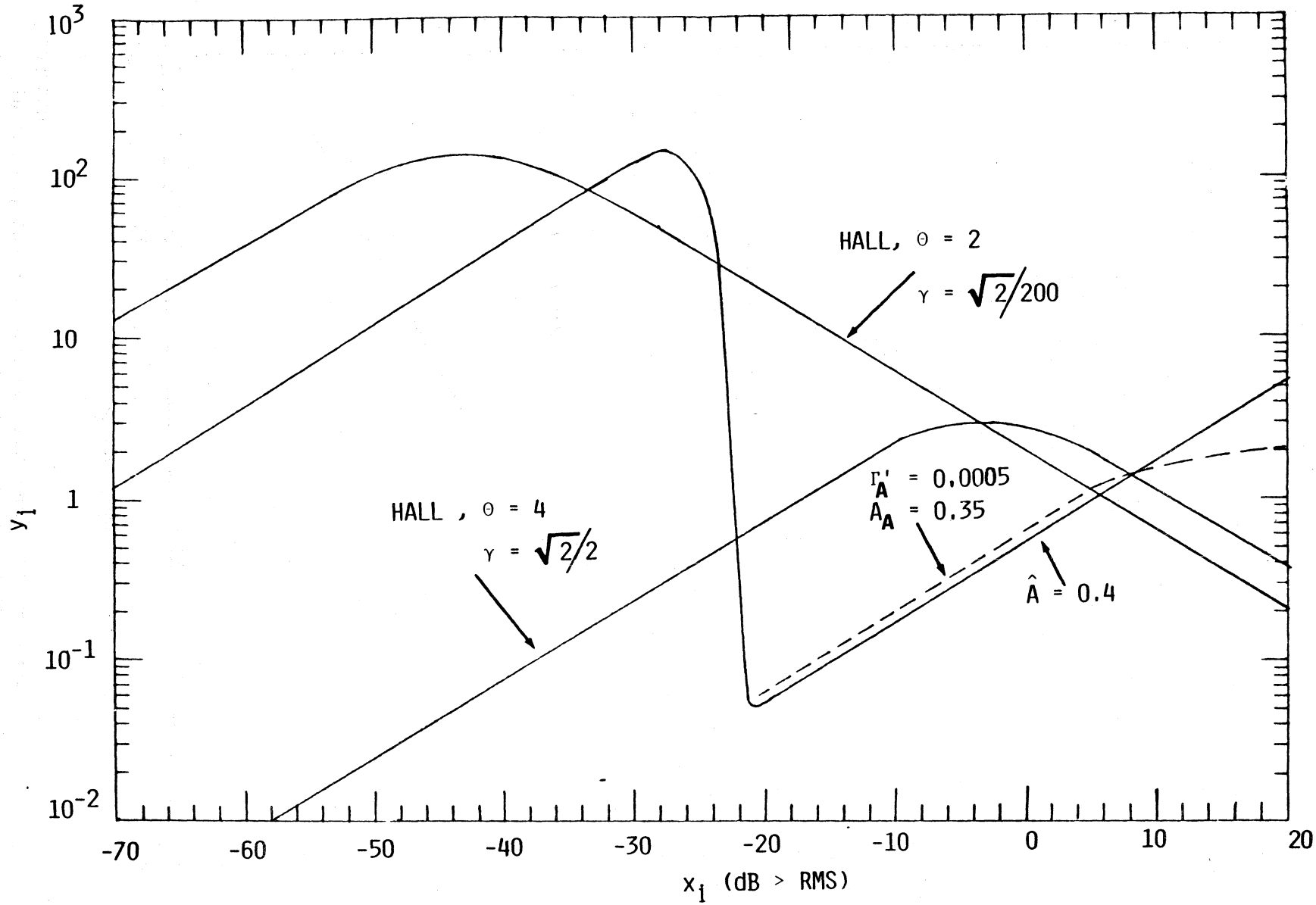

Figure 9.9. The LOBD nonlinearities.

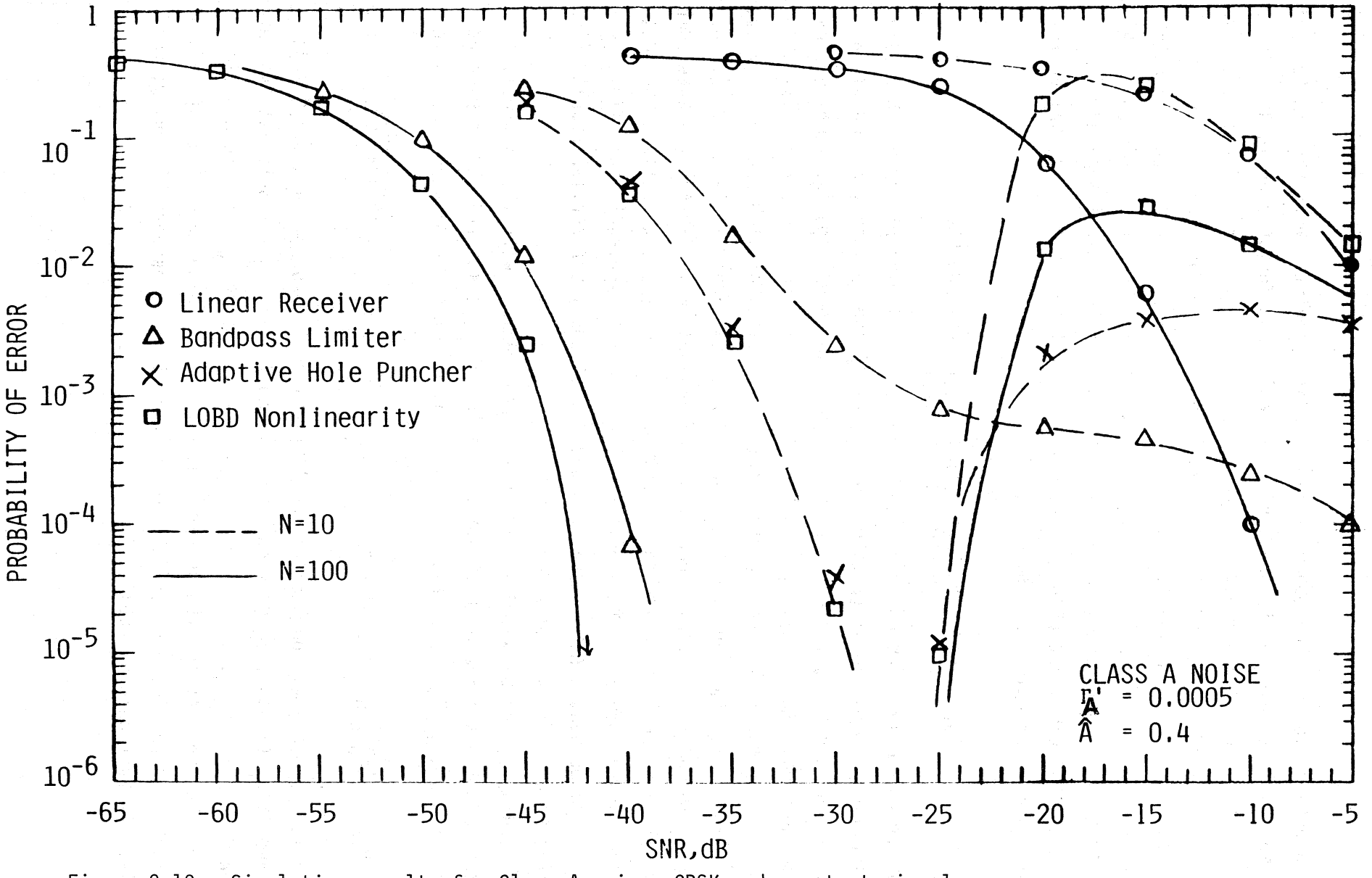

Figure 9.10. Simulation results for Class A noise, CPSK and constant signal.

The results for N = 100 behave more as theory predicts, with the limiter being approximately 3 dB inferior to the LOBD, but, again, performance again degrades rapidly as the SNR increases past -27 dB. Results also are given for an adaptive hole puncher (i.e., a nonlinearity identical to the LOBD nonlinearity for $|x_i| > -24$ dB, but $y_i = o$ for $|x_i| > -24$ dB), for N = 10. Performance is essentially the same as the LOBD for SNR < -27 dB, but also degrades rapidly for higher SNR as one would expect. This dramatically illustrates that the "small enough" signal requirement that gives the LOBD must be met, at least for some cases, before any kind of "good" performance can be expected.

10. REMARKS ON THRESHOLD RECEIVER PERFORMANCE IN NON-UNIFORM FIELDS

We have already remarked in Section 5 above on the possibility of increasing the effective performance of threshold detectors by appropriate location of the array sensors in the EMI field. Improvement by independent spatial sampling, as well as the usual time sampling, is achieved, provided that the signal field remains coherent across the array, and provided that the noise from each sensor is (spatially) independent. This limiting situation can be described analytically [60,62], but is only approximated in practice, because of the non-spatially "white" (in wave number space) nature of real noise fields. However, it is possible to replace the ideal J total independent sensors with a number, $J'(\leq J)$, which represents the effective number of independent sensors, and then proceed to apply our earlier results (for J) by replacing J by J', as indicated.

Accordingly, let us briefly illustrate these remarks with (1), a specific coherent, optimum threshold detection algorithm, $g^*_{J\text{-coh}}$; and (2), the structure factor, here $\sigma^{*2}_{oJ\text{-coh}}$, cf. (8.6a,b), by which performance is measured. We have

$$g^*_{coh} = (\hat{B}^*_{J\text{-coh}} + \log \mu) - \bar{a}_o\sqrt{2} \sum_{m=1}^{M} \sum_{n=1}^{N} \ell(x_{m,n})\, e^{-(\Delta\omega_d t_n)^2/2}, \qquad (10.1)$$

where m=1,....,M denote the spatial sampling points (sensors), n=1,....,N, the time samples t_n (= $n\Delta t$), $\bar{a}_o$ = av.coh. signal amplitude; $\Delta\omega_d$ = doppler spread parameter; and $\ell_{m,n} = \ell(x_{m,n})$ is just $w_1(x_{m,n}|H_o)$ again, where $x_{m,n}$ is the nth time sample of the input at the mth sensor. Here J = MN. (With no doppler spread, or very little spread, $\Delta\omega_d \doteq o$, and the exponential term is essentially unity; for details, see Section 8 of [60]).

The associated statistic $\sigma_{oJ}^{(x)^2}$ ($\equiv \mathrm{var}_{H_o} g_J^*$), used in (8.6a,b) to obtain performance measures, is found to be [60]

$$\sigma_{o\text{-coh}}^{*\,2} = 2\overline{a_o^2}\,(1-\eta)\,J\,L^{(2)}\,H_1(N\Delta t\Delta w_d), \qquad J = MN \tag{10.2}$$

where $1-\eta = \bar{a}_o^2/\overline{a_o^2}$ (≤ 1) is a fading ratio, and $H_1(x) = \sqrt{\pi}\theta(x)/2x$. With no fading, $\bar{a}_o^2 = \overline{a_o^2}$, and no doppler spread, i.e., $H_1(o) = 1$, we get

$$\sigma_{o\text{-coh}}^{*\,2} = 2\,\overline{a_o^2}\,J\,L^{(2)}\ , \tag{10.3}$$

which shows in this case that the processing gain π_{coh}^* and minimum detectable signal, $a_{o\text{-min-coh}}^{*2}$, are

$$\pi_{coh}^* = J\,L^{(2)}\ ;\quad (a_o^2)_{min\text{-coh}}^* = \overline{a_o^2} = \bar{a}_o^2 = a_o^2). \tag{10.4}$$

The former represents now the <u>space-time bandwidth product</u>, $MNL^{(2)}$, which is to be compared with $\phi^*/2$ in (8.7),(8.8). There the processing gain in $NL^{(2)}$; ($M = 1$ effectively, as the EMI field is assumed uniform). Here the processing gain is $M \cdot NL^{(2)}$, for these independent spatial samples, as well.

Thus, if we can sample the noise independently in space, we can increase our processing gains, or, equivalently, <u>lower</u> the minimum detectable signals, of our reception process (for the same performance). For $M = 10$, this means a 10 dB gain over the cases where the EMI field is uniform over the receiving array. Accordingly, it can be worthwhile to investigate the EMI field structure, to see to what extent it is possible to sample "independently"; cf., Section 5 earlier.

A full development of the combined spatial-temporal sampling models, in the threshold detection, for classes of realistic field models, is given in [60,73].

11. CONCLUDING REMARKS

From the discussion above, we can make the following general remarks with regard to the implications of these interference models for measurement and system design and performance determination.

1. These canonical models provide a needed, general apparatus for real-world EMI measurements and EMI assessment. Their canonical nature gives them global application, invariant of the particular source mechanism. They have been, and are, experimentally verified, tractable, and defined by measurable physical parameters.
2. Because of the canonical character of these general noise models, and their experimental establishment in real interference environments, we are now able to pursue systematically the development of (threshold) optimum reception systems, and determine their structures (algorithms) and performance, as well as to compare them with current suboptimal systems [14, 59,60].
3. In addition, from a practical standpoint, in various applications large improvement over conventional processing can be expected. This is shown typically by the comparison between the performance of conventional receivers optimized for the usual Gaussian noise assumptions, and receivers that truly adapt to the actual highly non-Gaussian EMI environment in which they must operate.
4. When reception in non-uniform EMI fields (over the receiving array) takes place, spatial processing, as well as temporal processing, can lead to additional improvements in performance. The canonical nature of the optimum threshold algorithms does not change, but adaptive beam forming naturally appears in the structure of these algorithms. Performance measures remain unchanged in form, but the detailed nature of var g* is modified to account for the spatial character of both the desired signal and the EMI environment.

We emphasize once more that it is this development of verified, tractable, canonical noise models that makes possible a general treatment of the real, non-Gaussian, interference world. We can now exploit the classical methods of Statistical Communication Theory for both measurement and signal processing.

The general approach, reviewed tutorially here, may be described as "parametric adapive" as distinct from other important approaches [69,70], which are "distribution free" or nonparametric. The former requires specific statistical-physical model building, with a consequent greater sensitivity to environment changes than the latter.

Finally, we must point out that our models, and the signal processing consequent upon them, are not confined to (EM) telecommunications alone. They are canonically applicable to other spectral domains, and other physical media and propagation mechanisms (e.g., underwater acoustics [60]), where information transfer in space-time is the aim, whether it be for the purposes of remote sensing or human communications.

12. REFERENCES

[1] D. Middleton, Statistical-physical models of electromagnetic interference, IEEE Trans. Electromagn. Compat., EMC-19, August 1977, pp. 106-127.

[2] ____, Canonical non-Gaussian noise models: Their implications for measurement and for prediction of receiver performance, IEEE Trans. Electromagn. Compat., EMC-21, Aug. 1979, pp. 209-220.

[3] ____, Probability models of received scattered, and ambient fields, Proc. 6th Princeton Conf. on Information Sciences and Systems, Mar. 23-24, 1972, Dept. of E.E., Princeton Univ., Princeton, NJ, and Proc. IEEE 1972 Internat'l Conf. Engineering in Ocean Environemtn, Newport, RI, September 13-16, 1972, IEEE Pub. 72 CHO-660-1-OCC.

[4] ____, Statistical-physical models of urban radio-noise environments, Part I: Foundations, IEEE Trans Electromagn. Compat., EMC-14, pp. 38-56, May ,1972.

[5] ____, Man-made noise in urban environments and transportation systems, IEEE Trans. Commun., COM-21, pp. 1232-1241, Nov. 1973.

[6] ____, Statistical-physical models of man-made radio noise, Part I: First-order probability models of the instantaneous amplitude, Office of Telecommunications Technical Report OT-74-36, Apr., 1974 (NTIS Order No. COM75-10864/AS).

[7] ____, Statistical-physical models of man-made and natural radio noise, Part II: First-order probability of the envelope and phase, Office of Telecommunications Technical Report OT-76-86, Apr., 1976 (NTIS Order No. PB253949).

[8] ____, Statistical-physical models of man-made and natural radio noise, Part III: First-order probability models of the instantaneous amplitude for Class B interference, National Telecommunications and Information Administration Report NTIA-CR-78-1, June, 1978 (NTIS Order No. PB 284862/AS).

[9] ____, Statistical-physical models of man-made and natural radio noise, Part IV: Determination of the first-order parameters of Class A and B interference, National Telecommunications and Information Administration Report NTIA-CR-78-2, Sept., 1978 (NTIS Order No. PB 288467).

[10] ____, Procedures for determining the parameters of the first-order canonical models of Class A and B electromagnetic interference, IEEE Trans. Electromagn. Compat., EMC-21, Aug., 1979, pp. 190-208.

[11] _____, First-order non-Gaussian Class C interference models and their associated threshold detection algorithms, May, 1986 (informal report, available from NTIA/ITS, Boulder, Colo. 80303).

[12] A. D. Spaulding, Man-made noise: The problem and recommended steps toward solution, Office of Telecommunications Report OT-76-85, Apr., 1976 (NTIS Order No. PB 253745/AS).

[13] A. D. Spaulding and D. Middleton, Optimum reception in an impulsive interference environment, Office of Telecommunications Report OT-76-67, June, 1975 (NTIS Order No. COM 75-11097/AS).

[14] A. D. Spaulding and D. Middleton, Optimum reception in an impulsive interference environment, Part I: Coherent detection, Part II: Incoherent reception, IEEE Trans. Comm. COM-25, Sept. 1977, pp. 910-934.

[15] D. Middleton, An Introduction to Statistical Communication Theory, New York: McGraw-Hill, 1960.

[16] ____, Topics in Communication Theory, New York: McGraw-Hill, 1965.

[17] ____, Canonically optimum threshold detection, IEEE Trans. Informa. Theory, IT-12, pp. 230-243, 1966.

[18] T. D. Plemons, J. A. Shooter, and D. Middleton, Underwater acoustic scattering from lake surfaces I. Theory, experiment, and validation of the data, JASA 52, No. 5 (Part 2), pp. 1481-1502, 1972.

[19] H. Cramér, Mathematical Methods of Statistics, Princeton Univ. Press, 1946; chapter 13.

[20] S. S. Wilks, Mathematical Statistics, New York: Wiley, 1962; Chapters 8 and 9.

[21] A. D. Spaulding, Optimum threshold detection in broadband impulsive noise employing both time and spatial sampling, Proc. of 3rd Sym. and Technical Exhibition on Electromag. Compat., Rotterdam, May 1-3, 1979, pp. 377-385.

[22] J. H. Van Vleck and D. Middleton, A theoretical comparison of the visual, aural, and meter reception of pulsed signals in the presence of noise, J. Appl. Phys. 17, pp. 940-971, Nov., 1946.

[23] J. W. Adams, W. D. Bensema, and M. Kanda, Electromagnetic noise, Grace Mine, National Bureau of Standards Report NBS IR 74-388, 1974 (NTIS Order No. COM-74-11687).

[24] W. D. Bensema, M. Kanda, and J. W. Adams, Electromagnetic noise in Robena No. 4 coal mine, National Bureau of Standards Technical Note 654, 1974 (NTIS Order No. COM-74-50698).

[25] E. C. Bolton, Simulating LF atmospheric radio noise and comparative characteristics of man-made and atmospheric radio noise at 60, 76, 200 kHz, Office of Telecommunications Technical Memorandum OT-TM-97, 1972 (available only from author).

[26] L. R. Espeland and A. D. Spaulding, Amplitude and time statistics for atmospheric radio noise, ESSA Technical Memorandum ERLTM-ITS 253, 1970 (available only from authors).

[27] R. A. Shepherd, Measurements of amplitude probability distributions and power of automobile ignition noise at HF, IEEE Trans. Vehicular Techn., VT-23, No. 3, August 1974, pp. 72-83.

[28] A. D. Spaulding and L. R. Espeland, Man-made noise characteristics on and in the vicinity of military and other government installations, Office of Telecommunications, Technical Memorandum OT-TM-48, 1971 (available only from authors).

[29] K. Furutsu and T. Ishida, On the theory of amplitude distribution of impulsive random noise, J. Appl. Phys. (Japan), 32, pp. 1206-1221, July 1960.

[30] A. A. Giordano, Modeling of Atmospheric Noise, Ph.D. dissertation, Dept. of Electr. Eng., Univ. of Pennsylvania, Philadelphia, 1970.

[31] A. A. Giordano and F. Haber, Modeling of atmospheric noise, Radio Science 7, No. 11, pp. 1011-1023, 1972.

[32] H. M. Hall, A new model for "impulsive" phenomena: application to atmospheric noise communications channels. Stanford Univ. Electronics Laboratories Tech. Report Nos. 3412-8 and 7050-7, SU-SEL-66-052, 1966.

[33] D. Middleton, Performance of telecommunication systems in the spectral-use environment: I. Objectives and approaches for the general data base, Jan. 31, 1975 (Office of Telecommunications Policy (OTP) Research Paper, NTIA, Office of Spectrum Management, 179 Admiral Cochrane Drive, Annapolis, MD 21401).

[34] ____, Performance of telecommunications systems in the spectral-use environment: II. An approach to cost, values, policies, and payoffs for decision-making in system performance, June 30, 1975 (Research Paper, OTP).

[35] ____, Performance of telecommunication systems in the spectral-use environment: III. Large scale interacting systems, March 31, 1976 (Research Paper, OTP).

[36] ____, Performance of telecommunication systems in the spectral-use environment: IV. Statistical criteria, EMI environments, and scenarios, Sept. 1977 (Research Paper, OTP).

[37] ____, Performance of telecommunications systems in the spectral-use environment: V. Land-mobile and similar scenarios in Class A interference, NTIA Report NTIA-CR-79-4, June 1979 (NTIS Order No. PB 80-112097).

[38] ____, Performance of telecommunications systems in the spectral-use environment: VI. Analytical results for land-mobile scenarios in Class B interference with fading and multipath, NTIA Report NTIA-CR-81-12, June 1981 (NTIS Order No. PB 81-249344).

[39] D. Middleton and R. Esposito, Simultaneous optimum detection and estimation of signals in noise, IEEE Trans. Information Theory, IT-14, No. 3, May 1968, pp. 434-444.

[40] D. Middleton, A tutorial review of the new EMI models and their effects on receiver performance, NTIA Report NTIA-Contractor Report-80-7, May 1980 (NTIS Order No. PB 80-211188).

[41] R. J. Dinger, W. D. Meyers, and J. R. Evans, Experimental Measurement of Ambient electromagnetic noise from 1.0 to 4.0 kHz, Naval Research Laboratory Report 8413, July 31, 1980.

[42] V. P. Pevnitsky and L. V. Tigin, A stochastic model of a cumulative process of man-made radio interference and objective evaluation of signal distortions produced by these interferences, Proc. of the 1st Sym. on EMC, Montreux, March 1975.

[43] V. P. Pevnitsky and Y. V. Polozok, On the agreement of two methods of construction of stochastic models of cumulative interference processes, Proc. of 4th Sym. and Tech. Exhibition on EMC, Zurich, March 10-12, 1981, pp. 537-542.

[44] J. de Riffye, Modeling of certain discontinuous physical random phenomena and applications to telecommunications, Doctoral Thesis in Applied Mathematics, Univ. of Pierre and Marie Curie, Paris, France, May 1982.

[45] L. A. Berry, Comparisons of analytical and numerical calculations of communications probability, NTIA Report 80-41, June 1980 (NTIS Order No. PB 80-211394).

[46] L. A. Berry, Understanding Middleton's canonical formula for Class A noise, IEEE Trans. on EMC, EMC-23, No. 4, Nov. 1981, pp. 337-344.

[47] D. Middleton, New results in the development of canonical and quasi-canonical EMI probability models, Proc. 4th Sym. and Tech. Exhibition on EMC, Zurich, March 10-12, 1981, pp. 25-32.

[48] ____, Performance of telecommunication systems in the spectral-use environment: VII, Interference scenarios and the canonical and quasi-canonical (first order) probability models of Class A interference, NTIA Report CR-82-18, March 1982 (NTIS Order No. PB 82-226861).

[49] ____, Canonical and quasi-canonical probability models of Class A interference, IEEE Trans. on EMC, EMC-25, No. 2, May 1983, pp. 76-106.

[50] A. D. Spaulding, Atmospheric noise and its effects on telecommunciation system performance, Chapter 7, Handbook of Atmospherics, Vol. 1, H. Volland, Ed., 1982 (CRC Press, 2000 N. W. 24th St., Boca Raton, Florida, 33431).

[51] A. D. Spaulding, Optimum threshold signal detection in broad-band impulsive noise employing both time and spatial sampling, IEEE Trans. on Communications, COM-29, No. 2, February 1981, pp. 147-152.

[52] D. Middleton, Channel characterization and threshold reception for complex underwater media, EASCON, Sept.-Oct. 1980, Vol. IEEE-0531-6863/80-0000-171, pp. 171-180.

[53] A. D. Spaulding, Robustness of LOBD's for non-Gaussian noise, Proc. 5th Sym. on EMC, Wrocław, Poland, Sept. 17-19, 1980, pp. 143-152.

[54] J. E. Evans and A. S. Griffiths, Design of a Sanguine noise processor based on worldwide extremely low frequency (ELF) recordings, IEEE Trans. on Communications, COM-22, No. 4, April 1974, pp. 528-539.

[55] R. F. Ingram and R. Houle, Performance of optimum and several suboptimum receivers for threshold detection of known signals in additive white, non-Gaussian noise, NUSC Tech. Report 6339, Nov. 24, 1980, Naval Underwater Systems Center, New London, Conn. 06320.

[56] R. F. Ingram, Performance of locally optimum threshold receiver and several suboptimum nonlinear receivers for ELF noise, IEEE J. of Oceanic Engineering, Vol. OE-9, No. 3, July 1984, pp. 202-208.

[57] A. D. Spaulding, Locally optimum and suboptimum detector performance in non-Gaussian noise, Conference Record, IEEE International Conf. on Communications, Philadelphia, June 13-17, 1982, pp. 2H.2.1-2H.2.7 (IEEE Catalog Number 82CH1766-5).

[58] W. A. Gardner, Structural characterization of locally optimum detectors in terms of locally optimum estimators and correlators, IEEE Trans. on Information Theory, IT-28, No. 6, Nov. 1982, pp. 924-932.

[59] D. Middleton and A. D. Spaulding, Optimum reception in non-Gaussian electromagnetic interference environments: II. Optimum and suboptimum threshold signal detection in Class A and B noise, NTIA Report 83-120, May 1983 (NTIS Order No. PB 83-241141).

[60] D. Middleton, Multiple-element threshold signal detection of underwater acoustic signals in non-Gaussian interference environments, NOSC Contractor Report 231, May 18, 1984, Naval Ocean Systems Center, San Diego, CA 92152.

[61] _____, Threshold detection in non-Gaussian interference environments: Exposition and interpretation of new results for EMC applications, IEEE Trans. on EMC, EMC-26, No. 1, February 1984, pp. 19-28.

[62] _____, Threshold signal detection for EMC in non-uniform, non-Gaussian EMI fields, Proc. of 7th International Sym. of EMC, Wrocław, Poland, June 17-19, 1984, pp. 515-527.

[63] A. D. Spaulding, Locally optimum and suboptimum detector performance in non-Gaussian interference environment, IEEE Trans. on Communications, COM-33, No. 6, June 1985, pp. 509-517.

[64] A. D. Spaulding, Locally optimum and suboptimum detector performance in non-Gaussian "broadband" and "narrowband" interference environments, Proc. of 6th International Sym. and Technical Exhibition on EMC, Zurich, March 5-7, 1985, pp. 437-442.

[65] A. D. Spaulding and J. S. Washburn, Atmospheric radio noise: Worldwide levels and other characteristics, NTIA Report 85-173, April 1975 (NTIS Order No. PB85-212942).

[66] L. T. Reminzov, Natural Radio Noise, Nauka Press, 1985 (Moscow, USSR).

[67] A. D. Spaulding, Stochastic modeling of the electromagnetic interference environment, Conf. Record, International Conf. on Communications, ICC '77, Chicago, June 12-15, 1977, pp. 42.4-114-123 (IEEE Catalog No. 77CH-1209-GCSCB).

[68] J. O. Gibson and J. L. Melsa, Introduction to Nonparametric Detection and Applications, Mathematics in Science and Engineering, Vol. 119, Academic Press, New York, 1975.

[69] J. B. Thomas, Nonparametric detection, Proc. of IEEE, 58, 1970, pp. 623-631.

[70] S. A. Kassan, A bibliography of non-parametric detection, IEEE Trans. on Information Theory, IT-26, No. 5, Sept. 1980.

[71] D. Middleton, Adaptive processing of underwater acoustic signals in non-Gaussian noise environments: I. Detection in the space-time threshold regime, Adaptive Methods in Underwater Acoustics, pp. 527-536, NATO ASI Series, Riedel Pub. Co. Dordrecht, Holland, Series C, Vol. 151, 1985.

[72] D. Middleton, Threshold signal and parameter estimation in non-Gaussian EMC environments, Proc. of 6th International Sym. and Exhibition on EMC, Zurich, March 5-7, 1985, pp. 429-435.

[73] D. Middleton, Space-time processing for weak signal detection in non-Gaussian and nonuniform electromagnetic interference (EMI) fields, NTIA Contractor Report 86-36, Feb. 1986 (NTIS Order No. PB 86-193406).

APPENDIX. NOISE MODEL STATISTICS AND PARAMETERS

In this Appendix, we summarize various statistical results: analytical forms for the APD's (and pdf's) of Class A and B interference, moments, etc., which have been derived in detail earlier (cf. [1,6-11]). These constitute the theoretical descriptions of the new EMI models, which in turn are needed in the telecommunications applications outlined in Part II. They are sufficiently detailed to provide entrée to those concerned with their foundations and derivations in the references just cited.

A.1 CLASS A STATISTICS

A brief summary of the principal first-order envelope statistics is given next. A comprehensive discussion, with the details of the derivation, is given in [1,7] (and for the statistics of the instantaneous amplitude in [6,8]. The principal statistics we shall need here are the exceedance probability (or APD), the probability density function (pdf) and various (even) moments. These are:

$$P_1(\mathcal{E} \geq \mathcal{E}_0)_A \simeq e^{-A_A} \sum_{m=0}^{\infty} \frac{A_A^m}{m!} \exp(-\mathcal{E}_0^2/2\hat{\sigma}_{mA}^2) \tag{A.1}$$

$$w_1(\mathcal{E})_A \simeq e^{-A_A} \sum_{m=0}^{\infty} \frac{A_A^m \mathcal{E}}{m!\hat{\sigma}_{mA}^2} \exp(-\mathcal{E}^2/2\hat{\sigma}_{mA}^2) \quad (\mathcal{E} \geq 0) \tag{A.2}$$

for the APD and pdf, respectively, for the normalized envelope $\mathcal{E}$ and envelope threshold $\mathcal{E}_0$, where

$$(\mathcal{E},\mathcal{E}_0) \equiv (E,E_0)/\sqrt{2\Omega_{2A}(1 + \Gamma_A')} \equiv (E,E_0)a_A \ . \tag{A.3}$$

The pdf of the (normalized) instantaneous amplitude x ($\equiv X/\sqrt{\Omega_{2A}(1 + \Gamma_A')}$), which is often employed in signal reception analyses, is

$$w_1(x)_A \tilde{=} \exp(-A_A) \sum_{m=0}^{\infty} \frac{A_A^m}{m!\sqrt{4\pi\hat{\sigma}_{mA}^2}} \exp(-x^2/4\hat{\sigma}_{mA}^2). \tag{A.4}$$

Here, also, we have

$$2\hat{\sigma}_{mA}^2 \equiv (m/A_A + \Gamma_A')/(1 + \Gamma_A') ,$$

with

$$a_A^2 = \{2\Omega_{2A}(1 + \Gamma_A')\}^{-1} . \tag{A.5}$$

The various even-order moments of ε are obtained most readily from the (exact) characteristic function (c.f.) (cf. [7,9]), which gives

$$\langle \mathcal{E}_A^{(0)} \rangle = 1; \quad \langle \mathcal{E}_A^2 \rangle = 1;$$

$$\langle \mathcal{E}_A^4 \rangle = \Omega_{4A}/\Omega_{2A}^2 \, (1 + \Gamma_A')^2 + 2 ;$$

$$\langle \mathcal{E}_A^6 \rangle = \frac{\Omega_{6A}}{\Omega_{2A}^3(1 + \Gamma_A')^3} + \frac{9\Omega_{4A}}{\Omega_{2A}^2(1 + \Gamma_A')^2} + 6, \text{ etc.} \tag{A.6}$$

(The unnormalized moments $\langle E_A^{2k} \rangle$, $k \geq 0$, follow directly from $E_A = \mathcal{E}_A a_A^{-1}$.)

A.2 A PROCEDURE FOR OBTAINING $\mathcal{P}_{3A}$

An approach based on the first three even moments $\langle E_A^{2k} \rangle$, $k = 1,2,3$, yields the explicit results ([10], Sec. 3.2)

$$A_A \doteq \frac{9(e_4 - 2e_2^2)^3}{2(e_6 + 12e_2^3 - 9e_2e_4)}$$

$$\Gamma'_A \doteq \frac{2e_2(e_6 + 12e_2^3 - 9e_2e_4)}{3(e_4 - 2e_2^2)^2} - 1 \qquad (A.7)$$

$$\Omega_{2A} \doteq \frac{3(e_4 - 2e_2^2)^2}{4(e_6 + 12e_2^3 - 9\, e_2e_4)}$$

$$e_{2k} \equiv \left\langle E_A^{2k} \right\rangle ,$$

where, of course, each parameter of $\mathcal{P}_{3A}$ exceeds zero.

Finally, an exact (for infinite ensembles) procedure for obtaining $\mathcal{P}_{3A}$ (and all higher degree, first-order parameters) requires (cf. [10]),

(i) 2nd moment:

$$\left\langle E_A^2 \right\rangle_{\text{ideal-xpt}} \equiv \left\langle E_A^2 \right\rangle = 2\Omega_{2A}(1 + \Gamma'_A) . \qquad (A.8a)$$

(ii) APD at limitingly small thresholds:

$$[P_1 \Big|_{\mathcal{E}_o^2 \to 0}]_{\text{i-xpt}} = (P_1 \Big|_{\mathcal{E}_o^2 \to 0})_{\text{analytic}} \qquad (A.8b)$$

(iii) slope of APD as $\mathcal{E}_o^2 \to 0$:

$$\{[dp_1/d\mathcal{E}_o^2]_{\mathcal{E}_o^2 \to 0}\}_{\text{i-xpt}} = [(dP_1/d\mathcal{E}_o^2) \Big|_{\mathcal{E}_o^2 \to 0}]_{\text{analytic}}, \qquad (A.8c)$$

which provides the necessary three relations for the set $\mathcal{P}_{3A}$. (See [8,10] for details and further discussion.)

A.3. CLASS A STATISTICS-EXTENSIONS

The results summarized above in Section A.1 are for the "strictly canonical" Class A models, which are distinguished physically from other types of Class A model by requiring, in general, that the interfering sources be equidistant from the receiver. (See Section IV of [49] for the detailed analysis.)

Other types, or extensions of the earlier canonical Class A models of Section A.1, are:

(1) the approximately canonical Class A models, where some distributions are such that few, if any, comparatively small "correction terms" are needed in the canonical results of Section A.1. The anatomy of these "approximate" cases is fully described, with typical examples, in Section V of [49]. The principal effect of the approximations is slightly to modify the shape of the pdf and APD vis-à-vis the strictly canonical forms. How this may be calculated also is described in Section V, [49].

(2) When the distribution of interfering sources, $\sigma_s(\underline{\lambda})$, is such that there may be a considerable source density near the receiver (unlike the strictly canonical cases, where the sources are equidistant from the receiver), we have what we have called the general, quasi-canonical Class A model. Analytically, it is distinguished from the others by a significant "correction term," modifying the exponential forms displayed in (A.1),(A.2), etc., which noticeably shifts the magnitude and location of the large-amplitude portion of the pdf, cf. Figures 6 and 7 [49], as well as modifying the resultant APD, cf. Figure 8, [49]; (see also [46]).

A.4. CLASS B STATISTICS

Unlike Class A interference, an adequate (first-order) description of Class B noise ultimately requires a pair of approximating characteristic functions, with their corresponding APD's and pdf's [Ref. 1, Section 2.3; 2.6II, Section 3, etc.], which are suitably joined at some appropriate value (here, E_B, of the envelope), cf. [Ref. 10, Section 2.3]. In addition, as we have already noted, we require now a basic set of six global parameters, $\mathscr{P}_{6B} = \{A_B, \Gamma'_B, \Omega_{2A}, \alpha, b_{1\alpha}, N_I\}$, also described above. The two APD's (and pdf's) needed here, which are joined at $\mathscr{E} = \mathscr{E}_B$, are

$$P_1(\mathcal{E}>\mathcal{E}_o)_{B=I} = 1 - \hat{\mathcal{E}}_o^2 \sum_{n=0}^{\infty} \frac{(-1)^n \hat{A}_\alpha^n \Gamma(1 + \frac{\alpha n}{2})}{n!} {}_1F_1(1 + \alpha n/2; 2; -\hat{\mathcal{E}}_o^2) \quad (\mathcal{E} \leq \mathcal{E}_o \leq \mathcal{E}_B)$$

with

$$\hat{\mathcal{E}}_o \equiv \mathcal{E}_o/\sqrt{\Omega}$$

$$\hat{\mathcal{E}}_o \equiv \mathcal{E}_o N_I/2G_B;\ G_B^2 \equiv (\frac{4 - \alpha}{2 - \alpha} + \Gamma_B')/4(1 + \Gamma_B') \tag{A.9}$$

$$\hat{A}_\alpha \equiv A_b(b_{1\alpha} a_B/G_B)^\alpha = A_\alpha 2^{-\alpha} G_B^{-\alpha},$$

where $a_B^2 = \{2\Omega_{2B}(1 + \Gamma_B')\}^{-1}$, cf. (A.5), the normalizing factor; e.g., $(\mathcal{E}_o, \mathcal{E}) = (E_o, E)a_B$, cf. (A.3), and ${}_1F_1$ is a confluent hypergeometric function [2]. The second APD is given by

$$P_1(\mathcal{E}>\mathcal{E}_o)_{B\text{-}II} \cong \exp(-A_B) \sum_{m=0}^{\infty} \frac{A_B^m}{m!} \exp(-\mathcal{E}_o^2/2\sigma_{mB}^2) \quad (\mathcal{E}_B \leq \mathcal{E}_o \leq \infty) \tag{A.10}$$

with

$$2\hat{\sigma}_{mB}^2 \equiv (m/\hat{A}_B + \Gamma_B')/(1 + \Gamma_B');\ \hat{A}_B \equiv (\frac{2 - \alpha}{4 - \alpha})\ A_B. \tag{A.11}$$

The associated pdf's for the two regions ($\mathcal{E} \gtrless \mathcal{E}_B$) are

$$w_1(\mathcal{E}) \equiv \hat{w}_1(\hat{\mathcal{E}})_{B\text{-}I} \cong 2\hat{\mathcal{E}} \sum_{n=0}^{\infty} \frac{(-1)^n}{n!} \cdot \hat{A}_\alpha^n \Gamma(1 + \alpha n/2)\, {}_1F_1(1 + \frac{\alpha n}{2};\ -\hat{\mathcal{E}}^2) \tag{A.12}$$

$$(\hat{\mathcal{E}} = \mathcal{E}/\sqrt{\Omega}) \qquad (0 \leq \mathcal{E} \leq \mathcal{E}_B)$$

and

$$w_1(\mathcal{E}) \cong \exp(-A_B) \sum_{m=0}^{\infty} \frac{A_B^m \mathcal{E} \exp(-\mathcal{E}^2/2\hat{\sigma}_{mB}^2)}{m!\hat{\sigma}_{mB}^2} \quad (\mathcal{E}_B \leq \mathcal{E} \leq \infty). \tag{A.13}$$

(The corresponding pdf's for the instantaneous amplitudes are [8]:

$$w_1(\hat{x})_{B\text{-}I} \simeq \frac{1}{\pi} \sum_{n=0}^{\infty} \frac{(-1)^n \hat{A}_\alpha^n}{n!} \Gamma\left(\frac{1+n\alpha}{2}\right) {}_1F_1\left(\frac{1+n\alpha}{2};\frac{1}{2};-\hat{x}^2\right); (-\hat{x}_B \leq \hat{x} \leq \hat{x}_B) \qquad (A.14a)$$

$$w_1(x)_{B\text{-}II} \simeq \exp(-A_B) \sum_{m=0}^{\infty} \frac{A_B^m \exp(-x^2/4\hat{\sigma}_{mB}^2)}{(4\pi\hat{\sigma}_{mB}^2)^{1/2}} \quad (x < -x_B;\ x > x_B) \qquad (A.14b)$$

with $\hat{x} \equiv xN_I/2\sqrt{2}G_B$, $\hat{x}_B = x_B N_I/2\sqrt{2}G_B$, $\hat{x} = x/\sqrt{\Omega}$.

The (even) moments of $\mathcal{E}$ are given (exactly) by (A.6), with $A \to B$, e.g., $A_A \twoheadrightarrow A_B$, etc.

A.5. CLASS B MODELS: SINGLE-FORM, THREE-PARAMETER MODELS

The general approximation outlined in Section A.3 for Class B cases gives an adequate (first-order) description of the desired APD and pdf here, with proper behavior at the "tails" (i.e., "rare-event" portions) of the distribution, in that the resultant second-moments $\overline{\mathcal{E}^2}$ (or $\overline{x^2}$) are <u>finite</u>, as required physically. However, these two-distribution analytic model fits can be cumbersome, so that it is usually desirable in applications to use a modified, three-parameter version of (A.7) and (A.10), which can be suitably adjusted to give good approximation to empirical observations over the effective range of distribution values.

Accordingly, it has been shown [59,63,69] that the APD and pdf of the normalized <u>input envelope</u>, $\mathcal{E}$, can be represented in the aforementioned three-parameter Class B models, by

$$P_1(\mathcal{E}>\mathcal{E}_o)_B \simeq e^{-\mathcal{E}_o^2/\Omega} \{1 - \frac{\mathcal{E}_o^2}{\Omega} \sum_{n=1}^{\infty} \frac{(-1)^n}{n!} \hat{A}^n \Gamma(1+\frac{n\alpha}{2}) {}_1F_1(1-\frac{n\alpha}{2};\alpha;\mathcal{E}_o^2/\Omega)\} \qquad (A.15)$$

and

$$w_1(\mathcal{E})_B \simeq \frac{2\mathcal{E}e}{\sqrt{\Omega}} e^{-\mathcal{E}^2/\Omega} \sum_{n=0}^{\infty} \frac{(-1)^n}{n!} \hat{A}_\alpha^n \Gamma(1+\frac{n\alpha}{2}) {}_1F_1(-\frac{\alpha n}{2};1;\mathcal{E}^2/\Omega) \ . \qquad (A.16)$$

A similar relation holds for the (normalized) instantaneous amplitude, x, viz.:

$$w_1(x)_B \simeq \frac{e^{-x^2/\Omega}}{\pi\sqrt{\Omega}} \sum_{m=0}^{\infty} \frac{(-1)^m}{m!} \hat{A}_\alpha^m \Gamma\left(\frac{m\alpha + 1}{2}\right) {}_1F_1\left(-\frac{m\alpha}{2}; 1/2; x^2/\Omega\right) \quad (-\infty < x < \infty) \qquad (A.17)$$

These models have the three parameters α, $\hat{A}_\alpha$, and Ω. The parameters α, $\hat{A}_\alpha$ are explicitly described in Section 3.1, B, and (A.7a) above, and depend on the physical processes involved in the EMI scenario in question. The parameter Ω, however, is a (dimensionless) normalization parameter, which is used here to normalize the process ($\mathcal{E}$ or z values) to the measured energy in the process. [We cannot normalize to the computed energy, since for (A.14) and (A.15) the second moment does not exist (nor does any other).] This unbounded second-moment and unbounded moment behavior in general is a typical problem with such models of broadband, "impulsive" noise. Using (A.13) - (A.15) in conjunction with measured data, as well as for analytic calculations, requires a suitable truncation of the pdf, at some large level $\mathcal{E}_0^1$ (or z_0^1), which in turn establishes Ω, cf. [67].

FORM **NTIA-29**
(4-80)

U.S. DEPARTMENT OF COMMERCE
NAT'L. TELECOMMUNICATIONS AND INFORMATION ADMINISTRATION

BIBLIOGRAPHIC DATA SHEET

	1. PUBLICATION NO.	2. Gov't Accession No.	3. Recipient's Accession No.
	NTIA Report 86-194		

4. TITLE AND SUBTITLE
A Tutorial Review of Elements of Weak Signal Detection in Non-Gaussian EMI Environments

5. Publication Date
May 1986

6. Performing Organization Code
NTIA/ITS.S3

7. AUTHOR(S)
David Middleton and A. D. Spaulding

9. Project/Task/Work Unit No.
910 1518

8. PERFORMING ORGANIZATION NAME AND ADDRESS
NTIA/ITS.S3
325 Broadway
Boulder, CO 80303

10. Contract/Grant No.

11. Sponsoring Organization Name and Address
NTIA/DoD
Herbert C. Hoover Building
14th & Constitution Ave., NW
Washington, DC 20230

12. Type of Report and Period Covered

13.

14. SUPPLEMENTARY NOTES

15. ABSTRACT *(A 200-word or less factual summary of most significant information. If document includes a significant bibliography or literature survey, mention it here.)*

New models of electromagnetic interference (EMI) have been developed by Middleton [1-11,48,49] over the last decade (1974-1983), which have provided canonical, analytically tractable, and experimentally well-established quantitative descriptions of nearly all EMI environments. These models are (1) physically derived; (2) are canonical in the sense that they are invariant of the nature and waveform of the source and details of propagation, as far as their formal analytical structure is concerned; (3) are highly non-Gaussian; and (4) are analytically and computationally manageable. Their principal quantitative and most widely applied form is embodied in the first-order probability distributions of the (instantaneous) amplitude, and envelope, of the received waveform following the linear front-end stages of a typical receiver. Three basic EMI models are distinguished: Class A, B, and C, respectively involving sets of three, six and eight, physically derived parameters, which are
(CONTINUED ON REVERSE)

16. Key Words *(Alphabetical order, separated by semicolons)*
Class A, B, C noise; electromagnetic interference environments (EMI); optimum and suboptimum detectors; optimum signal detection; performance comparison

17. AVAILABILITY STATEMENT	18. Security Class. *(This report)*	20. Number of pages
☒ UNLIMITED.	UNCLASSIFIED	102
☐ FOR OFFICIAL DISTRIBUTION.	19. Security Class. *(This page)* UNCLASSIFIED	21. Price:

measurable from observed EMI amplitude (or envelope) data. These three basic classes are defined in terms of receiver bandwidth vis-à-vis that of the EMI.

When receivers conventionally optimized for Gauss noise (i.e., matched-filter systems) are used in these highly non-Gaussian EMI environments, receiver performance can be greatly degraded [Q(20-40 dB), typically], vis-à-vis that of receivers optimized to the actual EMI in force (e.g., Class A, B, or C noise) [2,13,14,21]. Specific examples of this behavior are provided. The physical bases and practical implications of the EMI models themselves and their impact on the reception process also are discussed.

The principal aim of this Report is to present a Tutorial Review of the main features of the work to date (<1985) on these models and their current and potential applications, particularly for weak-signal detection. Accordingly, this Report represents an updated and expanded version of an earlier tutorial review ([40], 1980). Various analytical details are reserved to an Appendix, and the full technical analysis and results are specifically cited in the extensive list of references, which themselves are briefly appraised from the viewpoint of the reader's further interest.

☆U.S. GOVERNMENT PRINTING OFFICE:1986—676-002/40022